


DEVELOPING A NEW DESIGN PASSIVE HOUSE WITH A PARTIAL DOUBLE-
SKIN FAÇADE, DOUBLE-SKIN ROOF, UNDERGROUND SPACE AND EARTH
TUBE BASED ON ENERGY AND AIRFLOW PERFORMANCE



by
Ruhan Pak

Submitted to Graduate School of Natural and Applied Sciences
in Partial Fulfillment of the Requirements
for the Degree of Doctor of Philosophy in
Systems Engineering

Yeditepe University
2015

DEVELOPING A NEW DESIGN PASSIVE HOUSE WITH A PARTIAL DOUBLE-
SKIN FAÇADE, DOUBLE-SKIN ROOF, UNDERGROUND SPACE AND EARTH
TUBE BASED ON ENERGY AND AIRFLOW PERFORMANCE

APPROVED BY:

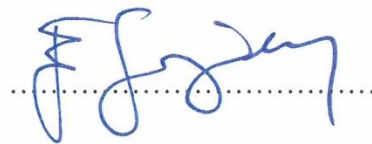
Assist. Prof. Dr. Zeynep Ocak
(Thesis Supervisor)



Assoc. Prof. Dr. Dilek Tüzün Aksu



Assoc. Prof. Dr. Esra Sorgüven Öner



Assist. Prof. Dr. Uğur Yıldırım



Assist. Prof. Dr. Zeynep Parlar



DATE OF APPROVAL: ... / ... / 2015



*To my wife Eser, my mother Mehlika,
my father Hasan, my brother Serhan...*

TABLE OF CONTENTS

ACKNOWLEDGEMENTS.....	iiix
ABSTRACT.....	ix
ÖZET.....	x
LIST OF FIGURES.....	xi
LIST OF TABLES.....	xiv
LIST OF SYMBOLS/ABBREVIATIONS.....	xvi
1. INTRODUCTION.....	1
1.1. SUSTAINABILITY.....	1
1.2. PASSIVE HOUSE.....	1
1.3. DOUBLE-SKIN HOUSES.....	4
1.4. WORK PLAN OF THE MANUSCRIPT.....	5
2. LITERATURE REVIEW.....	7
2.1. PASSIVE HOUSE ENVELOPE DESIGN PARAMETERS.....	7
2.2. PASSIVE HOUSE ADVANCED DESIGN PARAMETERS.....	9
2.2.1. Double-skin Façade (DSF).....	9
2.2.2. Experimental Studies on Double-skin Façade.....	13
2.2.2.1. Energy Performance.....	14
2.2.2.2. Mechanical Ventilation.....	14
2.2.2.3. Natural Ventilation.....	15
2.2.2.4. Thermal Mass.....	16
2.2.3. Numerical studies on double-skin façade.....	17
2.2.3.1. Energy Performance.....	17
2.2.3.2. Energy Simulation.....	18
2.2.3.3. Computational Fluid Dynamics Simulation.....	18
2.2.3.4. Calibration.....	18
2.2.3.5. Validation.....	19
2.2.3.6. Energy and Computational Fluid Dynamics Simulation Coupling.....	19
2.2.4. Double-skin Roof (DSR).....	23

2.2.5.	Experimental Studies on Double-skin Roof.....	24
2.2.5.1.	Energy Performance.....	24
2.2.5.2.	Natural Ventilation.....	25
2.2.6.	Numerical Studies on Double-skin Roof.....	25
2.2.6.1.	Computational Fluid Dynamics Simulation.....	25
2.2.7.	Underground Space and Earth Tube	26
2.3.	CONCLUSIONS.....	26
3.	OBJECTIVE OF THE STUDY.....	28
4.	METHODOLOGY.....	29
4.1.	METHODOLOGY APPLICATION.....	29
5.	NUMERICAL MODELING OF DSF.....	34
5.1.	NUMERICAL MODEL AND ASSUMPTIONS.....	34
5.2.	ENERGY MODEL FOR DSF.....	35
5.2.1.	Energy Model for Cavity.....	35
5.2.2.	Energy Model for Indoor Room.....	38
5.3.	AIRFLOW MODEL FOR CAVITY AIR.....	39
5.4.	TURBULENCE MODEL FOR CAVITY AIR.....	41
5.5.	COUPLED ENERGY AND AIRFLOW MODEL FOR CAVITY AIR.....	44
6.	VALIDATION OF ENERGY – CFD SIMULATION COUPLING.....	46
6.1.	ENERGY MODEL SETUP.....	47
6.2.	GEOMETRY CALIBRATION.....	48
6.3.	COMPUTATIONAL FLUID DYNAMICS MODEL SETUP.....	50
6.3.1.	Model Geometry.....	50
6.3.2.	Boundary Conditions.....	51
6.3.3.	Model Grid.....	52
6.3.4.	Numerical Methods.....	55
6.4.	VALIDATION OF ENERGY – CFD SIMULATION COUPLING.....	57
7.	NEW PASSIVE HOUSE DESIGN.....	59
7.1.	DESIGN COMPONENTS.....	60
7.1.1.	Design Components of New House.....	60

7.1.2.	Design Components of Reference House.....	62
7.2.	ENERGY ZONE LAYOUTS.....	62
7.2.1.	Energy Zone Layouts of New House.....	63
7.2.1.1.	Underground Space.....	64
7.2.1.2.	Living Quarters.....	65
7.2.1.3.	Double-skin Roof.....	65
7.2.1.4.	South-side Partial Double-skin Façade	66
7.2.1.5.	North-side Partial Double-skin Façade.....	67
7.2.1.6.	Earth Tube.....	68
7.2.1.7.	Component Combinations.....	68
7.2.2.	Energy Zone Layout of Reference House.....	69
7.2.2.1.	Living Quarters.....	69
8.	ENERGY PERFORMANCE OF NEW HOUSE.....	70
8.1.	ENERGY MODEL SETUP.....	70
8.2.	ENERGYPLUS SIMULATION RESULTS.....	70
8.2.1.	Passive House Criteria.....	71
8.2.2.	Energy and Airflow Behaviour of New House.....	71
8.3.	ENERGY PERFORMANCE COMPARISON.....	75
9.	AIRFLOW PERFORMANCE ANALYSIS OF NEW HOUSE.....	77
9.1.	COMPUTATIONAL FLUID DYNAMICS MODEL SETUP.....	77
9.1.1.	Model Geometry.....	77
9.1.2.	Boundary Conditions.....	78
9.1.3.	Model Grid.....	80
9.1.4.	Numerical Methods.....	86
9.2.	FLUENT SIMULATION RESULTS.....	86
9.3.	AIRFLOW PERFORMANCE ANALYSIS.....	90
10.	FINANCIAL ANALYSIS OF NEW HOUSE.....	91
10.1.	CONSTRUCTION COSTS.....	91
10.2.	ENERGY SAVINGS AND PAYBACK PERIOD.....	91
11.	DISCUSSION OF FINDINGS.....	94

11.1. DESIGN IMPLICATIONS.....	94
11.2. ENERGY PERFORMANCE.....	94
11.3. AIRFLOW CONTRIBUTION.....	95
11.4. FINANCIAL ASPECTS.....	95
12. CONTRIBUTION AND FUTURE WORKS.....	96
12.1. CONTRIBUTION.....	96
12.2. LIMITATION AND RECOMMENDATIONS FOR FUTURE WORK.....	96
REFERENCES.....	98
APPENDIX A	111
APPENDIX B.....	113
APPENDIX C.....	114
APPENDIX D.....	117
APPENDIX E.....	121
APPENDIX F.....	122
APPENDIX G.....	123
APPENDIX H.....	124
APPENDIX I.....	128
APPENDIX J.....	137
APPENDIX K.....	138
APPENDIX L.....	142
APPENDIX M.....	149
APPENDIX N.....	154
APPENDIX O.....	155
APPENDIX P.....	158
APPENDIX Q.....	159
APPENDIX R.....	164

ACKNOWLEDGEMENTS

I am deeply grateful to my supervisor Asst. Prof. Dr. Zeynep Ocak for her enthusiasm, support and inspiring lead. Without her I would not finish the program.

I am also grateful to Assoc. Prof. Dr. Esra Sorgüven. Her constructive guidance and remarkable patience were invaluable in the advancement of this research.

I would like to thank all the members of the academic jury also including Asst. Prof Dr. Uğur Yıldırım, Assoc. Prof. Dr. Dilek Tüzün Aksu and Asst. Prof. Dr. Zeynep Parlar, for their wisdom and advices.

I would like to extend my gratitude to Prof. Dr. Murat Tunç and Prof Dr. Melek Başak. Without him I would not begin the program and without her I would not stay in.

My thanks and appreciation also go to all the other people in Yeditepe Systems Engineering Department who helped me along the way.

I have been fortunate to come across good friends and colleagues like Kutun Demirci and Meltem Bayraktar. I am thankful to him for patiently explaining my Fluent problems and her for my EnergyPlus problems.

My loving thanks to my business partner Zeynep Berkol and my friends for their constant help and genuine friendship.

And of course, I want to express my love to my wife Eser whose patience, affection and encouragement have supported me during all these years. Without her this thesis would not exist.

Above all, I want to express my greatest gratitude to my parents Mehlika and Hasan, my brother Serhan, Pak and Ozar families, for their never-ending support and understanding.

ABSTRACT

DEVELOPING A NEW DESIGN PASSIVE HOUSE WITH A PARTIAL DOUBLE-SKIN FAÇADE, DOUBLE-SKIN ROOF, UNDERGROUND SPACE AND EARTH TUBE BASED ON ENERGY AND AIRFLOW PERFORMANCE

This research originates from the interest in developing products with a holistic and interdisciplinary systems engineering approach, toward fostering sustainability. The study develops a new-design passive house with a double-skin envelope that delivers better energy consumption performance for heating and cooling relative to a conventional reference house, while achieving comfort-level indoor temperatures. A single-façade reference house is designed with the identical geometry, material and conditions of the new house living quarters, in order to demonstrate the performance of new house using a valid comparison. The new and reference houses are simulated cases and are not calibrated by actual models. The Soft Systems Methodology which enables designers to make better decisions at the earliest design stage is applied integrated with hard methods for the conceptual model development and performance comparison. Additionally, fluid dynamics behaviour of the air inside the double-skin envelope is analysed to demonstrate the airflow's contribution to the energy performance. The energy simulations demonstrate that the heating and cooling demands of new house are 19.1 per cent and 18.8 per cent lower than those of reference house, respectively. Furthermore, the computational fluid dynamics simulations reveal that turbulent airflow in the underground space on summer day increases heat transfer, and laminar airflow in the double-skin roof on winter night decreases such transfer.

ÖZET

ENERJİ VE HAVA AKIMI PERFORMANSLARI ÜZERİNE KİSMİ ÇİFT CİDAR CEPHESİ, ÇİFT CİDAR ÇATISI, YERALTI ALANI VE YERALTI BORUSU OLAN YENİ TASARIM BİR PASİF EV GELİŞTİRMEK

Bu araştırma sürdürülebilirliği teşvik etmeye yönelik bütünsel ve disiplinler arası mühendislik yaklaşımıyla ürün geliştirme ilgisinden kaynaklanmaktadır. Bu çalışma ev içinde konfor seviyesinde sıcaklıkları sağlarken geleneksel bir referans ev ile karşılaştırıldığında ısıtma ve soğutma için daha iyi enerji tüketim performansı gösteren yeni tasarım bir pasif ev geliştirdi. Yeni evin performansını geçerli bir kıyaslama ile gösterebilmek için, yeni evin yaşam alanının geometri, malzeme ve şartları ile aynı olan tek cidarlı bir referans ev tasarlandı. Yeni ve referans ev simüle vakadır ve gerçek modellerle kalibre edilmemiştir. Tasarımcıların tasarım aşamasının en başından daha iyi karar vermesini sağlayan Yumuşak Sistemler Metodolojisi kavramsal model geliştirme ve performans karşılaştırması için katı metodlar ile birleştirilip uygulandı. Bununla beraber hava akımının enerji performansına katkısını ortaya koyabilmek için çift cidar zarfın içindeki havanın akışkanlar mekaniği davranışı incelendi. Enerji simülasyonları yeni evin ısıtma ve soğutma talebinin referans evden sırasıyla yüzde 19.1 ve yüzde 18.8 daha düşük olduğunu gösterdi. Buna ek olarak, hesaplamalı akışkanlar mekaniği simülasyonları yaz günü yeraltı alanındaki türbülanslı hava akımının ısı iletimini artırdığını ve kış günü çift cidar çatıdaki laminar hava akımının bu iletimi azalttığını açığa çıkardı.

LIST OF FIGURES

Figure 1.1. Passive house components.....	3
Figure 1.2. Early full double-skin façade house with DSR, crawlspace and underground pipes.....	4
Figure 2.1. ElementHouse designed by University of Illinois at Urbana-Champaign.....	8
Figure 2.2. Box-window type double-skin façade.....	10
Figure 2.3. Shaft-box type double-skin façade.....	11
Figure 2.4. Corridor type double-skin façade.....	12
Figure 2.5. Multi-story type double-skin façade.....	13
Figure 2.6. Double-skin roof structure.....	23
Figure 2.7. Underground warming and cooling systems.....	26
Figure 4.1. SSM stages.....	30
Figure 4.2. SSM stage 4 Conceptual model development.....	32
Figure 4.3. SSM stage 5 Problem and conceptual model comparison.....	33
Figure 5.1. Salens DSF model.....	34
Figure 5.2. Energy balance on the interior surface of a wall.....	38
Figure 6.1. Vliet test building.....	46

Figure 6.2. DSF model energy zone layout.....	47
Figure 6.3. DSF model B in DesignModeler.....	50
Figure 6.4. Mesh with wall distance of 17 mm for model A and 10 mm for model B.....	55
Figure 7.1. New passive house.....	60
Figure 7.2. Full south-side DSF without DSE (Deutscher Ring Verwaltungsgebäude in Hamburg) and new house with DSE	61
Figure 7.3. Conventional reference house.....	62
Figure 7.4. DSE cavity of new house with zones.....	63
Figure 7.5. Living quarters of new house without and with DSE.....	64
Figure 7.6. Underground space energy zone.....	64
Figure 7.7. Living quarters energy zone.....	65
Figure 7.8. DSR energy zone.....	66
Figure 7.9. South-side partial DSF energy zone.....	67
Figure 7.10 North-side partial DSF energy zone.....	67
Figure 7.11. Earth tube energy zone.....	68
Figure 7.12. Reference house energy zone.....	69
Figure 8.1. Airflow paths at new house nodes on summer days and winter nights	72

Figure 9.1. Boundary conditions of new house for summer daytime and winter nighttime extremes.....	79
Figure 9.2. Fluid domain geometry	80
Figure 9.3. Meshes of new house.....	86
Figure 9.4. Summer daytime and winter nighttime static air temperatures at mid-section of new house	87
Figure 9.5. Summer daytime and winter nighttime vectors of velocity magnitude at mid-section of new house	88
Figure 9.6. Summer daytime and winter nighttime vectors of velocity magnitude along streamline at mid-section of underground space, inlet, DSR, south-side partial DSF and north-side partial DSF	88
Figure 9.7. Summer daytime and winter nighttime static air pressures at mid-section of new house	89
Figure 9.8. Summer daytime and winter nighttime turbulent Reynolds number (Re_y) at mid-section of new house	89

LIST OF TABLES

Table 6.1. Saelens' horizontal temperature stratification measurements.....	48
Table 6.2. DSF model calibration cases.....	49
Table 6.3. Inlet/outlet airflow velocities and Fluent boundary conditions.....	53
Table 6.4. Cavity wall distance estimation and airflow model determination.....	53
Table 6.5. DSF model validation cases.....	58
Table 8.1. New and reference houses under PH criteria	71
Table 8.2. Energy performance comparison	75
Table 9.1. Boussinesq model air properties at operating temperatures.....	79
Table 9.2. Vent airflow velocities for summer daytime extreme	81
Table 9.3. Opening airflow velocities for summer daytime extreme	82
Table 9.4. Opening airflow velocities for winter nighttime extreme	82
Table 9.5. Zone wall distance estimation and airflow model determination for summer daytime extreme.....	83
Table 9.6. Zone wall distance estimation and airflow model determination for winter nighttime extreme	84
Table 9.7. Airflow behavior for summer daytime and winter nighttime.....	90

Table 10.1. Component costs91

Table 10.2. Benefit/cost comparison of component combinations 92



LIST OF SYMBOLS/ABBREVIATIONS

A	Area (m^2)
A_i	Area of surface i (m^2)
a	Constant for h_{cv} correlation (-)
b	Constant for h_{cv} correlation (-)
C_p	Specific heat capacity (J/kgK)
C_q	Flow coefficient (-)
C_t	Turbulent natural convection constant ($\text{W/m}^2\text{K}^{4/3}$)
$C_{1\varepsilon}$	k - ε model constant (-)
$C_{2\varepsilon}$	k - ε model constant (-)
C_μ	k - ε model constant (-)
D_h	Hydraulic diameter (m)
e	Euler's number (-)
E	Flow energy ($\text{J/kg}\cdot\text{mole}$)
F	External body forces (N)
g	Gravitational acceleration (m/s^2)
H	Height (m)
h_{cv}	Convective heat transfer coefficient ($\text{W/m}^2\text{K}$)
$h_{i,kr}$	Radiative heat transfer coefficient between surfaces i and k ($\text{W/m}^2\text{K}$)
I	Turbulence intensity (-)
I	Unit tensor (-)
J_j	Diffusion flux of species j ($\text{kg}/(\text{m}^2/\text{s})$)
K	Thermal conductivity (W/mK)
k	Turbulent kinetic energy (m^2/s^2)
L	Length (m)
l	Length (m)
Ma	Mach number (-)
\dot{m}	Mass flow rate (kg/s)
N	Number of enclosure surfaces (-)
n	Flow exponent (n)

P_b	Production of buoyancy (W)
P_k	Production of turbulent kinetic energy (W)
p	Static pressure (Pa)
$Q_{heat\ extraction}$	Heat extraction rate of indoor room quarters (J)
Q_{other}	Heat gains from lights, people, appliances, infiltration, etc. (J)
q_i	Conductive heat flux on surface i (W)
$q_{i.c}$	Convective heat flux from surface i (W)
$q_{i.k}$	Radiative heat flux from surface i to surface k (W)
q_{ir}	Radiative heat flux from internal heat sources and solar radiation (W)
$q_{radiative}$	Radiative heat flux (W)
Pr	Prandtl number (-)
Ra	Rayleigh number (-)
Re	Reynolds numbers (-)
S	Source term (the mean rate of strain tensor) 1/s
S_m	Mass added to continuous phase from dispersed second phase (kg)
S_h	Heat of chemical reaction and any other volumetric heat sources (J)
S_ϕ	Source term (W)
s	Width of the air cavity (m)
T	Temperature (K), (°C)
U_i	Pressure, temperature and turbulent parameters in x_i direction (m/s)
u'	Root-mean-square of the turbulent velocity fluctuations (m/s)
u_{avg}	Mean flow velocity (m/s)
$u_{i,j,k}$	Components of the velocity according to i, j, k (m/s)
\dot{V}	Volumetric airflow rate (m ³ /s)
$V_{indoor\ room}$	Indoor room volume (m ³)
v	Velocity (m/s)
w	Wetted perimeter of the duct (m)
x	Width of the duct (m)
y	Height of the duct (m)
Z	Pressure drop factor (-)

α^*	Coefficient for a low Reynolds number correction (-)
β	Thermal expansion coefficient (1/K)
Γ_ϕ	Diffusion coefficient (Ns/m ²)
Δp	Pressure difference (Pa)
Δt	Sampling time interval (min)
Δx	Normal distance from a point near a wall to the wall (m)
ε	Solar absorptance (-)
ε	Turbulent dissipation rate (m ² /s ³)
μ	Dynamic viscosity (kg/ms)
μ_t	Turbulent viscosity (kg/ms)
ν	Kinematic viscosity (m ² /s)
ρ	Density (kg/m ³)
σ	Stefan-Boltzmann constant (W/m ² K ⁴)
σ_ε	k- ε model constant (-)
σ_k	k- ε model constant (-)
$\bar{\tau}$	Stress tensor (Pa)
ϕ	Flow variable such as the mean velocity component (m/s)
ϕ	Tilt angle of glazing (°)
ω	Specific dissipation rate 1/s

ASHRAE	American Society of Heating, Refrigerating, and Air-Conditioning Engineers
CFD	Computational fluid dynamics
DSE	Double-skin envelope
DSF	Double-skin façade
DSR	Double-skin roof
ES	Energy simulation
HVAC	Heating, ventilating and air conditioning
MoWiTT	Mobile Window Thermal Test
MSF	Multiple-skin façade
PH	Passive house
PHI	Passive House Institute

RANS	Reynolds-averaged Navier-Stokes
RNG	Re-Normalization Group
SST	Shear Stress Transport
TARP	Thermal Analysis Research Program



1. INTRODUCTION

1.1. SUSTAINABILITY

Sustainable development pursues growth of wealth without endangering the future generations and the eco-systems. Sustainable development is affected by the efficient use of energy [1]. In order to mitigate the risks associated with the level of pollutants and greenhouse gasses, the energy used in building's life cycle must be minimized. Victor Olgyay introduced "bioclimatic architecture" in response to early sustainability concerns in architecture. In addition to the aesthetical, functional and technological aspects, Olgyay introduced psychology, climatology and building physics. He also included the physical, regional and cultural context in building design and construction process [2]. The building activities consume significant quantities of energy. The energy consumption during building's life cycle includes the energy required for its construction, operation and disposal. During a building's life span, about 15 per cent of the total energy is used for the construction, 5 per cent for demolition and 80 per cent for its operation [3]. Therefore, the demand for thermal, naturally illuminated and ventilated energy-efficient buildings is expected to grow in the future. The functional and formal design, technology and health, safety and environmental impact of the building are key factors for achieving sustainability.

1.2. PASSIVE HOUSE

Passive house (PH) design has been a building sector solution to improve the quality of human life while supporting eco-systems since its introduction in 1991 [4]. The Passive House Institute (PHI) defines PH as a building for which thermal comfort (ISO 7730) can be achieved solely by post-heating or post-cooling of the fresh air mass, which is required to achieve adequate indoor air quality conditions without the need for additional recirculation of air.

PH certification criteria defined by the PHI [5] are as follows:

- i)** PH heating demand may not exceed 15 kWh/(m²yr).
- ii)** Primary energy use may not exceed 120 kWh/(m²yr).
- iii)** Air change rates are limited to (at max pressure of 50 Pa): 0.6/hr.
- iv)** In warmer climates and/or during summer months, excessive temperatures may not occur more than 10 per cent of the time.

PHs that have already been completed or are under construction, are also registered in PHI's database [6].

According to PHI, PHs have the following advantages [5]:

- i)** **Comfort:** PH standard delivers high comfort in summer and winter with reasonable construction costs. They utilize energy sources such as body and solar heat.
- ii)** **Quality:** PHs are efficient because of the insulation and air-tight design. Their well-insulated and thermal bridge free envelope manages the heat exposure effectively. Hence, cold corners, heat losses and moisture damages are prevented. PHs save energy because of their components and ventilation systems. Fresh air is provided for superior air quality without causing draughts. Additionally, heat recovery unit re-uses the heat of the exhaust air.
- iii)** **Ecology:** PHs are eco-friendly because they use less primary energy, leaving energy resources for the future without damaging the environment. The additional energy required for their construction, their embodied energy, is insignificant compared with their future savings. PHs offer energy savings of up to 90 per cent compared with typical central European buildings and over 75 per cent compared with average new constructions. In terms of heating oil, PHs use less than 1.5 liters per square meter of living space per year - far less than typical low-energy buildings. Similar energy savings have been demonstrated in warm climates where buildings require more energy for cooling than for heating.
- iv)** **Affordability:** PHs are both affordable and frugal over their life span. Even though PH standard requires high-quality building components, expensive HVAC systems

are eliminated. The increasing financial support in many countries makes building a PH all the more feasible.

- v) Versatility: A competent architect can design a PH. By combining individual measures any new building anywhere in the world can be designed to meet the PH standard. The versatile PH standard is also used for non-residential buildings such as administrative buildings and schools. The PH standard can also be achieved in retrofits using PH components.

PHI defines the PH components as insulation, thermal bridge free design, airtight construction, heat recovery, ventilation, highly insulating windows and innovative building services (Figure 1.1) [4].

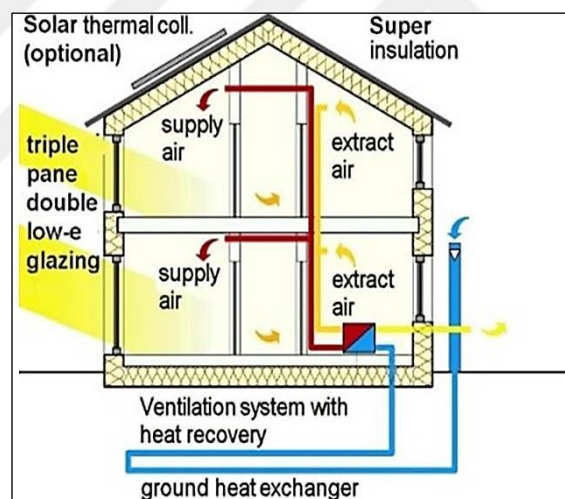


Figure 1.1. Passive house components [4]

Measurements carried out in 114 PH apartments which were part of the CEPHEUS project within the THERMIE Programme of the European Commission, Directorate-General Transport and Energy, showed average savings of approximately 90 per cent compared to conventional houses. Also according to this project, passive solar gain, superinsulation and subsoil heat exchangers are the major factors in building a PH [7].

1.3. DOUBLE-SKIN HOUSES

Since early 80s, PHs, double-skin façades (DSF) and double-skin roofs (DSR) have become more important in environmentally friendly and energy-efficient building design.

In 1979, Hartweg [8] developed a zero-energy design house with DSR, underground space, and pipes (Figure 1.2).



Figure 1.2. Early full double-skin façade house with DSR, crawlspace and underground pipes [8]

The DSF and DSR of this house acted as a thermal buffer reducing heating and cooling loads. The design included a water pool as the thermal mass to store solar energy. Additionally, underground space and pipes of the house benefited from earth ambient temperature year round. However, disadvantages of the house were as follows:

- i) The design required mechanical ventilation for the underground pipes.
- ii) The design required long underground pipes to be laid with a slope.
- iii) The double-skin cavity built up humidity, caused by the water pool.

In the early 90s, double-skin designs gained momentum when architects began to have more interest in energy-efficient buildings as the demand for such buildings grew. However, the external appearance was limited to an inner conventional façade with an additional façade made of glass panes and metal frame on the building outside [9]. By using the cavity as a natural or mechanical ventilation system, the energy needed for ventilation was reduced.

Since the early 90s, studies and applications have lacked a surrounding thermal zone from top to bottom, which improves the heat transfer rate around the house and an underground space to utilize earth ambient temperature. In Poirazis' study, 55 examples of buildings with DSFs (without any DSR integration) in Germany, Finland, Sweden, UK, Netherlands, Switzerland, Belgium, Czech Republic, USA and Australia are given [10].

1.4. WORKPLAN OF THE MANUSCRIPT

The manuscript has been divided into 12 chapters:

- Chapter 1 introduces sustainability, PH, double-skin house concepts.
- Chapter 2 reviews the literature on PH envelope and advanced design components: DSF, DSR, underground space and earth tube with their contribution to energy performance. The main advantages and disadvantages of these systems are discussed. Experimental studies on energy performance, mechanical and natural ventilation and thermal mass along with numerical studies on energy performance, energy simulation (ES), computational fluid dynamics (CFD) simulation, calibration, validation, Energy and CFD simulation coupling are presented.
- Chapter 3 introduces the objective of this study.
- Chapter 4 outlines the Soft Systems Methodology (SSM) integrated with hard methods for the conceptual model development and performance comparison. The methodology includes numerical modeling of DSF, validation of Energy - CFD simulation coupling, new passive house design, its energy performance comparison, airflow performance and financial analysis.
- Chapter 5 presents the governing equations for energy, airflow and coupled models of DSF.
- Chapter 6 achieves the validation of Energy - CFD simulation coupling using Saelens' experimental measurements and explains the applied method in details.
- Chapter 7 introduces the new house design with the integration of partial DSF, DSR, underground space and earth tube and the reference house design for a valid

comparison.

- Chapter 8 provides the energy and airflow behaviour of new house along with the new and reference house ES and the evaluation of results.
- Chapter 9 demonstrates the Energy and CFD simulation coupling of new house and evaluates results for determining the Fluid Dynamics behaviour of new house (the air inside partial DSF, DSR and underground space).
- Chapter 10 presents the financial cost and benefit comparison of new house.
- Chapter 11 discusses the performance findings and design implications.
- Chapter 12 acknowledges limitations and presents recommendations for future work.

2. LITERATURE REVIEW

In this chapter, PH envelope and advanced design parameters: DSF, DSR, underground space and earth tube with their contribution to energy performance are reviewed. The main advantages and disadvantages of these systems are discussed. Furthermore, experimental studies on energy performance, mechanical and natural ventilation and thermal mass along with numerical studies on energy performance, ES, CFD simulation, calibration, validation, energy and CFD simulation coupling are presented based on the literature review.

2.1. PASSIVE HOUSE ENVELOPE DESIGN PARAMETERS

The review of PH envelope design parameters lays the initial groundwork for a new design.

Sadineni, Madala and Boehm [11] made an extensive review of the envelope components and respective improvements from an energy efficiency perspective. Tavares and Martins [12] presented a case-study of a public building as an example of the adequacy of timely analysis of building performance, based on a preliminary architectural design with a systematic approach considering the aspects influencing building performance. Yıldız and Arsan [13] performed sensitivity and uncertainty analysis to determine the most significant parameters for buildings in hot-humid climates by considering the design of an existing apartment building in Izmir, Turkey. Wang, Esramb, Martinez and McCulley [14] reported a design and building process of a net-zero-energy modular house with 53 m² interior area, named ElementHouse (Figure 2.1) which entered the 2007 Solar Decathlon competition that was organized by the U.S. Department of Energy.



Figure 2.1. ElementHouse designed by University of Illinois at Urbana-Champaign [14]

A simplified energy model helped to form the building configuration at the preliminary design stage by showing how energy use was affected by various parameters, leading to optimization studies that provided design guidelines towards an energy-efficient building envelope and opening design.

Tommerup, Rose and Svendsen [15] gave a brief presentation of lower energy consumption, single-family houses which were built to demonstrate that it is possible to build typical single-family houses with an energy consumption that meets the demands without problems concerning building technology or economy. Filippin, Larsen, Beascochea and Lesino [16] showed the results of the thermal and energy behaviour of energy-efficient buildings for low-income students at La Pampa University. They concluded that without extra building cost, dwellers lived under good hygrothermal conditions at 50 per cent of the auxiliary energy consumed by conventional dwellings. Wang, Gwilliam and Jones [17] used the energy simulation program EnergyPlus to determine the façade design for a zero energy building in UK based on building materials, window sizes and orientations. Fath and Abdelrahman [18] investigated the micro-climatic environmental conditions inside a greenhouse distillation system. Turbulent, steady-state, flow, energy and humidity concentration equations were solved using the computational fluid dynamics simulation program Fluent. The results showed that, with the selected inlet flow conditions, the flow velocity, temperature, and relative humidity could be within the comfort values for plant growth. Persson, Roos and Wall [19] investigated the impact of decreasing the window size facing south and increasing the window size facing north on

the energy consumption of low energy houses in Gothenburg. The results showed that the size of the energy efficient windows did not have a major influence on the heating demand in the winter, but was relevant for the cooling need in the summer. Hassouneh, Alshboul and Al-Salaymeh [20] investigated the influence of glazing type, area and orientation combinations on the energy balance of apartment buildings in Amman. Lee, Kelly, Jagoda, Rosenfeld, Stube, Colaco, Gadgil, Akbari, Norford and Burik [21] described an ongoing project to demonstrate an affordable, safe, and energy-efficient housing technology based on expanded polystyrene (EPS) panels with a cementitious coating. Based on field investigation and quantitative analysis, Liu, Wang, Hu, Yang and Liu [22] presented an appropriate strategy for design, material use and building ES.

2.2. PASSIVE HOUSE ADVANCED DESIGN PARAMETERS

Review on DSF, DSR and underground space shows that these advanced parameters in particular improve thermal comfort, energy performance and sustainability.

2.2.1. Double-skin Façade (DSF)

Bestfacade project which is partially financed by European Commission actively promotes the concept of DSF in legislation and construction. As a result, investor's confidence is increased in operating performance, investment and maintenance costs. [23]. According to the project, the demand for natural ventilation in commercial buildings is increasing because of the growing environmental consciousness while at the same time energy consumption for buildings needs to be reduced. The project concludes that the DSF can provide thermal buffer zone, solar preheating of ventilation air, energy saving - sound protection, wind protection with open windows, pollutant protection with open windows, fire protection, nocturnal (night sky) cooling, aesthetics - site for incorporating PV cells.

Oesterle, Lieb, Lutz and Heusler [24] presented the categorization of DSF. Their definition is used by almost all researchers to classify the DSF system. They identified four different systems that are classified by the intermediate space division and the ventilation function: box-window, shaft-box, corridor and multi-story.

- i) Box-window is the first DSF introduced in the industry (Figure 2.2).



Figure 2.2. Box-window type double-skin façade [24]

The interior sheet is an inside opening window and the exterior sheet is a single-pane. The opening in the outside skin draws fresh air into the cavity allowing ventilation for the rooms, as well. The structure can be either segmented horizontally along the envelope, with vertical separations, or for each pane alone. Box type window is the only type that offers sound insulation in conventional openings. They are also used for retrofitting because their application to existing buildings is easier.

ii) Shaft-box is based on the box-window (Figure 2.3).



Figure 2.3. Shaft-box type double-skin façade [24]

Also developed this façade to benefit from the stack-effect based on solar radiation. The box-windows are horizontally segmented on the envelope and vertical shaft parts. The horizontally segmented box type windows are integrated to the vertical parts on each story by special openings. The stack-effect in the vertical part pulls air from the box type windows and generates airflow in the façade. Mechanical ventilation might also be included in the system. The system requires less opening in the outside skin because of the powerful thermal uplift of the stack-effect. Like Box-window, Shaft-box also offers acoustic benefits. This system is suitable for low-rises because of the height limitation of the stack-effect. An aerodynamic tuning is required to ventilate all of the box-windows integrated to a specific shaft to an equal degree. The vertical part can be positioned anywhere in the façade.

- iii) Corridor's façade is only segmented horizontally by each floor so that the cavity is open along the horizontal length of the envelope (Figure 2.4).



Figure 2.4. Corridor type double-skin façade [24]

The closures are at the corners where sometimes the pressure differentials are high. In systems with mechanical ventilation the airflow is controlled by a device called fish-head. Air intake and openings in the exterior layer which are staggered from bay to bay, are positioned close to floor and ceiling to prevent vitiated air extracted on one floor entering the space on the floor above. Corridor always has rooms attached to the individual spatial segments between the skins. Corridor does not have height limitations and it does not benefit from the stack-effect like shaft-box does because the intertwine effects are terminated on each floor.

iv) Multi-story is different in function and structure (Figure 2.5).

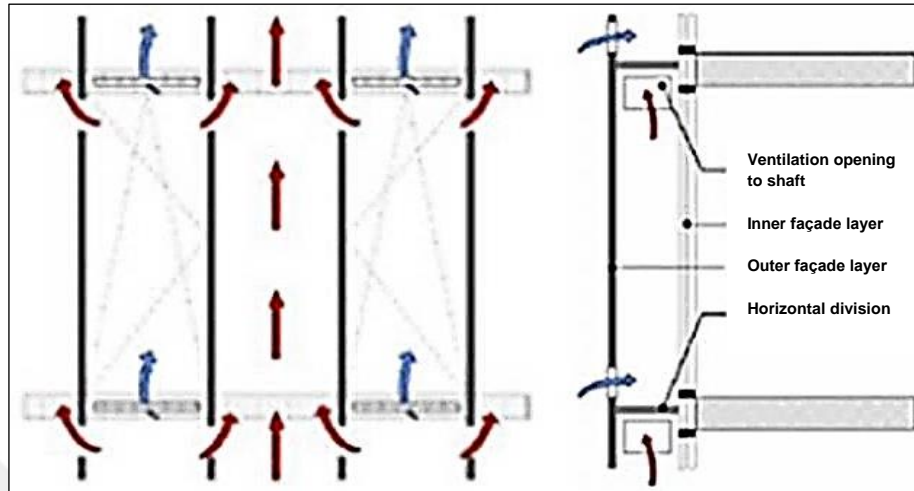


Figure 2.5. Multi-story type double-skin façade [24]

The façade is either not segmented horizontally or not segmented at all. It combines the typology of corridor and shaft-box. The air intake is situated near the bottom and the top to utilize the stack-effect. Multi-story provides sound insulation because openings do not need to be distributed over its height. Mechanical ventilation is required for the rooms behind the façade which can operate as a joint duct. The load on the service systems of the building can be reduced because Multi-story is an addition to the envelope.

2.2.2. Experimental Studies on Double-skin Façade

Reliable experimental data is required to study the thermal characteristics of a system integrated to a building. The experimental results are highly dependent on procedure and accuracy of the measurement. The consistency and the reproducibility of measurements can be achieved using a controllable experimental facility. Further development and characterization of DSFs require accurate control of the test conditions. Not only the solar radiation arriving on the façade surface, but also the thermal environment, both external and internal, should be controlled.

So far, there are not many experiments conducted to investigate thermal and energy performance of DSFs and there is no experimental study conducted at an actual building level mainly because experimental studies take long time to record the performances.

2.2.2.1. Energy Performance

Findings in studies of Xu and Ojima [25] and Chan, Chow, Fong and Lin [26] indicated that DSF was effective for energy conservation.

Xu and Ojima measured the temperature distribution, thermal performance in the double-skin space and its impact on air-conditioning load in rooms. Results showed that the DSF led to about 10-15 per cent energy saving for cooling in the peak of summer because of heat exhausted by natural ventilation, 20-30 per cent energy saving for heating in winter because of the green house effect. It was also concluded that the double-skin system in residential buildings conserved energy.

Chan, Chow, Fong and Lin used the data from their experiments in order to verify the theoretical model developed by EnergyPlus simulation program. After validating the model, they evaluated the energy performance of DSF with various configurations including glazing type, glazing position and glazing layers. The results indicated that a DSF system with single clear glazing as the inner pane and double reflective glazing as the outer pane could provide an annual saving of around 26 per cent for the cooling load, as compared to a conventional single-skin façade with single absorptive glazing.

2.2.2.2. Mechanical Ventilation

Even though some experiments provided reliable information about airflow, heat flux, solar radiation and temperature distribution in DSF, like the studies of Gavan [27], Gavan, Woloszyn, Kuznik and Roux [28], Jiru, Tao and Haghghat [29] and Fuliotto, Cambuli, Mandas, Bacchin, Manara and Chen [30], most of them analysed mechanical ventilation in DSF rather than natural ventilation.

Gavan's experimental campaign not only identified thermal behaviour of a room and its DSF and the most important modeling parameters and their relationships but also provided

an extensive set of data on air and surface temperatures of the DSF and the airflow rates.

Under controlled thermal and radiative environment, Gavan, Woloszyn, Kuznik and Roux measured and provided data on air and DSF surface temperatures and air velocities. The results of experiments can be used to validate the numerical models for ventilated DSFs with Venetian sun-shadings. However, experiments on natural ventilation in Gavan's Minibat test cell was not found feasible because of the limited height of DSF and the ineffective air velocity measuring technique with limited number of points.

Further studies on experiments of Gavan, Woloszyn, Kuznik and Roux were carried out by Kuznik, Katalina, Gauzere, Woloszyn and Roux [31] for numerical modeling of a DSF with a zonal model approach. An actual DSF with different airflow rates and shading angles were analysed.

Jiru, Tao and Haghghat conducted airflow and heat transfer simulation for a DSF system equipped with a venetian blind, using CFD simulation with Re-Normalization Group (RNG) $k-\epsilon$ turbulence model, Boussinesq hypothesis and surface-to-surface (S2S) radiation model for a three-level combination of slat tilt angle and blind position. The CFD simulation showed that the presence of venetian blinds influenced the surface heat transfer coefficients. The temperature and the air distribution in the DSF system, was validated using experimental data collected for a mechanically ventilated DSF equipped with venetian blinds.

Fuliotto, Cambuli, Mandas, Bacchin, Manara and Chen introduced a decoupling method for thermal performance evaluation and analysed the fluid behavior in a DSF. CFD simulations with the RNG $k-\epsilon$ turbulence model and Boussinesq hypothesis were used to analyse fluid flow and thermal effect on DSF. The numerical results provided by CFD simulation were validated with the experimental data.

2.2.2.3. Natural Ventilation

Studies on natural ventilation like Tascon's [32] and Mingotti, Chenvidyakarn and Woods' [33] focused generally on DSF overheating.

Tascon's full scale experiments and CFD simulation showed that natural ventilation through the cavity by a series of opening shafts on the upper and lower façade, the optical properties of the cavity elements, cavity depth size, solar control, and the basic operation of the façade were key parameters to reduce DSF overheating.

Mingotti, Chenvidyakarn and Woods investigated the natural ventilation of a DSF of a multistorey building and presented a fluid dynamics model. They showed how to prevent over-heating in summer and improve pre-heating in winter by adjusting the façade and the opening sizes.

In some studies the underlying geometry of test cell is hard to model like Kalyanova and Heiselberg's study [34]. Under the Subtask E: Modeling of a double-skin façade of International Energy Agency (IEA), Annex 34, Task 43, Kalyanova and Heiselberg performed empirical validation for buildings with double-skin façade (DSF), and assessed suitability and awareness of building energy analysis tools for predicting energy use, heat transfer, ventilation flow rates, solar protection effect and cavity air temperatures of DSF.

2.2.2.4. Thermal Mass

Fallahi [35] and Ding, Hapartial and Yamada [36] conducted experimental studies on DSFs with thermal mass. In his study, Fallahi introduced an innovative design approach. He integrated a thermal mass to the conventional DSF. He also introduced a numerical model to evaluate the thermal and energy performance of such system. The thermal mass was effective for reducing the energy loads in summer and winter.

Ding, Hapartial and Yamada conducted scaled model experiments and CFD simulation of a prototype building with a DSF and a solar chimney as the thermal storage space to evaluate the natural ventilation performance.

2.2.3. Numerical Studies on Double-skin Façade

2.2.3.1. Energy Performance

Shameria, Alghoul, Sopian, Zain and Elayeb [37] reviewed previous studies on DSF systems in buildings and concluded that DSF could decrease energy consumption.

Likewise, Aksamija [38] investigated the context and climate based DSF designs and their energy performances. The buffer zone between the interior and exterior of DSF reduced the energy loads. In her study, smaller air cavity size, effective window size, adaptive ventilation modes and airflow types, shadings, overhangs and glazing types that decreased cooling loads, were presented as the hot and arid climate design strategies for minimizing energy consumption. In winter, the trapped air improved insulation and in summer, ventilation of the cavity reduced energy loads. Position of the double glazing on the exterior also affected energy performance.

In their study, Çetiner and Özkan [39] concluded that the most energy efficient DSF in Istanbul would be approximately 22.84 per cent more efficient than a single-skin façade.

Yılmaz and Cetintaş [40] used a new numerical method in DSF's heat loss calculations and theoretically compared heat loss of a single-skin and a DSF commercial building to demonstrate the energy performance. First, a previous method was modified to calculate inter-space temperature. Then, the inter-space temperatures found in the first step were assumed to be the outdoor air temperature and the heat transfer through the inner skin of the envelope was calculated by using finite difference approach. It was found that energy load decreased in DSF building for winter in Istanbul.

Developing a modeling environment for single-story MSFs, Saelens, Roels and Hens [41] changed the façade and heating, ventilating and air conditioning (HVAC) system settings for the optimization of energy performance. Furthermore, the energy demand was improved if the control strategies for the airflow rate and the recovery of air were implemented.

2.2.3.2. Energy Simulation

Papadaki, Papantoniou and Kolokotsa [42] performed a study for the DSF configuration in a hot season. The ventilation rate, the shading type and the cavity size were investigated on a building with 18,500 m² surface area. EnergyPlus simulations showed that the ventilation rate configurations were more effective for cooling. The DSF was less effective when the ventilation was low. Additionally, the external shadings yielded 24 per cent energy savings.

2.2.3.3. Computational Fluid Dynamics Simulation

Caroli [43] studied the thermo-convective flow in a stacked DSF. Fluent solved the natural convection and heat transfer in the zones. Then, the stacked DSF was compared with a reference wall based on heat transfer capacities.

Gan [44] investigated solar heated open cavities including solar chimneys and double façades for enhancing natural ventilation of buildings. CFD simulation was used to predict buoyant airflow and flow rates inside the cavity. The airflow model of the cavity, buoyancy-induced natural convection, involved both laminar and turbulent flows. It was concluded that the buoyancy driven flow inside the cavity was developed by slow convective flows.

2.2.3.4. Calibration

As indicated by Hensen, Bartak and Drkal, [45] calibration is a difficult issue. There aren't experimental results for all of the buildings. The only way to calibrate the model is to carefully analyse the predictions and make comparisons based on previous work. Therefore, in this study, thermal and airflow models are numerically validated along with the governing equations, by comparing simulation results with the previous experimental studies.

2.2.3.5. Validation

Baldinelli [46] analysed a glass DSF equipped with integrated movable shading devices with three different modeling levels: optics of materials, fluid dynamics of the DSF and building energy balance to optimize energy performance. The validation data were taken from the experimental study of Yin-Hao Chiu and Li Shao [47] in the Institute of Building Technology of Nottingham University. This experimental campaign aimed to investigate the influence of solar heat flux and geometric parameters on a DSF thermal performance.

Pasut and Carli [48] proposed a sensitivity analysis for a CFD simulation of a special building envelope. In this work the model was validated using experimental data collected from a full-scale DSF facility by Mei, Loveday, Infield, Hanby, Cook, Li, Holmes and Bates. [49].

In an effort to show the complex natural ventilation in the air gaps divided by venetian blind, Xu and Young [50] analysed the thermal process in glass double façade with venetian blind and compared the simulation results with the experimental data in Manz's study [51].

2.2.3.6. Energy and Computational Fluid Dynamics Simulation Coupling

Manz and Frank [52] described a method based on EnergyPlus-Fluent coupling of three different simulation models that is economical in terms of computing time and suitable for design purposes. The models were: spectral optical, CFD simulation and building ES.

Hensen [53] presented two approaches for coupling heat and airflow models.

- i) In the ping-pong method the airflow rates from the ventilation model were used by the thermal model. The calculated air temperatures were then entered in the ventilation model at the next time step.
- ii) In the onion method, the airflow rates were passed from the ventilation model to the thermal model, and air temperatures were passed back from the thermal model to the ventilation model. The process was repeated until convergence was reached.

Comparing the ping-pong and the onion for different time steps, Hensen found that both of them could provide accuracy if the time step for the ping-pong was reduced.

Zhai and Chen's study [54] coupled ES and CFD simulation with different methods. Then, they validated the simulations based on experimental data. Comparison revealed the advantages of coupled building simulation over a separate ES and CFD simulation.

Zhai, Chen, Haves and Klems [55] explained efficient methods to couple ES and CFD simulation. Generally, the coupling delivers more precise results compared to separate simulations. The underlying reasons are as follows:

- i)** CFD simulation gets more accurate and real-time thermal boundary conditions and can predict the interior conditions which are essential for assessing the interior air quality and thermal comfort.
- ii)** ES receives more precise data on convection heat and can deliver more accurate estimation of energy consumption and thermal behaviour of the building envelope. The coupling can be applied to envelopes with large interior temperature stratification and detectible airflow.

Srebric Chen and Glicksman [56] stated the discontinuities between ES and CFD simulation.

- i)** Time-scale: Time-scale of ES is hours for the heat transfer in envelope. On the other hand, the time-scale of CFD simulation is seconds for the airflow in an envelope.
- ii)** Modeling: the interior conditions predicted for each space in ES are spatially averaged while CFD simulation produces field distributions.
- iii)** Speed: ES calculates a zone in seconds with a small memory. However, CFD simulation's computing time for the same zone is hours despite the usage of a larger memory.

Zhai, Chen, Haves and Klems [55] developed coupling strategies to bridge discontinuities between ES and CFD simulation.

- i) Complete computation can be divided into a long-time process for ES and a short-time process for CFD simulation to bridge the time-scale.
- ii) Numerical approximation can bridge space model discontinuity provided that enclosure surfaces in ES, are sufficiently subdivided. There are two main coupling strategies:
 - Static coupling has one-step or two-step exchange of occasional (static) information between ES and CFD simulation, depending on the sensitivity of thermal performance and accuracy requirements. One-step static coupling is used when ES or CFD simulation are not very sensitive to the exchanged variables.
 - Dynamic coupling has continuous (dynamic) information exchange between ES and CFD simulation at every time-step. It is used when both ES and CFD simulation are sensitive to the transient boundary conditions.
- iii) As proposed by Chen and van der Kooi [57], virtual dynamic coupling can be used to decrease the computational costs. The room air temperatures and the convective heat transfer coefficients required by ES are generated by CFD simulation as the functions of energy loads for conditioned periods or indoor-outdoor air temperature difference for unconditioned periods. At each time-step, ES calculates air temperature differences and convective heat transfer coefficients by interpolation of CFD simulation results. Virtual dynamic coupling is appropriate for envelopes without major changes of energy loads and exterior air temperature. Envelope characteristics and the purpose define the most appropriate coupling strategy. For instance, virtual dynamic coupling may be suitable for an annual energy analysis, while one-step dynamic coupling may be better for thermal comfort and indoor air quality analysis.

In order to improve accuracy in natural ventilation simulations, Wang and Wong [58] introduced a coupling with a text-mode interface between ES and CFD simulation for thermal prediction in time series. CFD simulations and field measurements validated the coupling. The study showed that ES alone could not predict the interior thermal environment accurately. Wang and Wong concluded that coupling could enhance the accuracy in natural ventilation prediction by taking pressure boundary conditions for CFD

simulation.

Zhai, Chen, Haves and Klems [55] indicated that a CFD simulation could solve heat transfer in solid materials, using an appropriate radiation model and conjugate heat transfer method [59-62]. When the CFD simulation takes over such functions of ES, the calculation is more accurate but yet expensive [60] as the computing time increases [63]. Therefore, ES and CFD simulation coupling is more appropriate for design purposes. The convective heat transfer information is exchanged between coupled simulations. A fully iterated coupling can render solutions similar to the conjugate heat transfer method, provided that the ES generates grids with sufficiently high resolution to model any significant temperature variations. In the coupling, the time-step is large in ES, the impact of the transient variation is small for CFD simulation.

Chen and van der Kooi [57] simulated a CFD model of room air to show the effect of the temperature distribution on energy loads. Srebric Chen and Glicksman [56] built up on Chen and van der Kooi's study by coupling a CFD simulation with an ES for designing energy load calculation.

Zhang, Lam, Yao and Zhang [64] reported the limitations in representing the actual environment with spatial configurations in systems modeling. In general, energy models assume a nodal approach for the heat transfer process with a basic network of heat resistors and capacitors. In nodal approach, the room temperature is assumed to be uniform for medium room sizes. Requirement of priori and empirical knowledge of wind pressure coefficient, heat transfer coefficient, loss and friction factors, as input is one of the limitations. The other one is the difficulty in representing the effects of thermal and airflow patterns resulting from building spatial configurations, in the model.

Zonal model, COMIS [65], is applied to ventilation in complex buildings. Moreover, research [66] shows that zonal model does not give effective results even compared to coarse-grid CFD models under isothermal conditions. Finite Volume Method of CFD details temperature profile and calculates airflow field with first principle based Navier-Stokes set of equations and turbulence models. Coefficients, such as heat transfer, are the results of the simulation defined by a set of boundary conditions. However, cost of computation and calculation of coupling between solid and fluid, are the main drawbacks of CFD simulation compared to the nodal model. Therefore, coupling may combine the

advantages of the nodal and Finite Volume Method approach, offering higher accuracy and less computation time.

Zhai, Chen, Haves and Klems [55] showed that heat transfer coefficient between CFD simulation and empirical equation could differ from $1.42 \text{ W/ m}^2 \text{ K}$ to $111.41 \text{ W/ m}^2 \text{ K}$. Mora, Gadgil and Wurtz [66] investigated the zonal model for airflows in a large interior. A coarse-grid CFD simulation was performed. Velocity and pressure calculation of zonal models and coarse-grid $k-\varepsilon$ CFD model were compared to experimental measurements. In conclusion, the zonal model was not as effective as the coarse-grid CFD model.

2.2.4. Double-skin Roof (DSR)

Natural ventilation provides a healthy and comfortable building interior with a sustainable approach. Geometry of the building is one of the most significant factors determining the viability of natural ventilation in buildings. There are past studies carried out to enhance the natural ventilation of a building by attaching components on the roof like wind towers and wind catchers. Among the wind-driven ventilation techniques forwarded by Khan, Su and Riffat [67], DSR for building roofs is considered an effective method for energy-saving designs (Figure 2.6).

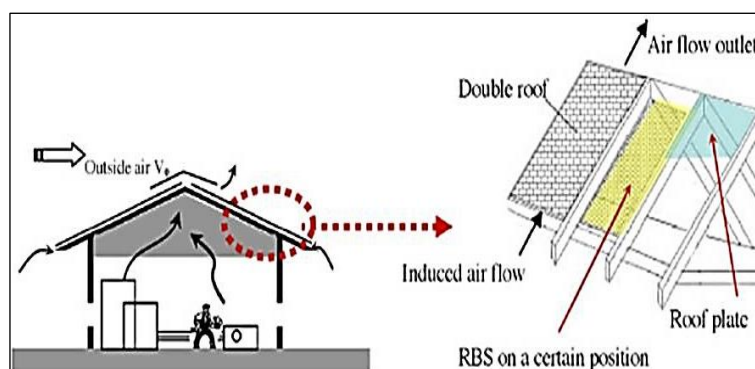


Figure 2.6. Double-skin roof structure [67]

Double-skin structure causes the mezzanine to form an air layer. In summer, the air layer with opened ends reduces the heat entering the room. In winter, the air layer with closed ends decreases the heat loss from inside to outside.

In the industry, generally a combination of high gloss roof and a low gloss ceiling finish underneath is used. These weather tight designs ensure that there are no leaks and the insulation eliminates mildew and condensation [68]. Despite of their higher investment costs when compared to single-skins, double-skin roof structures provide improved level of thermal efficiency, acoustic and fire performance [69] [70].

2.2.5. Experimental Studies on Double-skin Roof

2.2.5.1. Energy Performance

Chang, Chiang and Lai [71] designed double roof proto-types with double-skin structure and Radiant Barrier System (RBS) to reduce the solar heat gain. Experimental energy saving measurements showed that the DSR with a roof plate and aluminum foil-polypropylene board-RC slab achieved a high performance.

Biwole, Woloszyn and Pompeo [72] studied the DSRs with a metallic screen on sheet metal. In their investigation, radiation, convection and conduction heat transfers were analysed. Natural convection in the channel drove off the residual heat. The bi-dimensional numerical simulation of the heat transfers through the double-skin revealed that for a channel width over 6 cm the sheet metal surface emissivity, the screen internal and external surface emissivity, the insulation thickness and the inclination angle were the most significant factors for the system's efficiency. The impact of these factors on Rayleigh and Nusselt numbers was also analysed. Temperature and air velocity profiles on channel cross-sections were plotted and discussed.

Irwan, Ahmed, Ibrahim and Zakaria [73] concluded the best roof angle for optimum thermal and energy performance in local climate was at a roof slope of 10° at which the energy consumption could be saved up to 0.79 kWh or 4.13 per cent per day. At this angle the temperature inside the attic with respect to ambient temperature was only increased about 1.2 °C for non-insulated roof and was reduced by 0.5 °C for insulated roof.

Ong [74] tested six laboratory sized passive roof designs. It was concluded that:

- i) Bare metal roof with insulation underneath resulted in the highest roof temperature.

- ii) Roof solar collector design resulted in the coolest attic.
- iii) Solar collector roof provided the coolest ceiling.
- iv) Insulation under the tile is preferred to above the ceiling.

Lai, Huang and Chiou [75] used inclined parallel plates with upper plate heated by a lighting system to simulate DSRs exposed to solar irradiation. Heat transfer experiments were conducted for different inter-plate spacing and different inclined angles. The study also reported that placing a low-cost radiant barrier on the top of lower plate structure could be effective to prevent the roof heat from entering into the building.

2.2.5.2. *Natural Ventilation*

Susanti, Homma, Matsumoto, Suzuki and Shimizu [76] aimed to reduce the radiative heat gain of a roof cavity using natural ventilation. Experimental results for different combinations of heat production, inclination angles, and opening ratios were obtained from an inclined cavity heated on the upper surface. The heat and airflow resistance in the cavity was affected by the opening size. The higher resistance initiated low velocity and high temperature rise. Furthermore, natural ventilation in the cavity was effective for discharging solar incidence.

2.2.6. Numerical Studies on Double-skin Roof

2.2.6.1. *Computational Fluid Dynamics Simulation*

Hooff, Blocken, Aanen and Bronsema [77] used wind tunnel experiments and CFD simulation to investigate the flow in a venturi-shaped roof focusing on the underpressure in the narrowest roof section. This underpressure (contraction) could be the driver for natural ventilation in buildings. In their study, 3-D CFD simulations were performed with steady Reynolds-averaged Navier-Stokes (RANS) and the RNG k- ϵ model.

2.2.7. Underground Space and Earth Tube

Rabah [78] and Zhu, Lin and Yuan [79] referred to effective underground cooling and warming by ducts and tunnels utilizing ground heat (Figure 2.7).

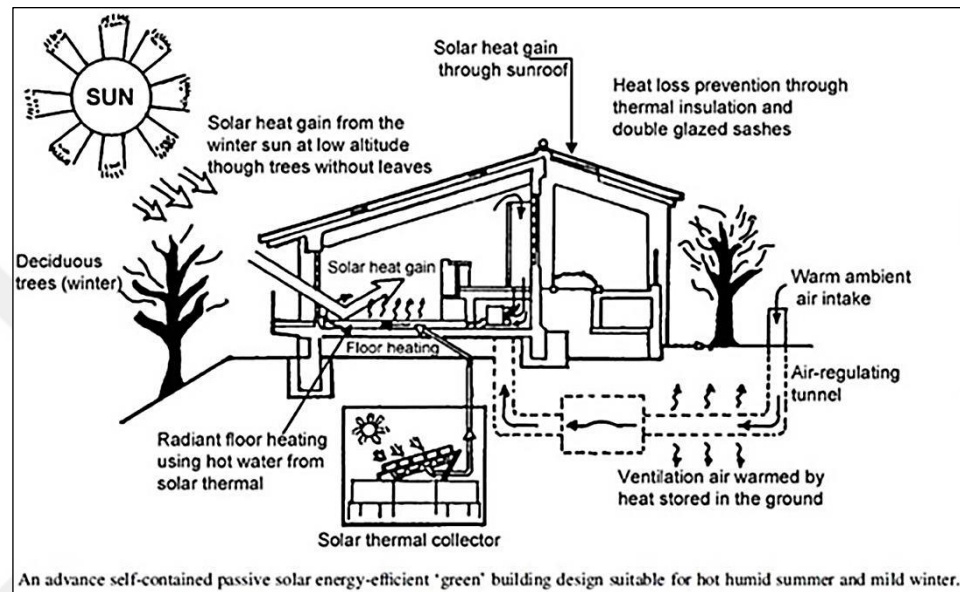


Figure 2.7. Underground warming and cooling systems [78]

Underground space heating based on the energy-storage capacity of the soil improves the indoor environment by pre-heating outside air in winter. In summer, an underground space's vent connected to an earth tube is open to suck fresh air from outside and cool it in the underground space.

2.3. CONCLUSIONS

According to Saelens, Roels and Hens [41], Multiple-skin Façade (MSF) systems to improve the energy efficiency is found in the literature. Sophisticated models to simulate MSFs are also presented in the studies. However, the ideas to enhance the energy efficiency calculation results or experimental results were seldom given. Furthermore, the researchers did not link the envelope level results to the building energy performance to model and assess the interaction between airflow in the façade, the HVAC system and the building energy management system.

A literature review of DSF, DSR and underground space shows that although there are academic studies on DSF and DSR separately, there has been no study of their full or partial integration. This finding and the possibility of eliminating the shortcomings of Hartweg's house inspired our objective of developing a new-design PH with full surrounding thermal zone, which delivers superior performance in energy consumption for heating and cooling while achieving comfort-level indoor temperatures relative to a conventional reference house.



3. OBJECTIVE OF THE STUDY

This research stems from the interest in developing products with a holistic and interdisciplinary systems engineering approach to foster sustainability. The study which is expected to contribute to the sustainable development, aims to develop a new design PH which delivers a better performance in consuming energy for heating and cooling while meeting comfort level indoor temperatures compared to a conventional reference house.

In order to actualize these performances, a new house with the first partial double-skin façade (DSF) design integrated with a double-skin roof (DSR), underground space and earth tube, is introduced by eliminating the shortcomings of the existing double-skin house designs. Additionally, the Fluid Dynamics behaviour of the air inside DSF, DSR and underground space is analysed in order to demonstrate airflow's contribution to the energy performance.

Hereafter, any integrated system of DSF and DSR including underground space and earth tube if exists, shall be referred to as double-skin envelope (DSE), new passive house as the new house and conventional reference house as the reference house.

4. METHODOLOGY

In this chapter, the methodology to develop a new design PH which delivers a better performance in consuming energy for heating and cooling while meeting comfort level indoor temperatures compared to a conventional reference house, is explained. The methodology includes numerical modeling of DSF, validation of Energy - CFD simulation coupling, new passive house design, its energy performance comparison, airflow performance and financial analysis.

4.1. METHODOLOGY APPLICATION

Soft Systems Methodology (SSM) is applied for achieving the goals of the research.

A new design PH development is complex and it has many system aspects. Like information systems projects, it assumes different characteristics during its development process. This problem situation initially has ill-defined boundaries. Hence, a soft systems approach is suggested. It is difficult to implement a hard systems approach when the system analyst is not sure of all the elements in a system. Consequently, as the study advances and achieves well-defined requirements or objectives, a hard method deems more suitable [80]. SSM can be applied in almost all situations where there is a need to enhance the analyst's understanding of a problem situation so that improvements can be made. On the other hand, hard systems approach, believes that the world contains interacting systems that can be engineered to achieve their goals. Therefore, the hard approach is applied to problems for which the main goal is to find the best solution [81].

SSM provides a process that can be applied at the earliest design stage to help designers make better decisions [82]. Furthermore, SSM with hard systems integration help the system analyst effectively address all the critical factors. Hence, while integrating hard methods which utilize simulation and quantitative models, into the stage 4 and 5 of SSM framework, this research provides a comprehensive and a distinct SSM for developing a new design PH with a partial double-skin façade, double-skin roof, underground space and earth tube based on energy and airflow performance. The stages of SSM and its application

are explained in Figure 4.1.

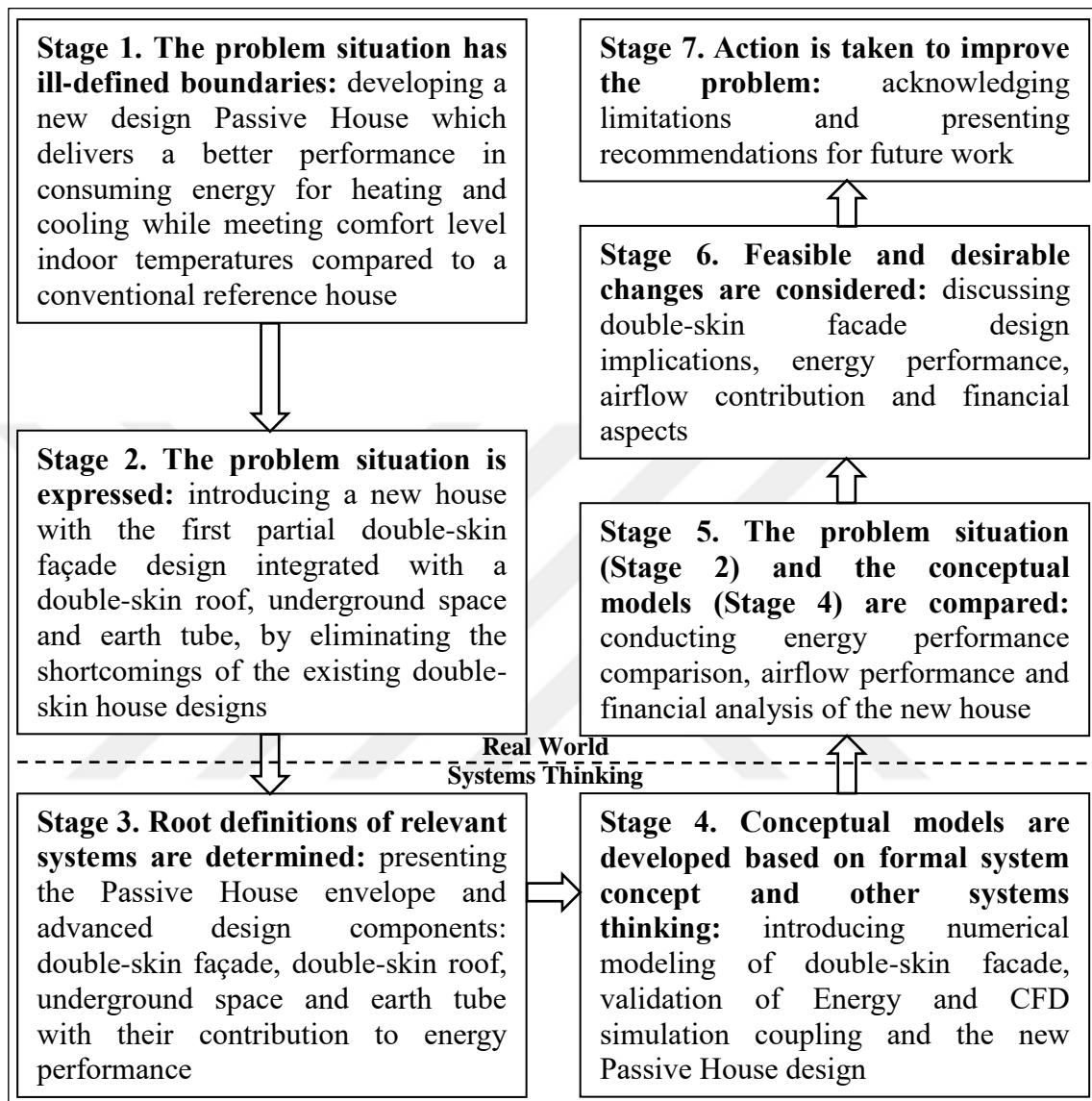


Figure 4.1. SSM stages

The essence of soft systems approach is to identify the problem area in a system and then to model only the processes which are relevant to that particular problem area. If there are complex processes, they are composed into sub-processes. SSM has the ability to provide different perspectives on a problem situation. Based on these different perspectives, a series of root definitions of the relevant systems can be developed, each of which is generated from the world view for that definition. In other words, world view reflects the underlying assumptions of the system such as “technology should surpass expectation in design, comfort, health and safety”. In addition to world view, the development of root

definitions includes the identification of the following key attributes:

- clients who are affected from the activities,
- actors who are responsible for carrying out the activities of the relevant system,
- owners who have the power to start up and shut down the system,
- transformation process which is the core process of the system that transfers its input into output,
- environmental constraints which affect the system activity.

Conceptual models illustrate the root definitions of the system showing the relationship between system activities. Taking the root definitions into consideration, conceptual model development may be problematic. Therefore, an iterative process of revisiting the root definitions and developing a conceptual model is carried out. The sub-processes of conceptual model should also monitor:

- Efficacy: to produce transformation's intended outcome.
- Efficiency: to achieve the transformation with the minimum use of resources.
- Effectiveness: to serve for some higher level or longer-term aim [83].

Finally, the conceptual model and the problem situation presented as a rich picture are compared in order to determine the feasible and desirable changes and future plans for improvement.

Based on Saelens, Roels and Hens' findings [41], Pappas and Zhai's hard methods [84], Zhai and Chen's [54] and Zhai, Chen, Haves and Klems' [55] studies, the methodology of this research follows a distinct approach for the stage 4 – conceptual model development. Both the similarities and the differences with Pappas and Zhai's approach [84] are summarized in Chapter 6 “Validation of Energy - CFD simulation coupling”. The application of stage 4 of SSM is explained in Figure 4.2.

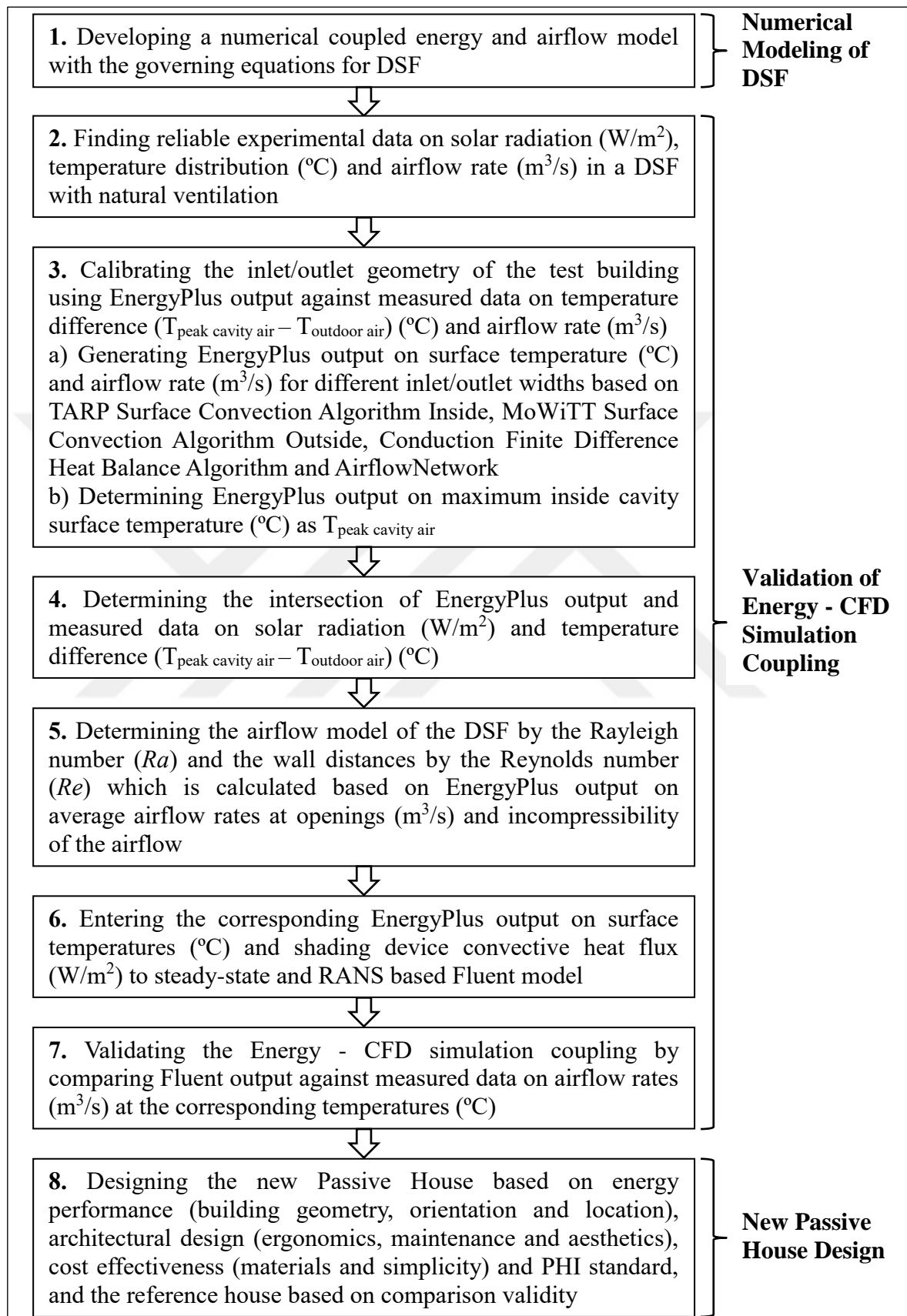


Figure 4.2. SSM stage 4 conceptual model development

As for stage 5 – conceptual model comparison, the simulated new house is compared with the simulated reference house in parallel with the hard methods applied in Mona Azarbayjani’s thesis [85]. The application of stage 5 of SSM is explained in Figure 4.3.

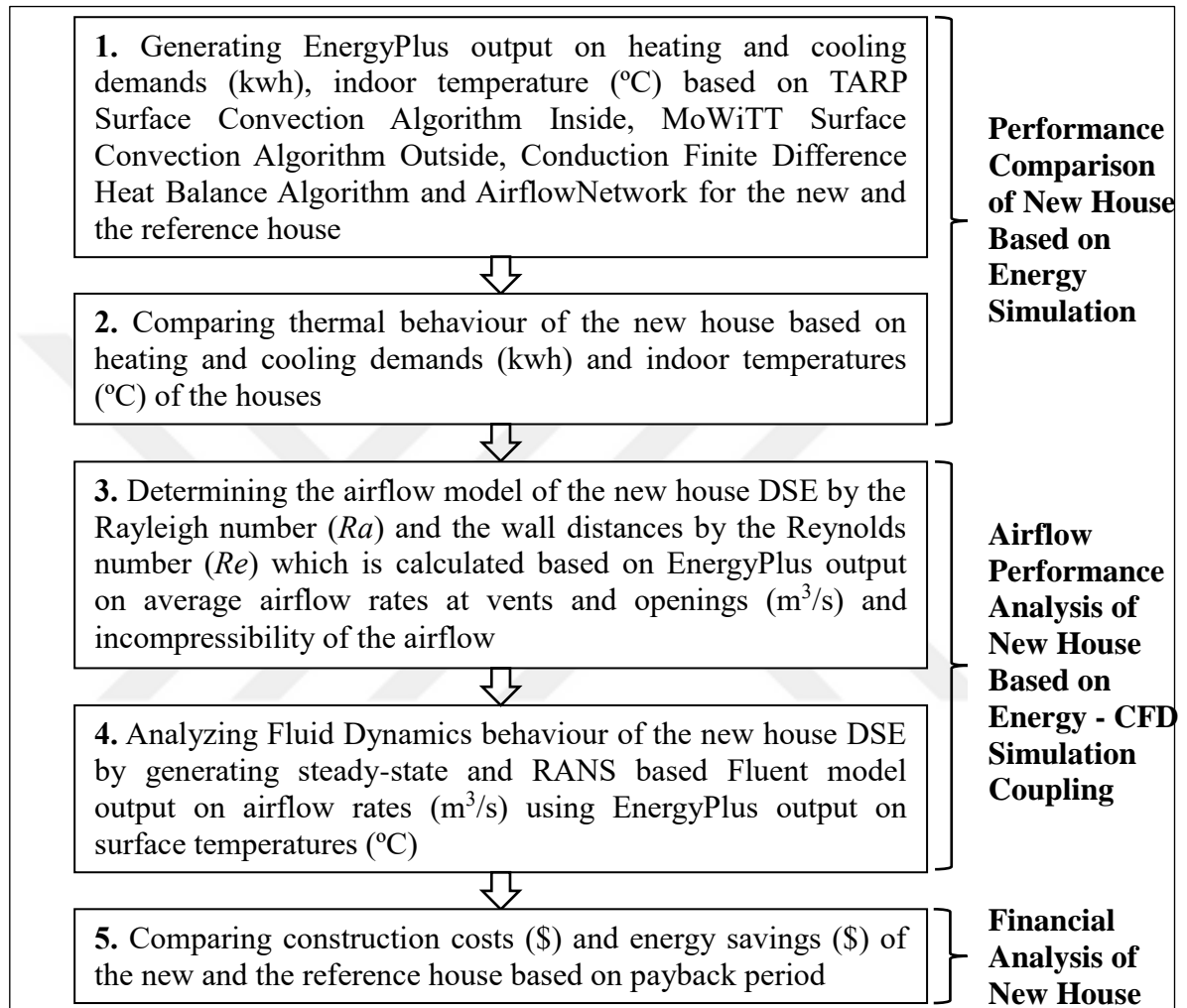


Figure 4.3. SSM stage 5 conceptual model comparison

Azarbayjani also suggested that coupling CFD simulation with an ES gives more accurate results than a CFD simulation or ES alone in building energy analysis. ES in this study provides building envelope thermal information such as surface temperatures which are used as boundary conditions in CFD model by thermal coupling.

5. NUMERICAL MODELING OF DSF

In this chapter, the governing equations for a numerical coupled energy and airflow model of DSF are presented. Energy, airflow and turbulence models are reviewed and adapted before coupling. Energy model is based on a nodal method and the airflow model is represented by pressure network approach where the pressure difference between inside and outside is the main driver of the airflow.

5.1. NUMERICAL MODEL AND ASSUMPTIONS

Saelens developed a two-dimensional numerical model of DSF based on cell-centered control volume approach [86]. DSF section was divided into vertical layers as illustrated in Figure 5.1.

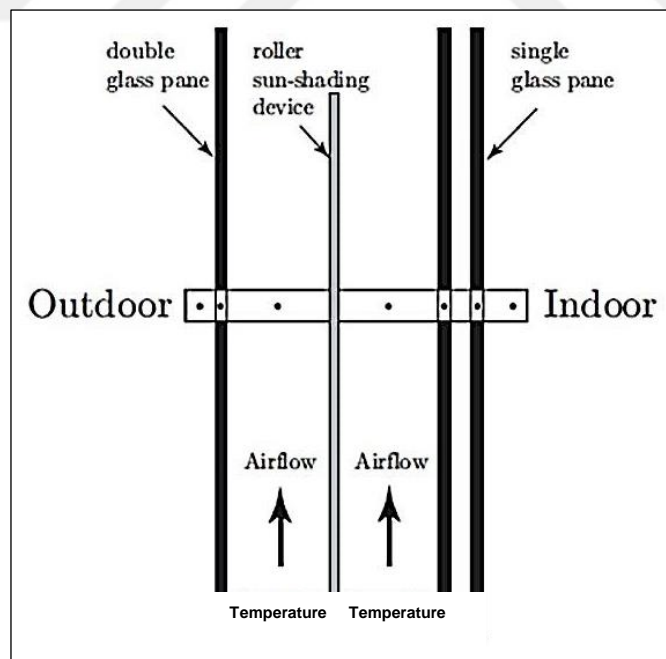


Figure 5.1. Saelens DSF model [86]

The number of vertical layers changed depending on the construction and the position of the sun-shading device. The vertical layers were discretized horizontally along the height. The heat balance equation was written for each control volume. Then, the outcome, the

thermal system, was solved. The direction of the airflow in the cavities was upward only which prevented the application of the model on DSFs with sun-shading devices because of Saelen's assumption that enthalpy flow was vertical only. Saelens developed airflow models for mechanical and natural ventilated DSFs. In mechanical ventilation model, the airflow rate variable was known. However, the airflow rate caused by the buoyancy and the pressure differentials at inlet and outlet, and the temperature profiles in natural ventilation model were dependent. This thermal system was then, solved by TRNSYS, an energy simulation (ES) program. Finally, the models were validated with the experimental data of Saelens.

5.2. ENERGY MODEL FOR DSF

ES programs such as EnergyPlus and TRNSYS solve energy balance equations for room air and surface heat transfer.

5.2.1. Energy Model for Cavity

ES program EnergyPlus [87] is used in this study to model the buoyant airflow between the inner and outer panes of DSF including the simulation of heat transfer in DSF based on a nodal approach (Figure 5.1). As explained by Chan, Chow, Fong and Lin [26], the DSF cavity is divided into zones. These zones are linked to an airflow network node. The network nodes are associated with AirflowNetwork model in EnergyPlus. EnergyPlus models heat transfer of long-wave radiant exchange, surface convection, solar transmission, reflection and absorption. The multizone airflow calculations are performed at each HVAC time step. The airflow rate inside DSF is determined by the inside and outside temperature difference, and the flow resistance of the path. A pressure-balance equation is adopted for evaluating airflow rate, temperature inside DSF and at the outlet. The pressure-balance equates the buoyancy pressure on the air inside DSF to the pressure losses generated by the airflow between the inlet and outlet. Pressure-balance equation is:

$$\Delta p_T = \Delta p_B + \Delta p_{HP} + \Delta p_Z \quad (5.1)$$

where Δp_T is the pressure difference between the air outside and inside DSF. This main driver of the airflow is given by:

$$\Delta p_T = \rho_o T_o g H \sin \phi |T_{gap} - T_{gap,in}| / T_{gap} T_{gap,in} \quad (5.2)$$

where ρ_o , T_o , g , H and ϕ are density of air at temperature T_o , reference temperature, gravitational acceleration, height of glazing and tilt angle of glazing, respectively. T_{gap} represents effective mean air temperature inside DSF and $T_{gap,in}$, air temperature at inlet. Δp_B is the result of the air accelerating to velocity ν . It is defined by its velocity pressure (Bernoulli's law):

$$\Delta p_B = \rho \nu^2 / 2 \quad (5.3)$$

where ρ is density of air at temperature T_{gap} . The term Δp_{HP} represents the pressure loss because of friction caused by the panes:

$$\Delta p_{HP} = 12 \mu H \nu / s^2 \quad (5.4)$$

where μ is viscosity of air at temperature T_{gap} . Δp_Z is calculated based on pressure losses at the openings:

$$\Delta p_Z = \rho \nu^2 (z_{in} + z_{out}) / 2 \quad (5.5)$$

where Z_{in} and Z_{out} are pressure loss factors at the openings:

$$Z_{in} = ((A_{gap} / 0.66 A_{eq,in}) - 1)^2 \quad (5.6)$$

$$Z_{out} = ((A_{gap} / 0.66 A_{eq,out}) - 1)^2 \quad (5.7)$$

where A_{gap} , $A_{eq,in}$ and $A_{eq,out}$ are cross-sectional area of DSF, equivalent inlet opening area and equivalent outlet opening area, respectively. The air temperature in DSF in terms of h ,

the distance from the inlet is:

$$T_{gap}(h) = T_{ave} - (T_{ave} - T_{gap, in})e^{-h/H_o} \quad (5.8)$$

where T_{ave} is the average inside surface temperature of the panes on DSF and H_o is the specific height expressed as:

$$H_o = \rho C_p s \nu / 2 h_{cv} \quad (5.9)$$

where C_p , h_{cv} and s represent specific heat capacity of air, convective heat transfer coefficient and width of the air cavity, respectively. The outlet air temperature is:

$$T_{gap, out} = T_{ave} - (T_{ave} - T_{gap, in})e^{-H/H_o} \quad (5.10)$$

The thermal equivalent mean temperature of the air cavity is expressed as:

$$T_{gap} = 1/H \int_H^0 T_{gap}(h)dh = T_{ave} - (T_{gap, out} - T_{gap, in})H_o/H \quad (5.11)$$

The thermal convection model is based on measurements taken at the Mobile Window Thermal Test (MoWiTT) facility [88]. The correlation is expressed as:

$$h_{cv} = [(C_t(\Delta T)^{1/3})^2 + a \nu_z^{b2}]^{1/2} \quad (5.12)$$

where ΔT is temperature difference between glazing surface and air, ν_z is local air velocity calculated at the height above ground of surface centroid and constants a , b ; and turbulent natural convection constant C_t are obtained from Yazdani and Klems's experiments.

5.2.2. Energy Model for Indoor Room

As Zhai, Chen, Haves and Klems [55] presented, the energy balance equation for indoor room air of DSF model is:

$$\sum_{i=1}^N q_{i,c} A_i + Q_{other} - Q_{heat\ extraction} = \rho V_{indoor\ room} C_p \Delta T / \Delta t \quad (5.13)$$

where $\sum_{i=1}^N q_{i,c} A_i$ is the convective heat transfer from envelope surfaces to indoor room air, $q_{i,c}$ is the convective flux from surface i , N is the number of envelope surfaces, A_i is the area of surface i , Q_{other} is the heat gains from people, lights, infiltration, etc., $Q_{heat\ extraction}$ is the heat extraction rate of indoor room, $\rho V_{indoor\ room} C_p \Delta T / \Delta t$ is the energy change in indoor room air. ρ is the air density, $V_{indoor\ room}$ is indoor room volume, C_p is the specific heat of air, ΔT is the temperature change of room air, and Δt is the sampling time, 2 minutes.

Heat extraction rate is equal to the energy load when indoor room air temperature is kept constant ($\Delta T = 0$). The convective heat flux from a wall is expressed by the energy balance equation for the wall surface. The same energy balance can be formulated for each window, as well. Energy balance equation for a surface is given by (Figure 5.2):

$$q_i + q_{ir} = \sum_{k=1}^N q_{i,k} + q_{i,c} \quad (5.14)$$

where q_i is the conductive heat flux on surface i , q_{ir} is the radiative heat flux from internal heat sources and solar radiation, and $q_{i,k}$ is radiative heat flux from surface i to surface k .

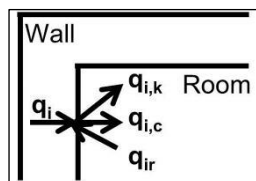


Figure 5.2. Energy balance on the interior surface of a wall

The q_i can be defined by transfer functions, by weighting factors, or by solutions of the discretized heat conduction equation for the envelope surface based on the finite difference method. Radiative heat flux is given by:

$$q_{i,k} = h_{i,kr} (T_i - T_k) \quad (5.15)$$

where $h_{i,kr}$ is the linearized radiative heat transfer coefficient between surfaces i and k , T_i is the temperature of interior surface i , and T_k is the temperature of interior surface k , and

$$q_{i,c} = h_c (T_i - T_{indoor\ room}) \quad (5.16)$$

where h_c is the convective heat transfer coefficient and $T_{indoor\ room}$ is indoor room air temperature. Convective heat transfer coefficient, h_c , is unknown. In general, energy simulations either predict h_c using empirical equations or assume it as constant. If indoor room air temperature, $T_{indoor\ room}$ is assumed as known and uniform, the interior surface temperatures, T_i , can be found by solving Equation (5.14). Cooling and heating load can then, be obtained using Equation (5.13). Coil load is derived from the heat extraction rate and the relevant air handling processes and HVAC system chosen. Based on a plant model and hourly calculation of the coil load, the energy consumption of the HVAC system for a building can be calculated.

5.3. AIRFLOW MODEL FOR CAVITY AIR

CFD simulation program Fluent [89] solves the energy equation explicitly and performs the thermo-convective analysis of the DSF air in a steady state flow by discretizing the governing equations including Navier-Stokes with the finite volume approach for both laminar and turbulent flows. Spatial continuum is divided into a finite number of discrete cells. Finite time-steps are applied to dynamic problems. Discrete equations are solved using boundary conditions. A converged solution is achieved by iteration. Continuity equation is valid for both incompressible and compressible flows [90]:

$$\frac{\partial \rho}{\partial t} + \nabla = S_m \quad (5.17)$$

The source S_m is the mass added to the continuous phase from the dispersed second phase. Momentum equation in inertial space is given by:

$$\frac{\partial(\rho \vec{v})}{\partial t} + \nabla \rho \vec{v} \vec{v} = -\nabla p + \nabla \bar{\tau} + \rho \vec{g} + \vec{F} \quad (5.18)$$

where p is the static pressure, $\bar{\tau}$ is the stress tensor, and $\rho \vec{g}$, \vec{F} , respectively, are the gravitational and external body forces. Stress tensor $\bar{\tau}$ is described by:

$$\bar{\tau} = \mu [(\nabla \vec{v} + \nabla \vec{v}^T) - 2(\nabla \vec{v} I)/3] \quad (5.19)$$

where μ is the dynamic viscosity, I is the unit tensor, and the second term from the right is the effect of volume dilation.

The model can be expressed as [91]:

$$\frac{\partial(\rho U_i \phi)}{\partial x_i} = \frac{\partial(\Gamma_\phi \frac{\partial \phi}{\partial x_i})}{\partial x_i} + S_\phi \quad (5.20)$$

The flow model is based on the continuity, momentum, heat transfer and turbulence equations. In this equation ρ is the air density (kg/m^3); ϕ is the flow variable such as the mean velocity; U_i (m/s) is the pressure, temperature and turbulent parameters in x_i (m) direction; Γ_ϕ represents the diffusion coefficient (N s/m^2); and S_ϕ is the source term.

The Boussinesq approach for buoyancy-driven flows assumes that the density is constant in all of the equations except for the buoyancy term in momentum equation:

$$(\rho - \rho_0)g \approx -\rho_0 (T - T_0) \quad (5.21)$$

where ρ is the actual density, ρ_0 is the constant density of the flow, T is the actual temperature and T_0 is the operating temperature. Based on the Boussinesq approximation which is valid when $\Delta T = (T - T_0) \ll 1$, actual density is:

$$\rho = \rho_0 (1 - \beta \Delta T) \quad (5.22)$$

where β is the thermal expansion coefficient. Energy equation can be expressed in the following form:

$$\frac{\partial(\rho E)}{\partial t} + \nabla \cdot (\vec{v} (\rho E + p)) = \nabla \cdot [k_{eff} \nabla T - \sum_j h_j \vec{J}_j + (\bar{\tau}_{eff} \vec{v})] + S_h \quad (5.23)$$

where k_{eff} is the effective conductivity ($k + k_t$), where k_t is the turbulent thermal conductivity determined depending on the turbulence model used, and J_j the diffusion flux of species j . The first three terms from the right represent energy transfer by conduction, species diffusion, and viscous dissipation, respectively. S_h is the heat of chemical reaction.

5.4. TURBULENCE MODEL FOR CAVITY AIR

As presented by Zhang, Zhang, Zhai and Chen [92], the turbulence models, k- ε Shear Stress Transport (SST) and k- ω RNG with enhanced wall function predict mean temperature and velocity closely for natural convection. K- ε and k- ω are RANS turbulence eddy-viscosity models. They use the same equation for the turbulent kinetic energy k [93]:

$$k = (\overline{u_i' u_i'})/2 \quad (5.24)$$

where $u_{i,j,k}$ are components of the velocity according to i, j, k [m s⁻¹] and an uncommon equation for the rate of energy kinetic dissipation [94]:

$$\varepsilon = (k^{3/2})/l \quad (5.25)$$

where ε is turbulence dissipation rate and l is length scale.

$$\omega = (k^{3/2})/l \quad (5.26)$$

where ω is specific dissipation rate [95].

Turbulent viscosity for the k- ε model is expressed as:

$$\mu_t = \rho C_\mu k^2 / \varepsilon \quad (5.27)$$

where μ_t is turbulent viscosity [$\text{kg m}^{-1} \text{s}^{-1}$], ρ is air density [kg m^{-3}] and C_μ is an empirical constant in k- ε equations equal to 0.09 for standard k- ε or 0.0845 per k- ε RNG.

Turbulent viscosity for the k- ω model is expressed as:

$$\mu_t = \rho \alpha^* k / \omega \quad (5.28)$$

where the coefficient α^* damps the turbulent viscosity for a low Reynolds number correction [96]. The μ_t equation for SST is complex. Further information is found in Fluent User's Guide.

Avva, Smith and Singhal [97] compared a high Reynolds number k- ε model with near wall functions and a Low Reynolds number k- ε model with near wall resolution. Avva, Smith and Singhal concluded that a high-Re model gave better results compared to a Low-Re model for the cases studied.

In order to predict heat transfer in developing flows, Raisee and Hejazi [98] compared predicted and measured data of a turbulent flow in rectangular channels using Low-Re k- ε models. Raisee and Hejazi concluded that the nonlinear Low-Re k- ε model made better heat transfer predictions.

The standard k- ε model is a high-Reynolds-number model but the RNG k- ε model introduces an analytically-derived differential formula for effective viscosity which is

suitable for low-Reynolds number effects. RNG k- ε model is also applied for the turbulence model of DSF in this study.

The transport equations of k- ε model stated in the studies of Launder and Spalding [99] [100] are as follows:

For the kinetic energy k :

$$\frac{\partial(\rho k)}{\partial t} + \frac{\partial(\rho k u_i)}{\partial x_i} = \left[\frac{\partial(\mu + \mu_t/\sigma_k)}{\partial x_j} \frac{\partial k}{\partial x_j} \right] + P_k + P_b - \rho \varepsilon - Y_M + S_k \quad (5.29)$$

For the turbulent dissipation ε :

$$\frac{\partial(\rho \varepsilon)}{\partial t} + \frac{\partial(\rho \varepsilon u_i)}{\partial x_i} = \left[\frac{\partial(\mu + \mu_t/\sigma_\varepsilon)}{\partial x_j} \frac{\partial \varepsilon}{\partial x_j} \right] + C_1(P_k + C_3 P_b)/k - C_2 \rho \varepsilon^2/k + S_\varepsilon \quad (5.30)$$

The production of k is expressed as:

$$P_k = -\rho \overline{u'_i u'_j} \frac{\partial u_j}{\partial x_i} \quad (5.30)$$

$$P_k = \mu_t S^2 \quad (5.31)$$

Source term S (the mean rate of strain tensor) is given by:

$$S \equiv 2(S_{ij} S_{ij})^{1/2} \quad (5.32)$$

Buoyancy effect on the flow is expressed as:

$$P_b = g_i (\mu_t / Pr) \frac{\partial T}{\partial x_i} \quad (5.33)$$

where Pr is the turbulent Prandtl number for energy; and g_i is the component of the gravitational vector in i directions. For the standard and realizable models, the default

value of Pr is 0.85. Coefficient of thermal expansion is given by:

$$\beta = - \left(\frac{\partial \rho}{\partial T} \right)_p / \rho \quad (5.34)$$

The model defines the following as constant:

$$C_{1\varepsilon} = 1.44, C_{2\varepsilon} = 1.92, C_\mu = 0.09, \sigma_k = 1.0, \sigma_\varepsilon = 1.3 \quad (5.35)$$

Bernard [101] compared two Reynolds numbers between the measured turbulent kinetic energy in channel flow and the prediction of various near-wall variants of the k- ε closure. The author detected a discrepancy between the high Reynolds number models and the measured experimental values of peak kinetic energy near the wall regions.

5.5. COUPLED ENERGY AND AIRFLOW MODEL FOR CAVITY AIR

As described by Zhai, Chen, Haves and Klems [55], the air temperature in the boundary layer of a surface and the convective heat transfer coefficient are the most significant parameters defining the convective heat transfer. Almost all the ESs assume a mixing in room air to solve the energy balance equation for room air. CFD simulation can determine the air temperatures near the surfaces from the air temperature distribution, and the convective heat transfer coefficients as:

$$h_{i,c} = C_p \mu_{eff} / Pr \Delta x \quad (5.36)$$

where C_p is the air specific heat, μ_{eff} is the effective kinematic viscosity, Pr is the Prandtl number, and Δx is the normal distance from a point near a wall to the wall. Then, using a direct coupling method, the air temperature, $T_{i,air}$, closed to a wall surface and the corresponding averaged convective heat transfer coefficient, $h_{i,c}$, is fed to ES. Thus, Equation (5.16) is improved to:

$$q_{i,c} = h_{i,c} (T_i - T_{i,air}) = h_{i,c} (T_i - T_{room}) - h_{i,c} \Delta T_{i,air} \quad (5.37)$$

where T_{room} is the desired air temperature of the room and $\Delta T_{i,air} = T_{i,air} - T_{room}$. ES uses the updated $T_{i,air}$ and $h_{i,c}$ from each CFD simulation input and substitutes them into Equation (5.37). Heat balance Equations (5.13) and (5.14) are solved together with Equation (5.37) for the surface temperatures and heat extraction to update the boundary conditions for the next CFD simulation run. The heat extraction rate from ES determines the inlet boundary conditions of the CFD simulation. For a constant-air-volume HVAC system with a known air supply airflow rate ν , the supply air temperature, T_{supply} , is expressed as:

$$T_{supply} = Q_{heat_extraction} / \rho C_p A \nu + T_{outlet} \quad (5.38)$$

where A is the diffuser air supply area and T_{outlet} is the return air temperature. For a variable-air-volume system, T_{supply} is constant, the ν is defined as:

$$\nu = Q_{heat_extraction} / \rho C_p A (T_{supply} - T_{outlet}) \quad (5.39)$$

CFD simulation has to run for each time-step because of the varying heat flows and surface temperatures in buildings.

6. VALIDATION OF ENERGY – CFD SIMULATION COUPLING

Based on Saelens, Roels and Hens' findings [41], Pappas and Zhai's [84], Zhai and Chen's [54] and Zhai, Chen, Haves and Klems' [55] studies, this study models the three-dimensional DSF cavity of Saelens [86] to validate the Energy - CFD simulation coupling method because of the available full-scale experimental data (Appendix A). The method is explained and validated with one step static coupled ES and CFD simulation based on temperature differences and airflow rates.

Saelens tests a mechanically and naturally ventilated DSF with a roller screen sun-shading device, the Vliet Test Cell [86]. However, because of the complex geometry of cavity opening grids on the Vliet Test Cell, the model is calibrated by different size of rectangular openings to find an equivalent opening size (Figure 6.1).

As depicted in Figure 4.2, a distinct methodology for validation of Energy - CFD simulation coupling is introduced. In order to validate the method, reliable experimental data on solar radiation (W/m^2), temperature distribution ($^{\circ}\text{C}$) and airflow rate (m^3/s) in a DSF with natural ventilation is required.

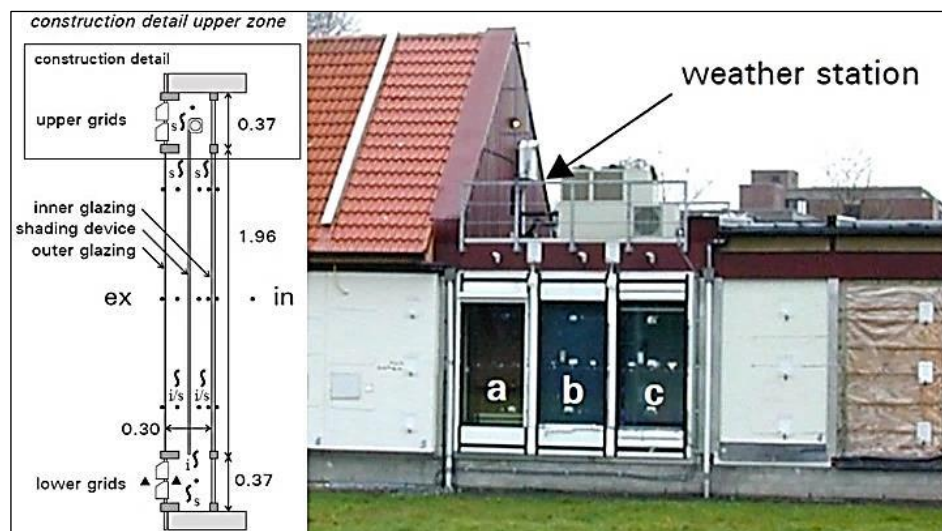


Figure 6.1. Vliet test building [86]

In order to calibrate this geometry, Saelens' Vliet test building with buoyancy-driven airflow is regenerated with two thermal zones in:

- Legacy OpenStudio Plug-in for SketchUp 1.0.10 [102] which creates and edits the building geometry in EnergyPlus input files allowing EnergyPlus simulation launches and viewing results without leaving SketchUp.
- OpenStudio 0.11.5 [103] which is a cross-platform collection of software tools for supporting building energy modeling of EnergyPlus.
- EnergyPlus 8.0 [87] which is an energy analysis and thermal load simulation program.

6.1. ENERGY MODEL SETUP

The EnergyPlus model consists of two zones: DSF cavity and the adjacent space with purchased air at 20 °C (Figure B.1) (Appendix C) (Appendix D). There is no mechanical ventilation for either zones. Figure 6.2 shows DSF model energy zone layout, with the cavity at the front.

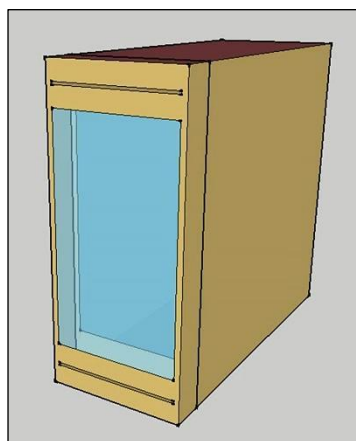


Figure 6.2. DSF model energy zone layout

The surfaces are concrete, with glazed openings in the cavity zone interior and exterior surfaces. The left and right sides of the cavity are adiabatic.

6.2. GEOMETRY CALIBRATION

Pappas and Zhai [84] calibrated and validated their model and modeling process also against Saelen's experimental data [86]. Then, the model was used to develop correlations which can be implemented in ES to exploit the accuracy of CFD simulations while reducing the computation time. Correlations were developed for airflow rate through cavity, average and peak cavity air temperature, cavity air pressure, and interior convection coefficient.

This study has the following similarities with Pappas and Zhai's approach in DSF model calibration:

- i) Glazing heat flux coefficients, dimensions, openings, and shading device details are all modeled accurately. When the exterior vents are open, the cavity draws outside air in from the bottom opening and exhausts the heated air from the top opening.
- ii) Saelen's experimental data showed that the airflow rate at the openings would be $111 \text{ m}^3/\text{hr}$ at a pressure difference of 2 Pa. Using the following volumetric airflow rate \dot{V} correlation:

$$\dot{V} = AC_q \Delta p^n \quad (6.1)$$

with flow coefficient $C_q = 1$ and flow exponent $n = 0.5$, opening area A is estimated as 0.022 m^2 . This value is used as a prelude for the calibration. One of the measured cases is used to calibrate the simulation: the case for which both horizontal and vertical cavity temperature stratification profiles are available as seen in Table 6.1.

Table 6.1. Saelens' horizontal temperature stratification measurements

Temperatures (°C)							
Outdoor air	Exterior glazing surface outside	Outer cavity air	Shade	Inner cavity air	Interior glazing surface inside	Interior glazing surface outside	Indoor air
3.6	11	15.7	20	14.5	16.5	23	18.8

- iii) EnergyPlus output on surface temperatures (°C), and airflow rates (m^3/s) for

different inlet/outlet widths (Table 6.2) based on TARP Surface Convection Algorithm Inside, MoWiTT Surface Convection Algorithm Outside, Conduction Finite Difference Heat Balance Algorithm and AirflowNetwork, are generated.

Table 6.2. DSF model calibration cases

Model	Opening height (m)	Opening size (m ²)	Simulated airflow rate (m ³ /sec)	Error compared to measured 31 (m ³ /sec)	ΔT (T _{peak cavity air} – T _{outdoor air}) (°C)	Error compared to measured 15.2 (°C)
A	0.016	0.018	30.95	– 0.2%	13.5	–11.4%
B	0.020	0.022	31.06	0.2%	14.0	–8.2%
C	0.024	0.026	31.06	0.2%	12.7	–16.6%

On the other hand, this study has the following differences from Pappas and Zhai's approach in DSF model calibration:

- i) The temperature difference (ΔT) (°C) is calculated using EnergyPlus output on maximum surface inside cavity temperature (T_{peak cavity air}) (°C) rather than calculating ΔT based on EnergyPlus output on mean zone temperatures and multiplying this ΔT by 2 to find the real ΔT .
- ii) Even though the shading device within the cavity absorbs a significant amount of solar radiation, contributing substantially to the air temperature rise in the cavity, the shading device is not taken into account in determination of T_{peak cavity air} because it does not exist when the solar radiation drops below 150 W/m².
- iii) The inlet/outlet geometry of the Vliet Test Cell is calibrated using EnergyPlus instead of Energy - CFD simulation coupling output against measured data on temperature difference (T_{peak cavity air} – T_{outdoor air}) (°C) and airflow rate (m³/s).

Consequently, the energy model with an opening 1.1 m wide by 0.020 m high (0.022 m²) provides an airflow rate through the cavity and air temperature stratification closest to the measured values. In this particular simulation, wind speed is low enough (4.475m/sec) to enable buoyancy analysis. The calibrated geometry predicts the exact airflow rate as the measured value, and an air temperature difference between indoor peak and outdoor 8.2 per cent above the measured value, shown as Model B in Table 6.2.

Thus, geometry calibration based on ES using Saelen's experimental measurements, is achieved within the limitations of the ES software. It is concluded that the calculation of airflow rates and temperatures are reasonable and reliable.

6.3. COMPUTATIONAL FLUID DYNAMICS MODEL SETUP

6.3.1. Model Geometry

The geometry is regenerated and meshed in:

- ICEM CFD 14.0 [104] which is a complete meshing solution with advanced mesh diagnostics, interactive and automated mesh editing, output to a wide variety of CFD and finite element analysis solvers and multiphysics post-processing tools.

DSF cavity geometry of model B (with the shading device) is shown in Figure 6.3. Geometry of model A is the same but without the shading device.

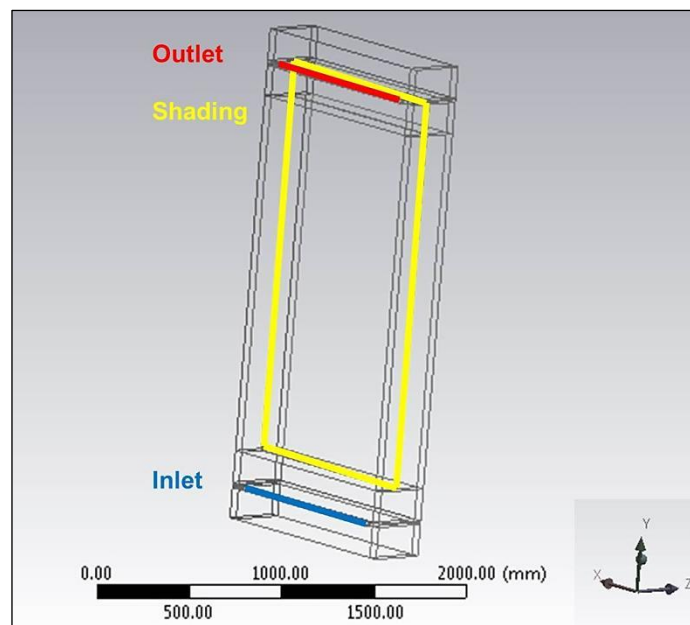


Figure 6.3. DSF model B in DesignModeler

6.3.2. Boundary Conditions

EnergyPlus output on cavity surface temperatures (°C) and shading device absorbed solar radiation rate (W) are generated for a specific radiation (W/m²) and outdoor air temperature (°C).

EnergyPlus 8.0 generates neither shading device surface temperature nor its convective heat flux. Surface temperatures taken from EnergyPlus account for the radiative heat flux from the shading device to cavity surface but it is necessary to differentiate the convective flux from the total shading device heat flux. Pappas and Zhai calculates shading device heat flux (W/m²) using shading device absorbed solar radiation rate, Saelens measurements (Table 6.1) and the following equation for radiative heat flux between the shading device and the exterior glazing, and between the shading device and the interior glazing:

$$q_{radiative} = A\sigma(T_1^4 - T_2^4)/(1/\varepsilon_1 + 1/\varepsilon_2 - 1) \quad (6.2)$$

where $A = 2.36 \text{ m}^2$ is shading device surface area, $T_1 = 20 \text{ °C}$ is shading device temperature, $T_2 = 12 \text{ °C}$ is outer cavity air temperature, $\varepsilon_1 = 0.39$ is shading device solar absorptance, $\varepsilon_2 = 0.84$ is exterior glazing solar absorptance and $\sigma = 5.67 \times 10^{-8} \text{ Wm}^{-2}\text{K}^{-4}$ is Stefan-Boltzmann constant. Thus, the radiative heat flux to the exterior glazing is calculated as 37.6 Watts. Using the interior glazing surface inside temperature, $T_2 = 17.5 \text{ °C}$, the heat flux to the interior glazing is calculated as 12.1 Watts. EnergyPlus calculates a total shading device absorbed heat flux as 187.6 Watts. As a result, convective heat flux portion of the total heat flux is found to be $[187.6 - (37.6 + 12.1)] / 187.6 = 0.74$.

Eventually, this shading device heat flux (W/m²) and cavity surface temperatures (°C) in Table E.1 are used in Fluent as boundary conditions. Fluent operating conditions along with air properties can be found in Table E.2 and Table E.3, respectively. Outlet target mass flow rates (kg/s) are not defined in Fluent boundary conditions so that Fluent can generate airflow rates (m³/hr) output freely for a valid comparison.

6.3.3. Model Grid

The airflow model inside the cavity (DSF) is determined based on the estimate of the Rayleigh number (Ra). Ra characterizes the natural convection flows, the flow can be laminar ($Ra < 6 \times 10^4$), transitional ($6 \times 10^4 < Ra < 10^9$) or turbulent ($10^9 < Ra$). It is calculated as follows:

$$Ra = C_p g \rho^2 \beta (T_{node} - T_{zone}) L^3 / k \mu \quad (6.3)$$

where μ is the dynamic viscosity of the fluid, C_p is the specific heat of the fluid; g is the gravitational force; k is the thermal conductivity of the fluid, ρ is the fluid density, β is the fluid thermal expansion coefficient, L is the vent/opening length, $T_{node} - T_{zone}$ is the fluid temperature difference between node and flow zone.

Airflow rate inside the cavity can be calculated provided that the flow is incompressible. Since the density variation of the fluid is negligible and the flow is steady state the Mach number (Ma) is calculated to determine the compressibility of the airflow. Ma is a dimensionless quantity representing the ratio of speed of an object moving through a fluid and the local speed of sound.

$$Ma = v_{object} / v_{sound} = 0.00207 \text{ m/sec} / 340.3 \text{ m/sec} = 0.000006 \quad (6.4)$$

where v_{object} is the velocity of the source relative to the medium, and v_{sound} is the speed of sound in the medium. Since $Ma_{max} < 0.3$, the airflow in model A and B is assumed to be incompressible. Thus, based on the flow cross sections, airflow rate inside the cavity (Table 6.4) can be deduced from inlet velocity (Table 6.3) which is generated by EnergyPlus.

Table 6.3 Inlet/outlet airflow velocities and Fluent boundary conditions

Inlet/outlet airflow velocities and Fluent boundary conditions	Model A	Model B
Section width (m)	1.100	1.100
Section length (m)	0.020	0.020
Hydraulic diameter (boundary layer length) (m)	0.039	0.039
Density (kg/m ³)	1.216	1.157
Dynamic viscosity (kg/ms)	0.000018248	0.000018973
Max airflow rate (m ³ /s)	0.00377	0.01222
Max freestream velocity U _∞ (m/s)	0.17145	0.5555
Reynolds	230	680
Turbulent intensity I	11.0%	9.6%
Outlet target mass flow rate (kg/s)	free	free

Table 6.4. Cavity wall distance estimation and airflow model determination

Cavity y+ wall distance estimation	Model A	Model B
Section width (m)	1.200	1.200
Section length (m)	0.300	0.300
Hydraulic diameter (boundary layer length) (m)	0.480	0.480
Temperature (°C)	17.55	32.31
Density (kg/m ³)	1.216	1.157
Dynamic viscosity (kg/ms)	0.000018248	0.000018973
Max airflow rate (m ³ /s)	0.00023	0.00075
Max freestream velocity U _∞ (m/s)	0.00064	0.00207
Desired y+	1	1
Reynolds	20	61
Estimated wall distance (m)	0.072	0.038
Cavity airflow model determination	Model A	Model B
Turbulent intensity I	11.0%	9.6%
L (m)	2.700	2.700
Specific heat Cp (J/kgK)	1,006	1,007
Thermal conductivity K (W/mK)	0.0255	0.0266
Thermal expansion coefficient (1/K)	0.0035	0.0033
ΔT (T _{peak cavity air} – T _{outdoor air}) (°C)	1.30	20.51
Rayleigh	2.8x10 ⁹	3.5x10 ¹⁰
Airflow model	Turbulent	Turbulent

The wall distances are estimated based on Reynolds numbers (Re). The Reynolds number characterizes the relative importance of inertial and viscous forces in a flow. For flow in a pipe or tube, the Reynolds number is generally defined as:

$$Re = \rho v D_H / \mu = v D_H / \nu = Q D_H / \nu A \quad (6.5)$$

where D_H is the hydraulic diameter of the pipe, Q is the volumetric flow rate, A is the pipe cross sectional area, ν is the mean velocity of the fluid, μ is the dynamic viscosity of the fluid, ν is the kinematic viscosity of the fluid, ρ is the density of the fluid. Re values calculated for model A and B can be found in Table 6.3.

The turbulence intensity, I , is expressed as:

$$I \equiv u' / u_{avg} \quad (6.6)$$

where u' is the ratio of the root-mean-square of the turbulent velocity fluctuations and u_{avg} is the mean flow velocity. A turbulence intensity of 1 per cent or less is usually considered low and turbulence intensities greater than 10 per cent are considered high. The turbulence intensity at the core of a fully-developed duct flow can be estimated from the following formula derived from an empirical correlation for pipe flows:

$$I = 0.16 (ReD_h)^{-1/8} \quad (6.7)$$

where Re is Reynolds number and D_h is hydraulic diameter. The hydraulic diameter in a non-circular duct or pipe is given by:

$$D_h = 4A / w \quad (6.8)$$

where D_h is the hydraulic diameter, A is the area section of the duct, and w is the wetted perimeter of the duct. Based on this equation the hydraulic diameter of a rectangular duct or pipe can be calculated as:

$$D_h = 4xy / (2(x+y)) = 2xy / (x+y) \quad (6.9)$$

where x is the width of the duct and y is the height of the duct. Hydraulic diameter and turbulence intensity are defined in Fluent boundary conditions for both inlet and outlet (Table 6.3).

Based on the estimated wall distances in Table 6.4, 17 mm and 10 mm distances are selected for model A and B, respectively in order to improve the mesh quality. As a result, a non-uniform grid of 124,440 cells for the cavity with $8 \times 10^{-6} \text{ m}^3/\text{cell}$ maximum volume, 0.996 minimum orthogonal quality and 3.51×10^{-3} average skewness is generated for model A and a grid of 989,510 cells for the cavity with $1 \times 10^{-6} \text{ m}^3/\text{cell}$ maximum volume, 1 minimum orthogonal quality and 2.73×10^{-9} average skewness is generated for model B in ICEM (Figure 6.4).



Figure 6.4. Mesh with wall distance of 17 mm for model A and 10 mm for model B

6.3.4. Numerical Methods

Reynolds Averaged Navier Stokes (RANS) 3-D model CFD simulations are performed in:

- Fluent 14.0 [89] which contains broad physical modeling capabilities to model flow, turbulence, heat transfer, and reactions for industrial applications.

Fluent performs the thermo-convective analysis of the cavity air in a steady state flow. Fluent is run under the Boussinesq approximation with full buoyancy effects since the variations of temperature as well as the variations of density are small. The Boussinesq approach assumes that the density is constant in the pressure terms of the equations but variable in the volume terms as explained in Chapter 5.3 “Airflow model for cavity air”. This improves the calculation convergence as it prevents the instabilities of non-linear terms.

The conjugate and radiation heat transfers are not included in Fluent because they are accounted for in EnergyPlus simulation. Additionally, the RNG k- ϵ model with enhanced

wall treatment is used based on Chapter 5.4 “Turbulence model for cavity air” to simulate the overall turbulence effect on mean airflow because of its applicability to both turbulent and laminar flows even with low-Reynolds number models. Also, thermal effects, viscous heating and pressure based solver are chosen.

In solution methods, a second order upwind spatial discretization scheme is used. The pressure interpolation scheme is chosen as Presto which is recommended for a natural convection case. Standard pressure discretization interpolates the pressure on the faces based on the cell center values. However, Presto discretization for pressure computes pressure using staggered grids where velocity and pressure variables are not co-located. Presto provides more accurate results avoiding interpolation errors and pressure gradient assumptions on boundaries. This scheme is suitable for problems with strong body forces and high Rayleigh number flows such as natural ventilation but it is more costly because of the memory required for alternate grids.

Semi-Implicit Method for Pressure-Linked Equations (SIMPLE) pressure-velocity coupling scheme is chosen to be coupled with the default options. It is not necessary to completely resolve the linear pressure-velocity coupling in a steady-state problem as the changes between the iterations are not small. SIMPLE provides an approximation of the velocity field by solving the momentum equation. The pressure gradient is calculated based on the pressure distribution from the previous iteration or an initial guess. The pressure equation is formulated to obtain the new pressure distribution. Finally, velocities and a new set of conservative fluxes are calculated.

The under-relaxation factors for model A and B are determined based on solution convergence and Fluent and EnergyPlus output compatibility. The under relaxation factor for pressure is chosen as 0.25, for density as 1, for body forces as 1, for momentum as 0.25, for turbulent kinetic energy as 0.8, for turbulent dissipation rate as 0.67, for turbulent viscosity as 0.95 and for energy as 1.

In both model A and B, convergence criteria for continuity, x, y and z velocity, k and epsilon residuals is 10^{-3} and for energy residual 10^{-6} . The calculation is initialized with hybrid option and the convergences of model A (Figure F.1) and model B (Figure F.2) are estimated from the evolution graphs of the residuals. Equations for model A and B reached convergence with 8 GB memory and double precision after 2,466 (20 iterations per

minute) and 2,564 (3 iterations per minute) iterations, respectively.

6.4. VALIDATION OF ENERGY – CFD SIMULATION COUPLING

This study has the following similarities with Pappas and Zhai's approach [84] in DSF model validation:

- i) The intersection of EnergyPlus output and measured data on solar radiation (W/m^2) and temperature difference ($T_{\text{peak cavity air}} - T_{\text{outdoor air}}$) ($^{\circ}\text{C}$) is determined.
- ii) The corresponding EnergyPlus output on surface temperature ($^{\circ}\text{C}$) and shading device convective heat flux (W/m^2) is entered to steady-state and RANS based Fluent model.
- iii) The model is validated by comparing Fluent output against measured data on airflow rates (m^3/s) with the corresponding temperatures ($^{\circ}\text{C}$).

On the other hand, this study has the following differences from Pappas and Zhai's approach in DSF model validation:

- i) The airflow model of the DSF is determined by the Rayleigh number (Ra) and the wall distances by the Reynolds number (Re). Re is calculated based on EnergyPlus output on average airflow rates at openings (m^3/s) and incompressibility of the airflow.
- ii) Instead of a two step dynamic Energy - CFD simulation coupling, one step static [54] [55] Energy - CFD simulation coupling is applied.

Table 6.5 details the two cases used for validation, model A measured at night without incident solar radiation and shading device and model B in the morning with incident solar radiation and shading device. The cases had low wind velocities of 3.6 m/sec and 3.9 m/sec, respectively, enabling an analysis without the wind effect. Modeled and measured values for temperature difference between peak cavity air and outdoor air and airflow rate at the inlet are presented. In model A error is 0.1 per cent and in model B 1.5 per cent for the temperature differences ($^{\circ}\text{C}$). As for the airflow rates (m^3/hr) of model A and B, errors are 15.8 per cent and -22.9 per cent, respectively. In Saelen's study, the measurement

errors were estimated about 4 per cent for temperature and 10 per cent for airflow rate [86]. Comparison of the simulated and measured inlet airflow rates with the corresponding air temperatures confirmed the precision of the method for a manual static coupling process with one-step data exchange from Energy to CFD simulation.

Table 6.5. DSF model validation cases

Validation parameters	Model A	Model B
Inlet airflow rate (m ³ /hr)	Fluent output	
	15.0	29.3
	EnergyPlus output	
	13.6	44.0
	Measured	
	13	38
Error (Fluent output compared with measured)	15.8%	-22.9%
Error (EnergyPlus output compared with measured)	4.5%	15.8%
ΔT ($T_{\text{peak cavity air}} - T_{\text{outdoor air}}$) (°C)	EnergyPlus output	
	1.3	20.5
	Measured	
	1.3	20.2
Error (EnergyPlus output compared with measured)	0.1%	1.5%
Incident solar radiation (W/m ²)	EnergyPlus output	
	0	663
	Measured	
	0	579
Error (EnergyPlus output compared with measured)	0%	14.5%
Outdoor air temperature (°C)	EnergyPlus output	
	17.0	22.7
	Measured	
	16.2	23.3
Error (EnergyPlus output compared with measured)	4.9%	-2.4%

Within the limitations of the energy and airflow simulation softwares, it is concluded that the calculation of airflow rates, temperatures, solar heat gains and heat fluxes, are reasonable and reliable. Thus, the method can be applied to the new house to analyse its performance in details.

7. NEW PASSIVE HOUSE DESIGN

In this chapter, the new house geometry is designed by integrating advanced components: partial DSF, DSR, underground space and earth tube into a naturally ventilated, single storey PH with:

- Sketchup 8.0 [105] which is a 3D modeling program for applications such as architectural, interior design, civil and mechanical engineering.
- Solidworks 2013 [106] which is solid modeling computer-aided design software.

EnergyPlus, the next generation of American ES which is funded by the US DOE, is used because of the following features relevant to the analysis:

- i) Heat balance based solution technique for building thermal loads that allows for simultaneous calculation of radiant and convective effects at both in the interior and exterior surface during each time step.
- ii) Transient heat conduction through building elements such as walls, roofs, floors, etc. using conduction transfer functions.
- iii) Improved ground heat transfer modeling through links to three-dimensional finite difference ground models and simplified analytical techniques.
- iv) Airflow Network a multi-zone airflow model, to predict airflow between spaces.

The reference house is also designed in such a way that a valid energy performance comparison of both houses can be made as in Chapter 8 “Energy performance of new house”.

In addition to PHI’s PH standard explained in Chapter 1 “Introduction”, the following criteria are also considered in this study:

- i) Energy performance (based on building geometry, its orientation and location).
- ii) Architectural design (based on ergonomics, maintenance and aesthetics).
- iii) Cost effectiveness (based on materials and simplicity).

7.1. DESIGN COMPONENTS

7.1.1. Design Components of New House

The new house geometry is designed by integrating partial DSF, DSR, underground space and earth tube into a naturally ventilated, single storey PH. The new house is aligned on an east-west axis and located in Istanbul where strong solar radiation may be captured. The DSE design adds a second envelope on the roof, partly onto the floor, the north and south walls. Inclination of the DSR, underground space and earth tube shapes, and north-side and south-side partial DSF sizes contribute to thermal energy performance of the house. Figure 7.1 shows the basic design components of the new PH: 1. Underground space, 2. Living quarters, 3. DSR, 4. South-side partial DSF, 5. North-side partial DSF, 6. Earth tube, 7. Inlet air vent, 8. Outlet air vent, 9. North-side partial DSF bottom opening, 10. South-side partial DSF bottom opening, 11. DSR north opening, 12. DSR south opening, 13. Earth tube opening, 14. Glazing.

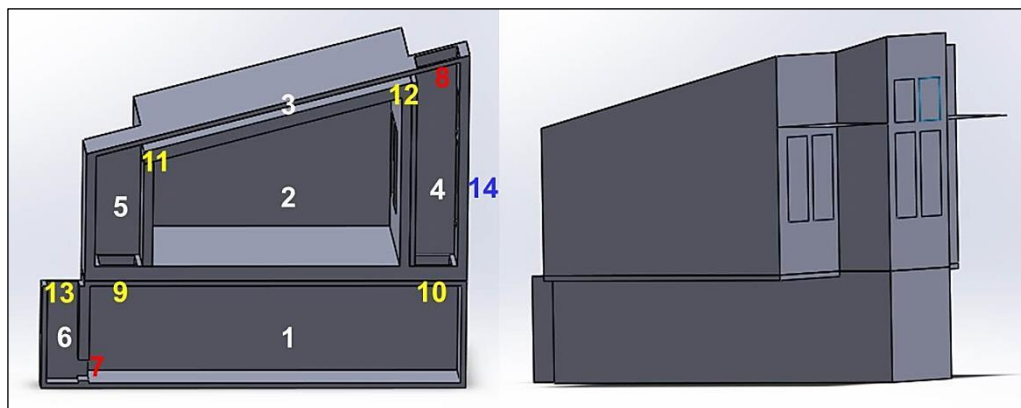


Figure 7.1. New passive house

The new PH is designed to operate with an underground space inlet and roof outlet vents that are open in summer and closed in winter. Vents of the new house control the airflow and thereby the temperatures in DSE. Major features considered in the new house design to save auxiliary energy within the indoor human comfort range are as follows:

- i) Full thermal zone from top to bottom with a DSR and partial DSF walls to improve the heat transfer rate around the house (Figure 7.2).

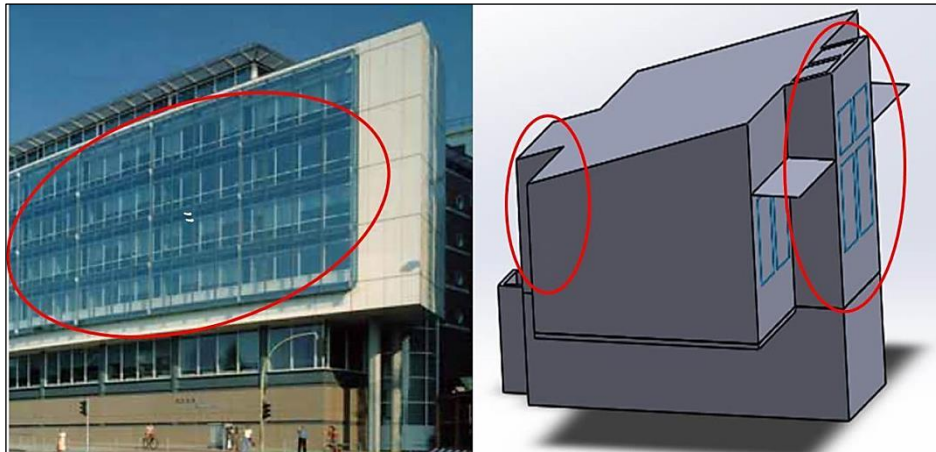


Figure 7.2. Full south-side DSF without DSE (Deutscher Ring Verwaltungsgebäude in Hamburg) [10] and new house with DSE

- ii) Underground space to utilize earth ambient temperature.
- iii) Earth tube and air vents for ventilation in summer.
- iv) Radiant Barrier Systems to avoid overheating in summer.
- v) Envelope built with Styrofoam for low conductivity [107] [108].
- vi) Compact envelope design with a minimized area in contact with outdoor air.
- vii) Double-glazed southern windows to maximize solar gain in winter, to benefit from natural daylight.
- viii) Minimized northern double-glazed area to prevent overcooling in winter.
- ix) Eliminated western and eastern glass to prevent overheating in summer.
- x) Single pane window on exterior partial southern DSF wall to increase solar radiation gain on winter days.
- xi) Well-insulated and unleaded PVC frames with low conductivity for both single-pane and double-pane windows.
- xii) Thermal insulation including foundation to retain earth ambient heat in winter.
- xiii) Natural ventilation to provide a less expensive and simple way for cooling in temperate regions where the nocturnal air temperature is lower than the comfort

temperature, and dissipate the heat accumulation.

xiv) Shades to provide shading in summer.

The partial DSF design resembles the multi-story DSF described in Chapter 2 “Literature Review” except for two differences: the partial DSF is connected to the surrounding thermal zone from top to bottom and it does not have an interior window inside DSE.

7.1.2. Design Components of Reference House

To demonstrate that the new house has better performance, a reference house was designed with naturally ventilated single façade living quarters (Figure 7.3).

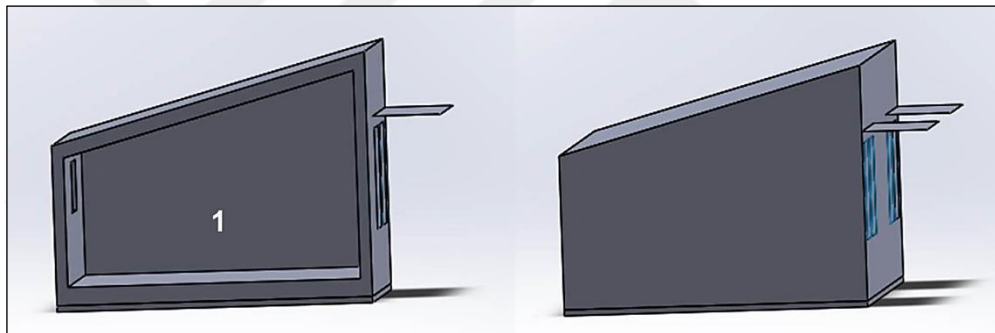


Figure 7.3. Conventional reference house

The size, design and material of the reference house living quarters are identical with those of the new house for a valid performance comparison.

7.2. ENERGY ZONE LAYOUTS

In general, energy consumption in buildings is determined by function, orientation, climate, building components, construction, control and settings. The climate and the ambiance are considered as boundary conditions in ES. Building function has also an important impact on energy use. Both building components and construction provide great potential for improvement of energy demand in such areas as adequate thermal insulation, a key component of energy consumption. In buildings, a proper selection of windows,

shading devices and heat recovery techniques should help to avoid additional solar gains. Designing a high-performance façade system will make a positive impact in minimizing energy consumption and optimizing the thermal condition.

7.2.1. Energy Zone Layouts of New House

The maximum height of the new house above the ground is 4,515 mm, with length 5,028 mm, and width 7,136 mm. Maximum room height is 3,976 mm. The window area comprises 29.1 per cent of the south façade including south-side partial DSF and 17 per cent excluding. Inspired by small size houses in competitions like 2007 Solar Decathlon [14], the total floor area of the new house is designed as 36 m² (2 residents x 18 m²/occupant).

A breakdown of energy zones and their components are presented in details below (Figure 7.4 and Figure 7.5).

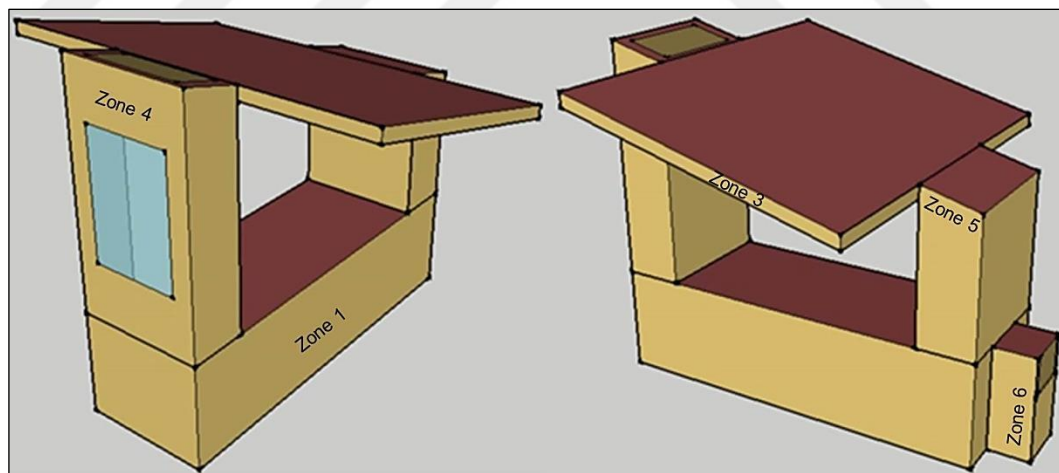


Figure 7.4. DSE cavity of new house with zones

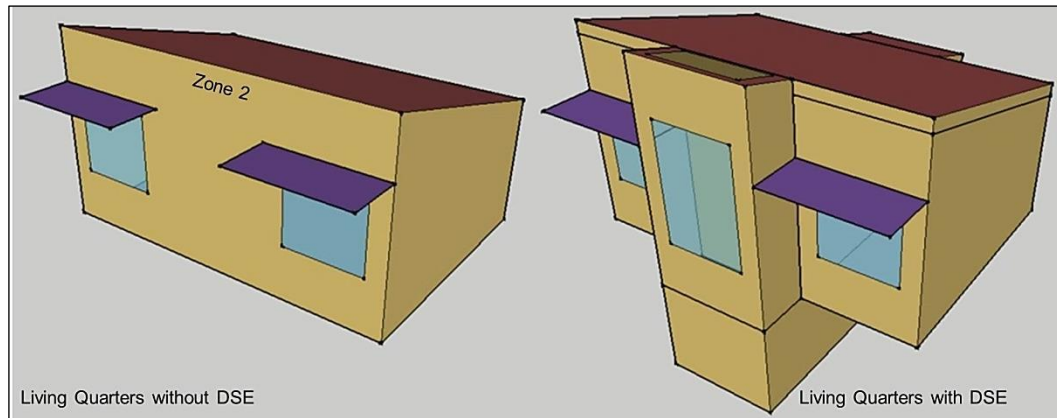


Figure 7.5. Living quarters of new house without and with DSE

7.2.1.1. *Underground Space*

In Zone 1, underground space of approximate volume 34 m³ is connected to the earth tube, south and north-side partial DSFs through air vents (Figure 7.6).

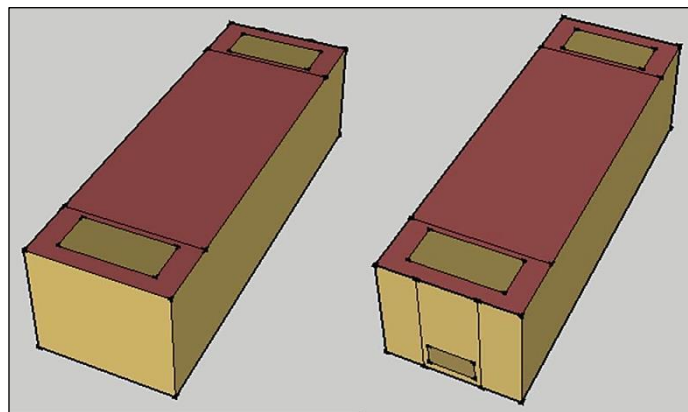


Figure 7.6. Underground space energy zone

Underground space uses earth ambient temperature at maximum depth 2 meters below the ground. Underground space is made of 100-mm-thick lightweight concrete, a low R factor material, to benefit from earth ambient temperature year round. Two of the air vents on the top are 700 mm x 1,600 mm in size to facilitate easy maintenance. One of the air vents that connects underground space to the earth tube is 400 mm x 800 mm in size. All of the air vents in the house are constructed with 0.5-mm-thick galvanized steel on top and 88.9-

mm-thick Styrofoam at the bottom.

7.2.1.2. Living Quarters

In Zone 2, the living quarters of new house is wrapped with 5 thermal zones: underground space connected to earth tube, south and north-side partial DSFs that are connected to DSR (Figure 7.7).

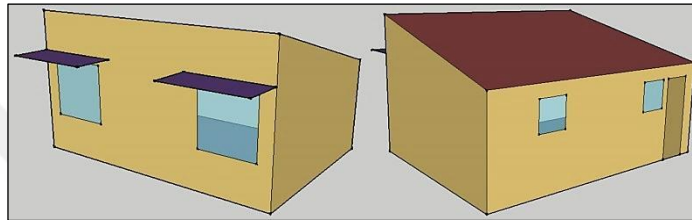


Figure 7.7. Living quarters energy zone

The living quarters has a rectangular shape with an open plan but its interior design is not within the scope of the study. Its 1:2.2 ratio of interior floor area (approximately 36 m²) to exterior surface area (~ 80 m²) shows the energy efficiency of the geometry. Styrofoam 88.9-mm-thick is used for the floor, ceiling and walls of the living quarters. The living quarters have two (1,600 mm x 1,600 mm) double pane (with 6.3 mm air gap) low-e glazings on the south side for daylight and two (800 mm x 800 mm) double pane (with 6.3 mm air gap) low-e glazings on the north side for ventilation. Also on the north side, a 2,384 mm x 800 mm size door made up of a metal sheet with 25-mm-thick insulation is modeled for the living quarters. The two (1,084 mm x 2,384 mm) outside shades with RBS above the south windows are also included.

7.2.1.3. Double-skin Roof

In Zone 3, DSR is connected to south and north-side partial DSFs through two (150 mm x 2,000 mm) air openings (Figure 7.8).

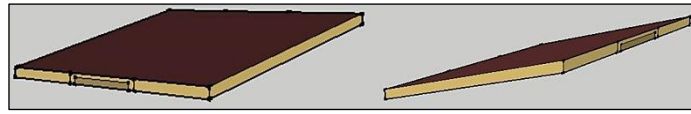


Figure 7.8. DSR energy zone

DSR design is mainly based on Chapter 2.2.5 “Experimental Studies on Double-skin Roof”. The experiments of Irwan, Ahmed, Ibrahim and Zakaria [73] identified the optimum roof pitch angle for thermal and energy saving potential in a local climate. The DSR slope angle is selected as 15° , within the 10° – 20° range of the latter study. Combination of a high-gloss roof and low-gloss ceiling finish underneath is generally used in the industry [68]. Chang, Chiang and Lai [71] designed prototypical double roofs inspired by the concepts of both the double-skin structure and RBS, specifically to reduce solar heat gain from the roof. Ong [74] tested six laboratory-sized passive roof designs side-by-side consecutively over a number of days, finding that a bare metal roof with insulation underneath resulted in the highest roof temperature. Based on these studies, the top skin of the DSR is composed of a 0.5-mm-thick white painted galvanized steel sheet [109] for effective passive solar design on top and 88.9-mm-thick Styrofoam, with a RBS [110] at the bottom. Lai, Huang and Chiou [75] used inclined parallel plates with an upper plate heated by a lighting system to simulate DSRs exposed to solar radiation. Heat transfer experiments were carried out for different inter-plate spacings and inclined angles. Lai, Huang and Chiou also showed that placing a low-cost radiant barrier on top of the lower plate structure could be very effective for preventing roof heat from entering the building. Susanti, Homma, Matsumoto, Suzuki and Shimizu [76] targeted a reduction of roof solar heat gain through the use of natural ventilation in a roof cavity. Natural ventilation in that cavity appeared to be highly applicable to solar incidence discharges. In parallel with these studies, the air gap in DSR is set to 150 mm. The sides of DSR are closed by 88.9-mm-thick Styrofoam with adequate conductive insulation.

7.2.1.4. South-side Partial Double-skin Façade

In Zone 4, south-side partial DSF uses 88.9-mm-thick Styrofoam for the floor and walls (Figure 7.9).

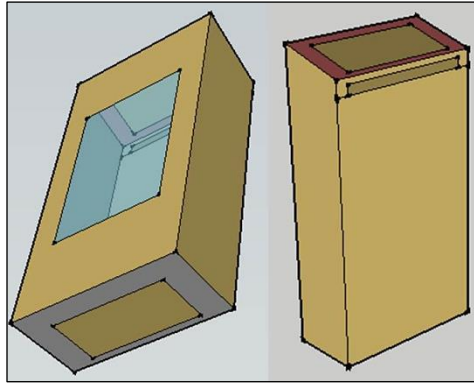


Figure 7.9. South-Side partial DSF energy zone

A 0.5-mm-thick galvanized steel sheet on top and 88.9-mm-thick Styrofoam with radiant barrier at the bottom are used for the ceiling. South-side partial DSF is connected to the underground space through an (700 mm x 1600 mm) air vent, DSR through an (150 mm x 2000 mm) opening, and outside through an (828 mm x 1800 mm) air vent. Window shades with radiant barriers, inside the cavity of the south-side partial DSF are directly behind 6-mm single-pane (2400 mm x 1600 mm) glazing.

7.2.1.5. North-side Partial Double-skin Façade

In Zone 5, north-side partial DSF is connected to the underground space through air vents (Figure 7.10).

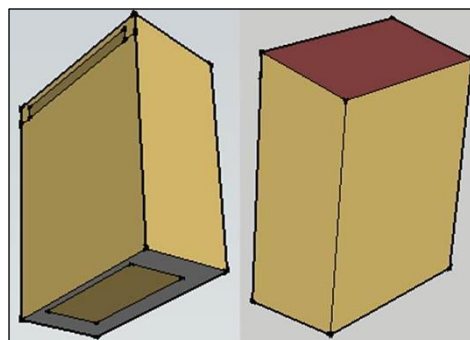


Figure 7.10. North-side partial DSF energy zone

Styrofoam 88.9-mm-thick is used for the floor and walls of this DSF. A 0.5-mm-thick galvanized steel sheet on top and 88.9-mm-thick Styrofoam with radiant barrier at the

bottom are used for the ceiling. North-side partial DSF is connected to underground space through an (700 mm x 1,600 mm) air vent and DSR through an (150 mm x 2,000 mm) opening.

7.2.1.6. *Earth Tube*

In Zone 6, earth tube which has an approximate volume of 1.6 m³ is made of 100-mm-thick lightweight concrete (Figure 7.11).

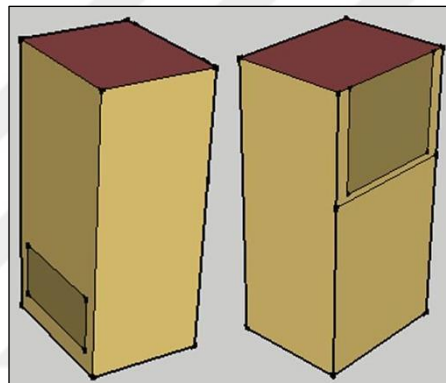


Figure 7.11 Earth tube energy zone

Through an (700 mm x 800 mm) air opening at the back, outside air enters the tube and passes to the underground space through an (400 mm x 800 mm) air vent in summer. Height of the earth tube is 2,000 mm, the same as that of the underground space.

7.2.1.7. **Component Combinations**

Based on energy modeling and simulations, the following component combinations are also introduced in the design process of new house:

- **Combination 1:** living quarters, underground space and earth tube.
- **Combination 2:** living quarters and Double-skin Roof.
- **Combination 3:** *living quarters, partial Double-skin Façade, underground space and earth tube.*

- **Combination 4:** living quarters and partial Double-skin Façade.
- **Combination 5:** living quarters, Double-skin Roof and partial Double-skin Façade.

These component combinations are further analysed in Chapter 8.3 “Energy Performance Comparison” and Chapter 10.2 “Energy Savings and Payback Period”.

7.2.2. Energy Zone Layout of Reference House

Living quarters’ of the new and reference houses have identical geometry and installations for a valid comparison. Maximum height of the reference house above ground is 4,224 mm.

7.2.2.1. Living Quarters

In Zone 1, the living quarters of reference house (Figure 7.12) is not wrapped by any thermal zone, and incorporates a single-skin roof, RBS, windows and shadings.

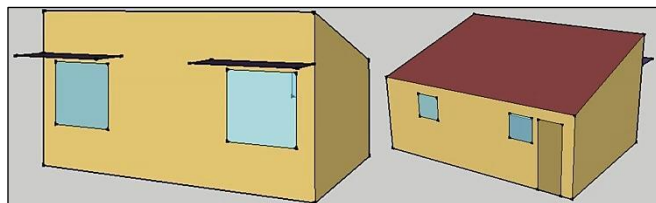


Figure 7.12. Reference house energy zone

The single-skin roof is designed with the same Styrofoam thickness (88.9 mm) as the living quarters of new house. Material properties of the living quarters and their components are the same as that of new house.

8. ENERGY PERFORMANCE OF NEW HOUSE

In this chapter, the energy and airflow behaviour of new house and the comparison of ES results for the new and reference houses are provided.

8.1. ENERGY MODEL SETUP

ES program EnergyPlus [87] is used to model the buoyant airflow inside DSE including the simulation of heat transfer in DSE based on a nodal approach. The main objective of the ES is to generate the performance data, heating and cooling demand and indoor temperature for both the new house and the reference house, by estimating thermal and airflow profiles inside DSE for extreme summer and winter conditions. ES results such as building envelope average surface temperature and average airflow rate at vents and openings serve as boundary conditions in a Computational Fluid Dynamics (CFD) model demonstrated in Chapter 9 “Airflow performance analysis of new house”.

The new house with 6 thermal zones (Figure G.1) (Appendix H) (Appendix I) and the reference house with 1 thermal zone (Figure J.1) (Appendix K) (Appendix L) are established with EnergyPlus 8.0 for ES. For solids, thermo-physical dependencies, corner and thermal bridge effects are ignored. Instead, conductivity, density and heat capacity at each time step are considered.

8.2. ENERGYPLUS SIMULATION RESULTS

Energy models are developed to solve for bulk airflows and temperatures at various nodes within a space. The major focus of the analysis is on the following five outputs:

- i)** PH criteria.
- ii)** DSE zone air temperatures.
- iii)** Airflow rates inside DSE.

- iv) Annual heating and cooling demands.
- v) Annual air temperatures in living quarters.

8.2.1. Passive House Criteria

EnergyPlus results demonstrate that the new house is a PH and that the reference house is nearly a PH, based on the following PH [2] criteria defined by the PHI [1] (Table 8.1).

Table 8.1. New and reference houses under PH criteria

PH criteria	New house	Reference house	PH criteria limits
Heat demand kWh/(m ² yr)	13.3	16.5	<15
Primary energy use kWh/(m ² yr)	0	0	<120
Air change per hour (at max pressure of 50 Pa)	0.195	0.195	<0.6
Time setpoint not met during cooling	0%	0%	<10%

8.2.2. Energy and Airflow Behaviour of New House

EnergyPlus generated the following results for the energy and airflow behaviour of new house in winter and summer.

- i) Partial DSF and DSR of the new PH operating at temperatures warmer than the cold winter extremes and cooler than hot summer extremes create a thermal zone around the interior shell (Figure M.1) (Figure M.2) (Figure M.3). That zone uses south-side solar gain and a natural convection airflow loop initiated by earth ambient temperature to heat the cold north walls of the house, equalizing the temperature differentials on the north/south and top/bottom of the house. Thus, throughout the year, the double-skin design minimizes the heat transfer rate by reducing the overall temperature difference and increasing thermal resistance year round, and evacuates a large part of the heat load on the living quarters in summer.
- ii) Underground space temperatures are correlated with ground temperatures. Based on the energy storage capacity of soil, underground space improves the indoor environment by heating air in winter and cooling it in summer (Figure M.4).

- iii) In summer, annual air outflow rates (m^3/s) at the roof and air inflow rates (m^3/s) at the underground space vent nodes are equal (Figure M.5), and airflow rates at the south-side partial DSF bottom opening node are higher than in winter (Figure M.6).
- iv) On a summer day, air flows from outside to the underground space (Figure M.5), from the underground space to the south-side partial DSF (Figure M.6), from the underground space to the north-side partial DSF bottom opening (Figure M.7), from the DSR south opening node (Figure M.8) to the south-side partial DSF, from the north-side partial DSF to the DSR north opening node (Figure M.9), and from the south-side partial DSF to outside (Figure M.5) (Figure 8.1).

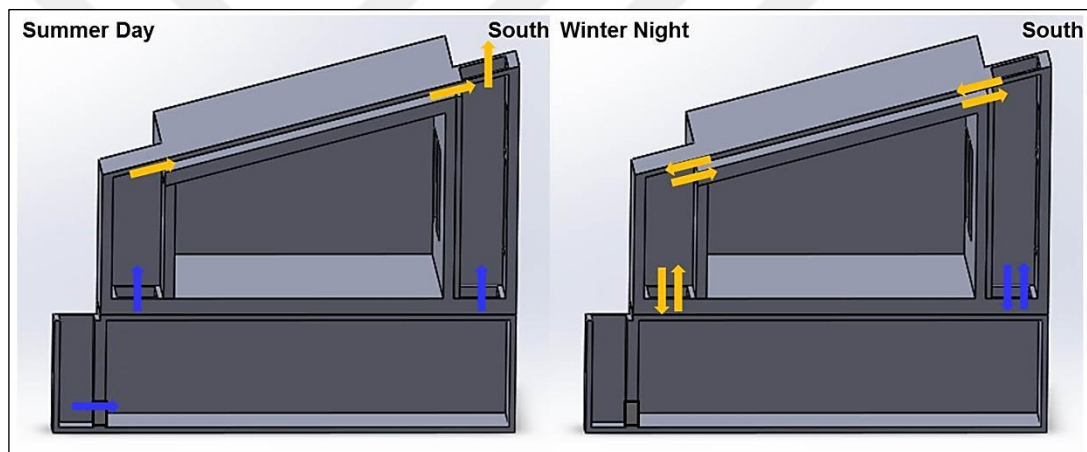


Figure 8.1 Airflow paths at new house nodes on summer days and winter nights

The airflow paths mainly depend on the house geometry, temperature differentials, wind velocity and direction.

- v) During summer daytime, the roof and underground space vents are open and the shading is active. The underground space vent sucks fresh air from outside, then cools it in the underground space and as the air temperature rises in DSFs and DSR, the air is exhausted from the roof vent by natural convection. Air circulation creates a thermal zone colder than outside temperatures and hence, contributes to the thermal performance of the house. The highest outside temperature is considered in the energy analysis.

- vi)** During summer daytime, density of the air in the thermal zone decreases as it rises, and continuously draws more heat out of the zone. The upward airflow rate through the north and south sides of the thermal zone is determined by the north/south/east/west temperature and air pressure differentials. Replacement air which is cooler than the peak outside air temperature is brought in by the earth tube and through the underground space. Instead of earth tube, angled cooling tubes connected to the underground space could be used on a sloping lot. Using a fan in the north-side partial DSF or the earth tube to augment the airflow loop not only complicates the operation but also increases the costs. Therefore, cool air from the vertical earth tube is drawn through a vent at the north bottom of the underground space by natural ventilation. Replacement air absorbs heat from its surroundings, becomes less dense, rises toward the roof, and is exhausted through the roof air vents. The well-insulated roof with RBS has an air vent that is open only in summer. For an effective natural convection, the tube and vent sizes must not be too small.
- vii)** Summer night is less critical than summer day because everything else being equal, the replacement and outside air temperatures are lower. Under these conditions, the house operates more effectively than on summer day.
- viii)** On winter nights, the air flows in both directions at all nodes (Figure M.5) (Figure M.6) (Figure M.7) (Figure M.8) (Figure M.9) (Figure 8.1).
- ix)** During winter nighttime, roof and underground space vents are closed and the shading is inactive. As the air in underground space gets warmer, it rises in DSFs, and as it gets colder at the top, it falls back to the underground space by natural convection. Air circulation creates a thermal zone warmer than outside temperatures and hence, contributes to the thermal performance of the house. The lowest outside temperature is considered in the energy analysis.
- x)** On winter night, differences in air density, pressure and temperature are automatically equalized inside the DSFs, DSR and the underground space. In contrast, single-skin conventional houses with mechanical heating systems cannot automatically equalize temperatures at all points, increasing discomfort and inefficiency. When air temperature of the thermal zone drops below the

temperature of the earth beneath the house, a thermal-siphon starts to draw heat out of the earth and keeps the thermal zone temperature higher. The larger the temperature differential becomes, the more effectively the nighttime thermal-siphon operates.

- xi)** Winter day is less critical than winter night because everything else being equal, the solar gain and outside air temperatures are higher. In winter, the interior of the south-side partial DSF gets warmer than the outside air because of the radiation caused by the low winter sunlight. Warm air is less dense and rises to the top of the south-side partial DSF entering the insulated DSR, cools and falls first on the north-side partial DSF then, into the underground space, and completes the cycle that partially blankets the house. Thus, the north-side partial DSF is naturally heated by high volume natural convection airflow from the south-side partial DSF. On cold days, heat is drawn outside from the insulated exterior north wall, making the air in the north-side partial DSF cooler and denser. That heavier air falls down through the north-side partial DSF and enters the underground space. The concrete underground space under the house creates a return airflow path for the bottom of the natural convection airflow loop. The temperature-based pressure differentials automatically regulate north/south and top/bottom convection airflow. The larger the differential becomes, the faster the airflow gets. That quickly equalizes the pressure and temperature differentials between the north and south-side partial DSFs. When inside and outside temperature differentials are low, pressure differentials are also low, and the convection airflow is at a much lower volume and slower flow. On such a warm, sunny day in the winter, solar heated air rises to the DSR, but because there is not much northern cooling, the downward airflow almost stops. In winter and spring when the solar radiation is higher than needed, the roof air vent can be used to exhaust the excess heat out of the DSR. Additionally, the south-side partial DSF window blinds help to block solar radiation when it is not needed.

8.3. ENERGY PERFORMANCE COMPARISON

Energy demands and the average temperatures of the living quarters for the component combinations introduced in Chapter 7.2.1.7 “Component Combinations” are presented in Table 8.2.

Table 8.2. Energy performance comparison

Component combination	Annual heating demand (kWh)	Living quarters average temperature difference compared to new house in winter	Annual cooling demand (kWh)	Living quarters average temperature difference compared to new house in summer	Total demand (kWh)	Total demand difference compared to new house
Combination 1	628	-1.4%	1,538	1.1%	2,166	21.5%
Combination 2	424	2.8%	1,694	1.1%	2,118	19.7%
Combination 3	626	-0.6%	1,397	1.7%	2,023	15.9%
Combination 4	586	1.5%	1,364	1.6%	1,950	12.8%
Combination 5	437	-1.1%	1,307	1.2%	1,744	2.5%
New house	478	0%	1,223	0%	1,701	0%
Reference house	591	-0.5%	1,507	1.9%	2,098	18.9%

As seen in Table 8.2, the new house design delivers the highest energy performance among all component combinations. When compared to the reference house, the new house heating demand, cooling demand and total demand are 19.1 per cent, 18.8 per cent and 18.9 per cent lower, respectively. Also, the new house living quarters delivers lower average temperatures in summer and higher average temperatures in winter than the reference house living quarters (Figure M.10) indicating that energy performances does not result from deteriorated living quarters temperatures.

Combination 1 and 2 perform worse than the reference house because of the lack of surrounding thermal zone which benefits from the earth ambient temperature and the airflow. In summer time, higher cooling demands result from higher mean temperatures of

the air inside the components:

- i)** The living quarters of reference house is exposed to a mean ground temperature of 16.6 °C compared to a mean temperature of 18.9 °C of Combination 1's underground space.
- ii)** The living quarters of reference house is exposed to a mean outdoor air temperature of 21.8 °C compared to a mean temperature of 22.2 °C of Combination 2's DSR.

In this energy performance analysis, the following conditions apply for all component combinations:

- i)** 509 heating degree days which is close to 609 cooling degree days shows no heating or cooling season dominance.
- ii)** Besides the cooling and heating demands, the largest components of the annual energy consumption are 1,113 kWh for interior equipment and 356 kWh for interior lighting.

9. AIRFLOW PERFORMANCE ANALYSIS OF NEW HOUSE

In this chapter, the new house, the design with the highest energy performance, is selected for demonstrating the airflow's contribution to the energy performance and hence, the CFD model of the airflow inside DSE along with the fundamentals of airflow model and airflow performance analysis based on Energy - CFD simulation coupling is presented.

9.1. COMPUTATIONAL FLUID DYNAMICS MODEL SETUP

CFD model of new house is designed in parallel with Chapter 6.3 "Computational Fluid Dynamics Model Setup". CFD simulation program Fluent [96] is used in this study to solve turbulent airflow inside the DSF in extreme summer and winter conditions. In parallel with the studies of Azarbayjani [85] in Chapter 4 "Methodology", Zhai and Chen [54] and Zhai, Chen, Haves and Klems [55] in Chapter 2 "Literature Review", a manual static coupling process with one-step data exchange from energy to CFD simulation is executed.

9.1.1. Model Geometry

New house DSE operates mainly in two ways:

- During summer daytime, roof and underground space vents are open and the shading is active.
- During winter nighttime, roof and underground space vents are closed and the shading is inactive.

Air inside DSE (Figure N.4) is the only domain under investigation and it is separated into the following subzones: 1. Underground space, 3. DSR, 4. South-side partial DSF, 5. North-side partial DSF (Figure 7.4).

9.1.2. Boundary Conditions

Results of EnergyPlus are entered as boundary conditions into Fluent. During summer daytime with open inlet and outlet vents, the underground space vent is defined as the mass flow inlet and the roof vent as the pressure outlet of the air domain. Backflow can occur depending on local density and temperature properties. For natural convection, static pressure at the openings is set as gauge pressure in Fluent. Gravity is taken into account, and zero pressure difference between the inlet and outlet is calculated. An operating pressure equal to atmospheric pressure is assumed owing to the fact that pressure variations around the static pressure are small. The external and internal walls are established as wall boundaries of the air domain. The external and internal walls are defined as adjacent to the external environment and living quarters, respectively.

For winter nighttime with closed inlet and outlet vents, fluid boundary conditions are modeled as a closed circuit because there is neither inlet nor outlet. In other words, the inlet and outlet are considered wall boundaries and the DSE domain is sealed with no air exchange outside the domain.

For both the external and internal wall boundaries of air inside DSE, the corresponding EnergyPlus output on surface temperatures ($^{\circ}\text{C}$) is illustrated in Figure 9.1. Additionally, the side walls of the air vents and openings covered with Styrofoam, are assumed to be adiabatic.

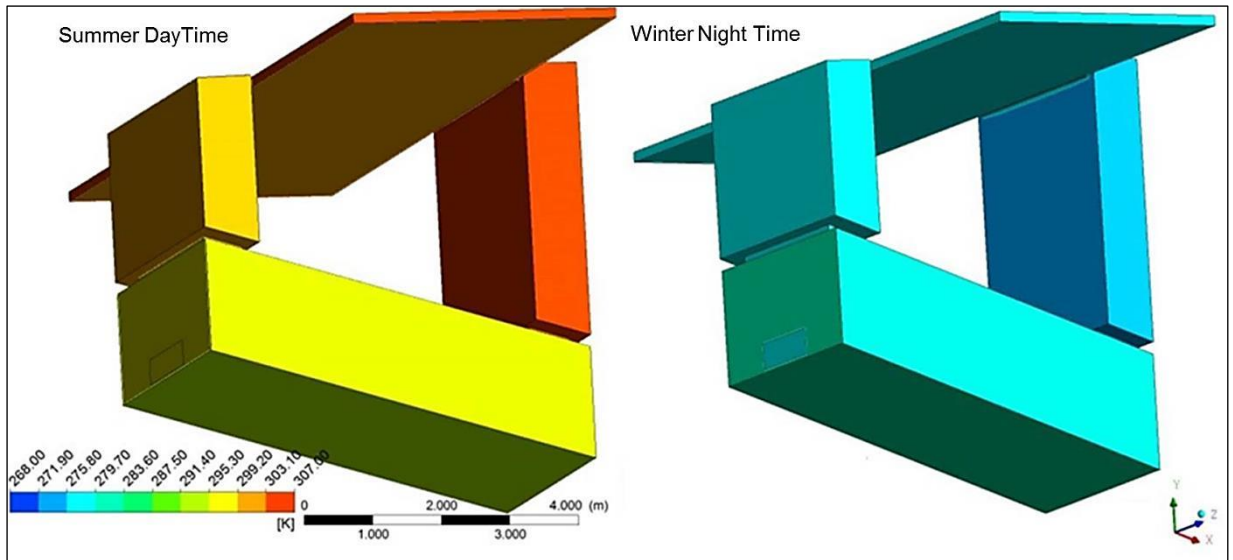


Figure 9.1. Boundary conditions of new house for summer daytime and winter nighttime extremes

There is only one calculation domain and the properties of this fluid domain are defined in Table 9.1. Air density is calculated based on the Boussinesq approximation explained in Chapter 5.3 “Airflow model for cavity air”.

Table 9.1. Boussinesq model air properties at operating temperatures

Boussinesq model air properties	Summer	Winter
Thermal expansion coefficient (1/K)	0.0033	0.0036
Density (kg/m ³)	1.1512	1.2587
Specific heat Cp (J/kgK)	1.007	1.006
Thermal conductivity K (W/mK)	0.0267	0.0248
Dynamic viscosity (kg/ms)	0.000019046	0.000017751

The infiltration of the DSR, south-side partial DSF and north-side partial DSF defined in EnergyPlus “Airflow Network Multizone Surface Crack” setup is taken into account only for summer in Fluent. In summer, the DSR, north-side partial DSF and south-side partial DSF surfaces all behave as outlets, with 0.00432, 0.00359 and 0.00491 kg/s mass flow rates, respectively. This infiltration is added to the outlet target mass flow rate (kg/s) in the Fluent boundary conditions.

Hydraulic diameter and turbulence intensity are also defined in the Fluent boundary conditions for vents. Details of the boundary conditions and operating conditions can be

found in Table O.1, Table O.2 and Table O.3.

9.1.3. Model Grid

The grids of new house are designed in parallel with the detailed explanations in Chapter 5.4.3 “Model grid”. The airflow model of the new house DSE is determined by the Rayleigh number (Ra). This number characterizes natural convection flows, which can be laminar ($Ra < 6 \times 10^4$), transitional ($6 \times 10^4 < Ra < 10^9$) or turbulent ($10^9 < Ra$). For an appropriate selection of airflow model, Rayleigh numbers for the following zones should be calculated for summer daytime and winter nighttime extremes: 1. Underground space, 3. DSR, 4. South-side partial DSF 5. North-side partial DSF (Figure 7.4).

Wall distances of the new house DSE are estimated by the Reynolds number (Re). Re is calculated based on EnergyPlus output for average airflow rates at vents and openings (m^3/s) and incompressibility of the airflow. For summer daytime extreme, EnergyPlus output of average airflow rates and temperatures at the following six nodes, and average surface temperatures including the glazing is produced (Figure 9.2): 1. Underground space inlet vent, 2. Roof outlet vent, 3. South-side partial DSF bottom opening, 4. North-side partial DSF bottom opening, 5. DSR north opening, 6. DSR south opening.

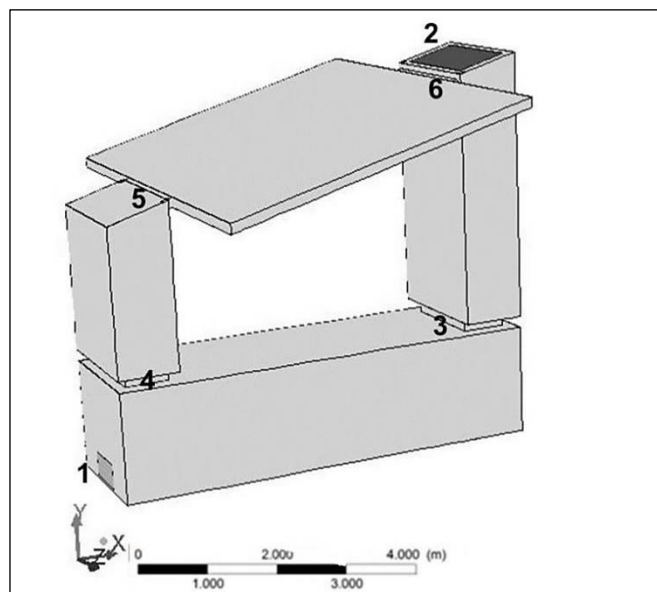


Figure 9.2. Fluid domain geometry

For winter nighttime extreme, output of average airflow rates is generated at the following four nodes (Figure 9.2): 3. South-side partial DSF bottom opening, 4. North-side partial DSF bottom opening, 5. DSR north opening, 6. DSR south opening. In this case, the underground space inlet vent and roof outlet vent are excluded, because they are treated as walls. Also, output of all surface temperatures is generated. Airflow rates inside the zones can be calculated provided that the flow is incompressible. Since density variation of the fluid is negligible and the flow is steady state, the Mach number (Ma) is calculated at 0.0002 for the maximum velocity. Because this is less than 0.3, airflow in summer and winter is assumed incompressible. Then, based on flow cross sections, vent (Table 9.2) and opening airflow velocities (Table 9.3 and Table 9.4) produced by EnergyPlus, airflow rates inside the zones in summer and winter (Table 9.5 and Table 9.6) are deduced. The relevant vent or opening with the maximum zone velocity is chosen. Thus, Re for summer (Table 9.5) and winter (Table 9.6) is calculated.

Table 9.2. Vent airflow velocities for summer daytime extreme

Vent airflow velocities for summer daytime extreme	Underground space vent	Roof vent
Boundary type	Inlet	Outlet
Section width (m)	0.800	1.800
Section length (m)	0.400	0.828
Hydraulic diameter (boundary layer length) (m)	0.533	1.134
Density (kg/m^3)	1.196	1.154
Dynamic viscosity (kg/ms)	0.00001848	0.00001902
Max airflow rate (m^3/s)	0.316	0.305
Max freestream velocity U_∞ (m/s)	0.989	0.205
Reynolds	34,000	14,000
Turbulent intensity I	4.3%	4.9%
Target mass flow rate (including infiltration) (kg/s)	0.35817	0.35817

Table 9.3. Opening airflow velocities for summer daytime extreme

Opening airflow velocities for summer daytime extreme	South-side partial DSF bottom opening	North-side partial DSF bottom opening	DSR north opening	DSR south opening
Section width (m)	1.600	1.600	2.000	2.000
Section length (m)	0.700	0.700	0.150	0.150
Hydraulic diameter (boundary layer length) (m)	0.974	0.974	0.279	0.279
Density (kg/m ³)	1.165	1.181	1.176	1.175
Dynamic viscosity (kg/ms)	0.00001887	0.00001867	0.00001874	0.00001874
Max airflow rate (m ³ /s)	0.286	0.030	0.028	0.024
Max freestream velocity U_{∞} (m/s)	0.255	0.027	0.095	0.082

Table 9.4. Opening airflow velocities for winter nighttime extreme

Opening airflow velocities for winter nighttime extreme	South-side partial DSF bottom opening	North-side partial DSF bottom opening	DSR north opening	DSR south opening
Section width (m)	1.600	1.600	2.000	2.000
Section length (m)	0.700	0.700	0.150	0.150
Hydraulic diameter (boundary layer length) (m)	0.974	0.974	0.279	0.279
Density (kg/m ³)	1.279	1.270	1.265	1.266
Dynamic viscosity (kg/ms)	0.00001752	0.00001763	0.00001768	0.00001767
Max airflow rate (m ³ /s)	0.118	0.113	0.110	0.111
Max freestream velocity U_{∞} (m/s)	0.105	0.101	0.368	0.370

As seen in Table 9.5, for summer daytime extreme, the airflow model is determined as turbulent in every zone except for the DSR based on its Ra , which is between 6×10^4 and 10^9 .

Table 9.5. Zone wall distance estimation and airflow model determination for summer daytime extreme

Zone y+ wall distance estimation for summer daytime extreme	Underground space	DSR	South-side partial DSF	North-side partial DSF
Section width (m)	2.168	6.958	2.190	2.190
Section length (m)	1.800	0.155	0.995	0.995
Hydraulic diameter (boundary layer length) (m)	1.967	0.304	1.368	1.368
Temperature (°C)	28.11	30.05	29.13	28.61
Density (kg/m ³)	1.173	1.166	1.169	1.171
Dynamic viscosity (kg/ms)	0.00001876	0.00001886	0.00001881	0.00001879
Max airflow rate (m ³ /s)	0.026	0.008	0.147	0.016
Max freestream velocity U _∞ (m/s)	0.007	0.007	0.067	0.007
Desired y+	1	1	1	1
Reynolds	860	130	5,700	600
Estimated wall distance (m)	0.022	0.014	0.003	0.020
Zone airflow model determination for summer daytime extreme	Underground space	DSR	South-side partial DSF	North-side partial DSF
L (m)	1.800	0.155	4.281	2.551
Specific heat Cp (J/kgK)	1,006	1,006	1,006	1,006
Thermal conductivity K (W/mK)	0.0263	0.0264	0.0263	0.0263
Thermal expansion coefficient (1/K)	0.0033	0.0033	0.0033	0.0033
Max temperature difference (°C)	5.80	2.61	1.58	2.52
Rayleigh	3.1x10 ⁹	0.9x10 ⁶	11.2x10 ⁹	3.8x10 ⁹
Airflow model	Turbulent	Transitional	Turbulent	Turbulent

Table 9.6 shows that for winter nighttime extreme, the airflow model is determined as turbulent in every zone except for the DSR based on its Ra which is between 6×10^4 and 10^9 .

Table 9.6. Zone wall distance estimation and airflow model determination for winter nighttime extreme

Zone y+ wall distance estimation for winter nighttime extreme	Underground space	DSR	South-side partial DSF	North-side partial DSF
Section width (m)	2.168	6.958	2.190	2.190
Section length (m)	1.800	0.155	0.995	0.995
Hydraulic diameter (boundary layer length) (m)	1.967	0.304	1.368	1.368
Temperature (°C)	5.05	4.27	3.34	4.38
Density (kg/m ³)	1.270	1.274	1.278	1.274
Dynamic viscosity (kg/ms)	0.00001762	0.00001758	0.00001753	0.00001758
Max airflow rate (m ³ /s)	0.034	0.031	0.061	0.058
Max freestream velocity U_{∞} (m/s)	0.009	0.028	0.028	0.027
Desired y+	1	1	1	1
Reynolds	1,300	620	2,800	2,700
Estimated wall distance (m)	0.016	0.004	0.006	0.006
Zone airflow model determination for winter nighttime extreme	Underground space	DSR	South-side partial DSF	North-side partial DSF
L (m)	1.800	0.155	4.281	2.551
Specific heat Cp (J/kgK)	1,006	1,006	1,006	1,006
Thermal conductivity K (W/mK)	0.0247	0.0246	0.0245	0.0246
Thermal expansion coefficient (1/K)	0.0036	0.0036	0.0036	0.0036
Max temperature difference (°C)	1.95	1.92	2.71	1.81
Rayleigh	1.5×10^9	1.0×10^6	2.9×10^{10}	4.0×10^9
Airflow model	Turbulent	Transitional	Turbulent	Turbulent

The Re is basically calculated using zone hydraulic diameters, airflow rates and temperatures yielding air density and dynamic viscosity (Table 9.5 and Table 9.6). The area of interest is airflow in the zones rather than at vents and openings. However, the airflow models are initially determined based on node airflow rates at the vents and openings output of EnergyPlus. Then, the airflow models are further elaborated based on Fluent output of airflow characteristics in the zones. To visualize the various responses to DSE while considering the computational resources available for this research, a 3D mesh of DSE for both summer and winter configurations are set up according to dimensions of the fluid geometry. Accurate analysis of convective airflows requires precise calculations

around boundaries. A hexahedral scheme is used because the fluid geometry is based on square section elements. A small size mesh is generated near the walls, where laminar flows are created. The wall treatment is not applied at the vents, openings or around the adiabatic walls of the openings. However, being the main object of interest, the wall treatment is applied to the underground space, DSR, south-side partial DSF and north-side partial DSF zones. Eventually, a single-mesh model is used for both summer and winter cases, taking the minimum estimated wall distances into consideration for the 1st layer. Wall distances (for $y^+ = 1$) of 16, 4, 3 and 6 mm are estimated for underground space, DSR, south-side partial DSF, and north-side partial DSF, respectively (Figure 9.3).

The temperature and the velocity gradients are important in the underground space and hence, wall distance of 16 mm is obtained at the floor (in y direction) and both sides (in z direction). The surface with inlet is meshed with 16 mm x 16 mm and 20 mm x 16 mm cells (on y-z plane) and a coarse mesh is extruded (in x direction) with a bias (16 mm - 675 mm - 16 mm).

The DSR grid side next to the north-side partial DSF is meshed with 10 mm x 4 mm cells (on y-z plane) and a coarse mesh is extruded (in x direction) with a bias (30 mm - 475 mm - 30 mm) while ensuring 4 mm wall distance at sides (in z direction).

To fit the roof slope, the south-side partial DSF is meshed by quadrangular cells (on x-y plane) beginning with a first layer distance of 100 mm from the top and growing to 175 mm at the bottom (in y direction) while ensuring 3 mm wall distance at sides (in z direction). Additionally, a coarse mesh is extruded (in x direction) with a bias (1.65 mm - 100 mm).

The north-side partial DSF is also meshed by quadrangular cells (on x-y plane) beginning with a first layer distance of 8 mm from the top and growing to 190 mm at the bottom (in y direction) while ensuring 6 mm wall distance at sides (in z direction). Additionally, a coarse mesh is extruded (in x direction) with a bias (6 mm - 22 mm - 6 mm).

As a result, a non-uniform grid of 3,523,904 cells for the cavity, with 2×10^{-3} m³/cell maximum volume, 0.916 minimum orthogonal quality and 6.31×10^{-2} average skewness is produced. Grid-independence studies show that this meshing gives results with the most reasonable accuracy per computing time.

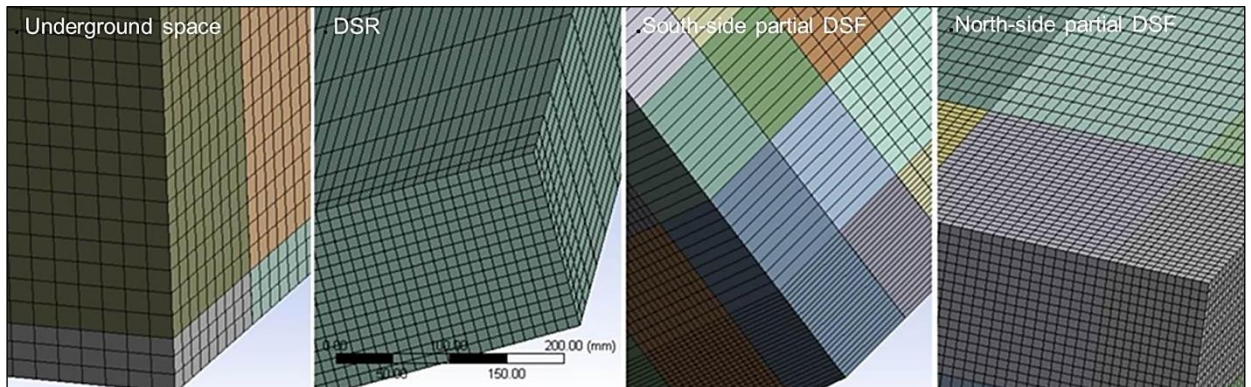


Figure 9.3. Meshes of new house

9.1.4. Numerical Methods

In parallel with Chapter 6.3.4 “Numerical methods” which explains the following concepts and calculations in details, the heat flow is calculated for convective heat transfer by the discretization of the equations of continuity, energy and turbulence based on Chapter 5 “Numerical Modeling of DSF”.

Turbulence is modeled via the RNG k - ε turbulence model based on Chapter 5.4 “Turbulence model for cavity air”. A second-order upwind spatial discretization scheme is used. A Semi-Implicit Method for Pressure-Linked Equations (SIMPLE) pressure-velocity coupling scheme is selected for coupling the default options. Convergence criteria is set to 10^{-3} for the momentum equations and 10^{-6} for energy.

The convergences of summer day (Figure P.1) and winter night (Figure P.2) are estimated from the evolution graphs of the residuals. Equations for summer day and winter night reached convergence with 8 GB memory and double precision after 1,607 (4/3 iteration per minute) and 1,526 (1 iteration per minute) iterations, respectively.

9.2. FLUENT SIMULATION RESULTS

Figure 9.4 to Figure 9.8 depict the zone temperatures, airflow rates, static pressures and turbulent Re for summer day and winter night extremes. The airflow is predominantly symmetric. Therefore, Fluent result demonstrations are mainly given at the mid-section (x - y plane) of new house. Contours of static temperatures for summer day and winter night

are generated for that mid-section (Figure 9.4). Temperatures range from 294 to 307 K for summer day and 268 to 281 K for winter night.

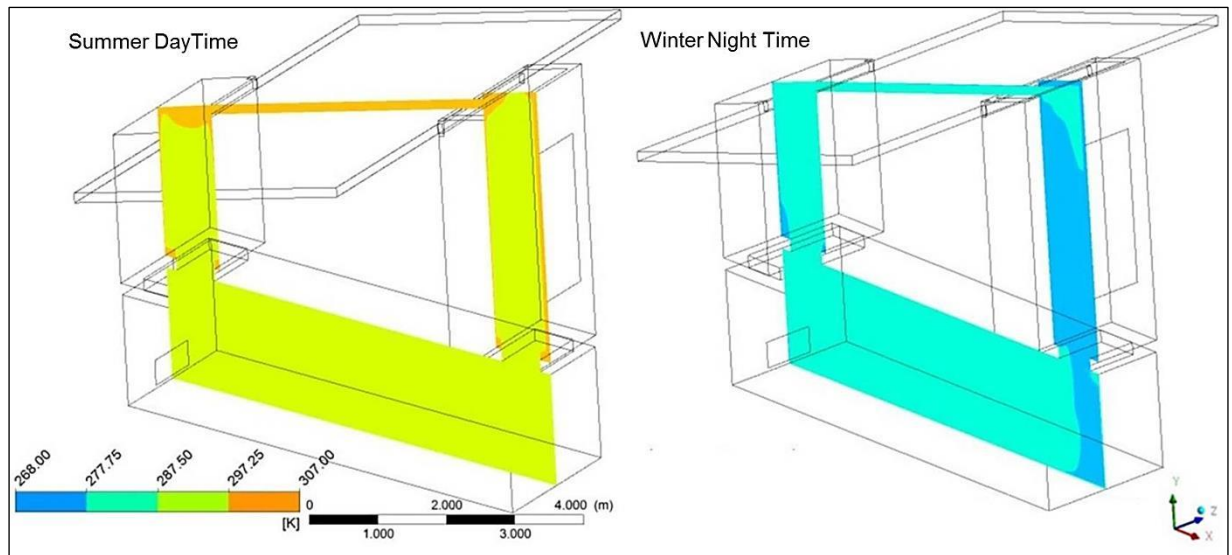


Figure 9.4. Summer daytime and winter nighttime static air temperatures at mid-section of new house

For summer day and winter night, vectors of velocity magnitudes are produced at the aforesaid mid-section (Figure 9.5), along a streamline at the mid-section of the underground space (x-z plane), inlet (x-z plane), DSR (x-y-z plane), south-side partial DSF (y-z plane) and north-side partial DSF (y-z plane) (Figure 9.6). Airflow rates are 0 - 1 m/s for summer day and 0 - 0.6 m/s for winter night.

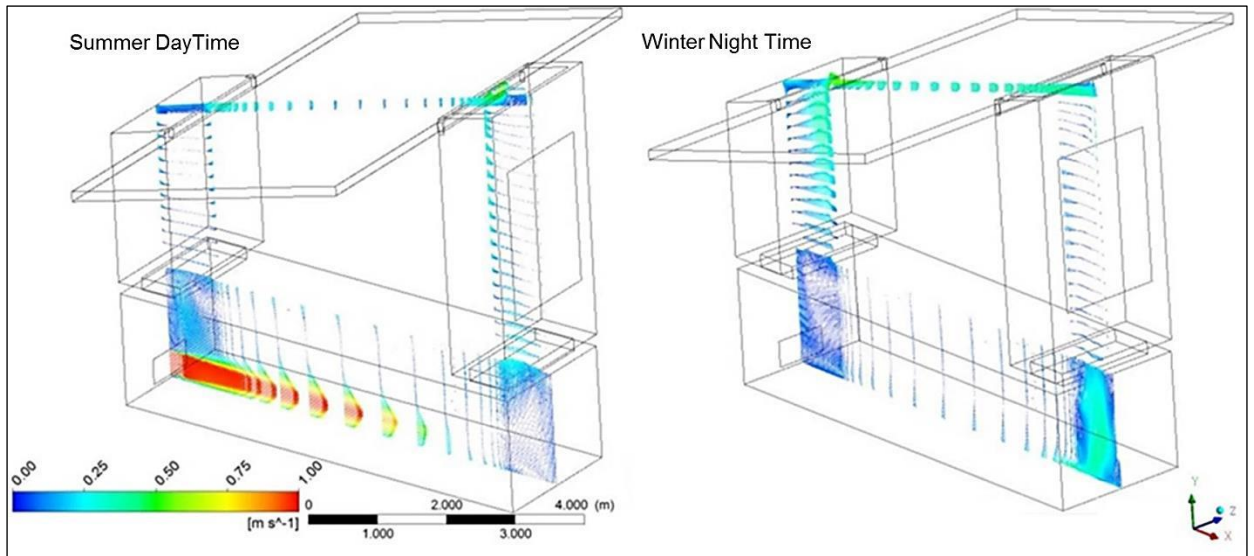


Figure 9.5. Summer daytime and winter nighttime vectors of velocity magnitude at mid-section of new house

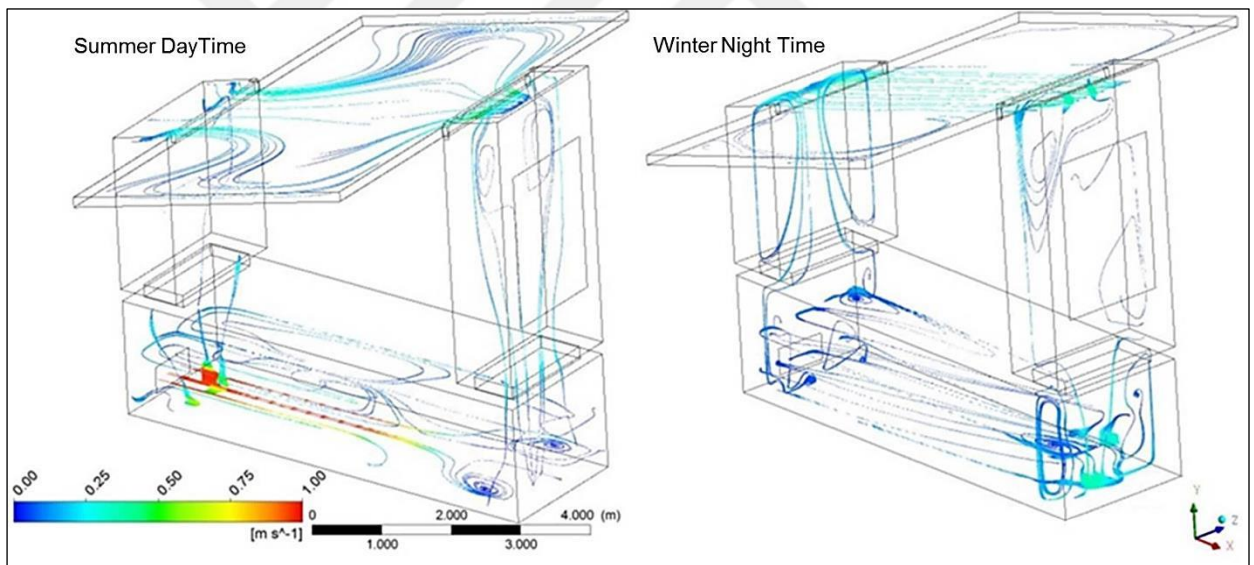


Figure 9.6. Summer daytime and winter nighttime vectors of velocity magnitude along streamline at mid-section of underground space, inlet, DSR, south-side partial DSF and north-side partial DSF

Contours of static pressure for summer day and winter night are generated at the mid-section (x-y plane) of new house (Figure 9.7). The pressures are 0.1 - 2.9 pa for summer day and -0.7 - 0.3 pa for winter night.

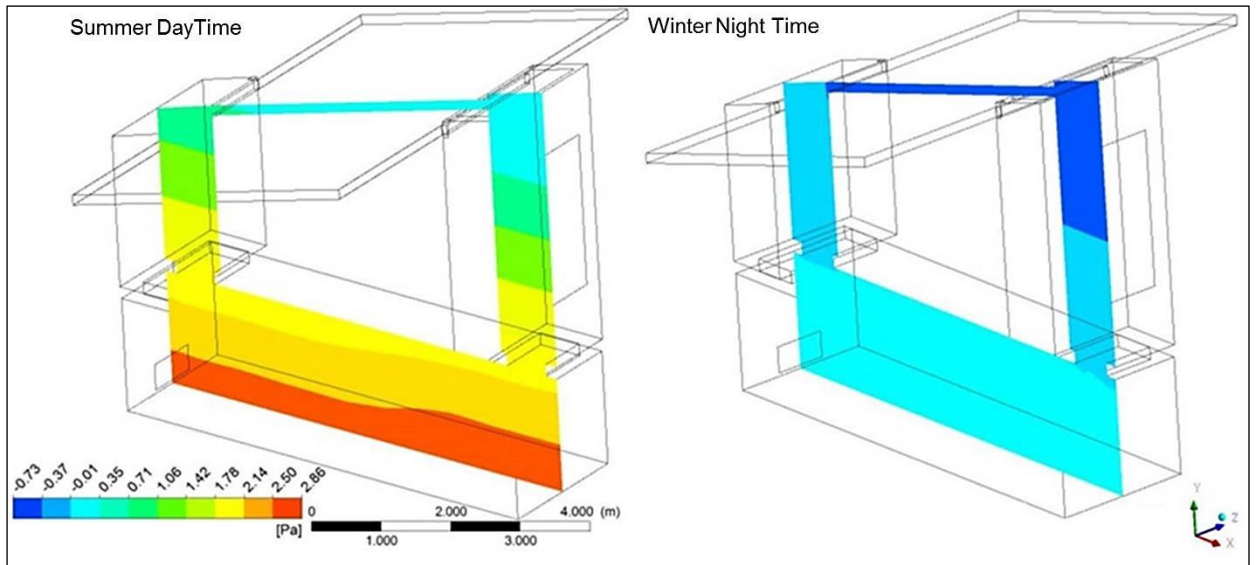


Figure 9.7. Summer daytime and winter nighttime static air pressures at mid-section of new house

Contours of turbulent Re (Re_y) for summer day and winter night are produced at the mid-section (x-y plane) of new house (Figure 9.8). The Re_y range from 0 to 6,771 for summer day and 0 to 3,118 for winter night.

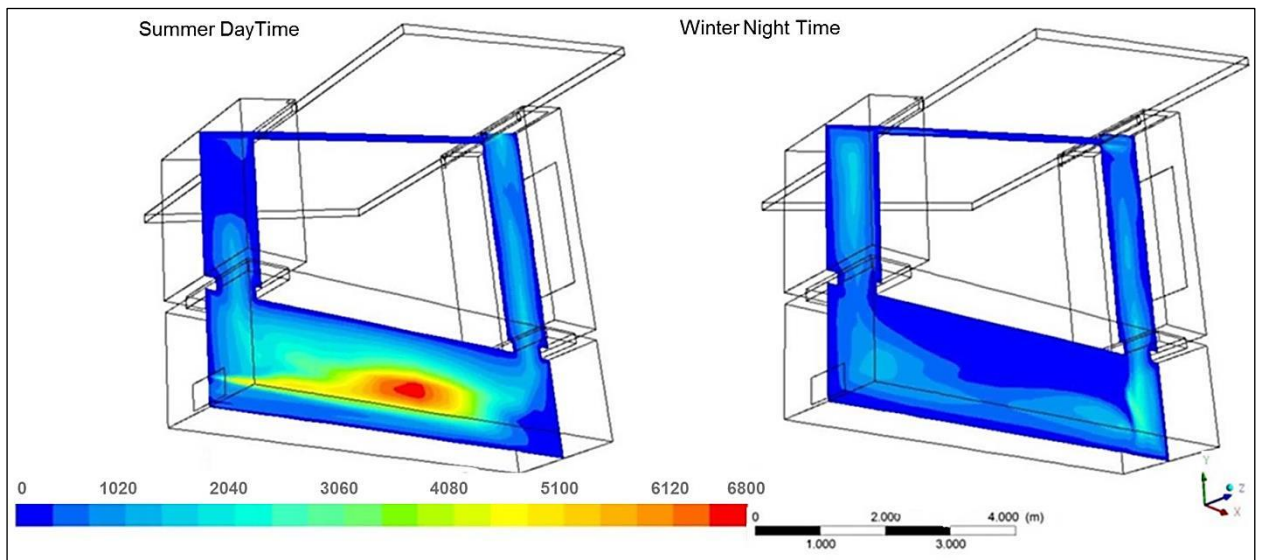


Figure 9.8. Summer daytime and winter nighttime turbulent Reynolds number (Re_y) at mid-section of new house

9.3. AIRFLOW PERFORMANCE ANALYSIS

The static temperature, flow rate, static pressure and turbulent Reynolds number ranges of the air inside DSE for summer day and winter night extremes are presented in Table 9.7.

Table 9.7. Airflow behavior for summer daytime and winter nighttime

Air inside DSE	Range at Summer Daytime Extreme	Range at Winter Nighttime Extreme
Static Temperature (K)	294 - 307	268 - 281
Flow Rate (m/s)	0 - 1	0 - 0.6
Static Pressure (pa)	0.1 - 2.9	-0.7 - 0.3
Turbulent Reynolds Number (Re_y)	0 - 6,771	0 - 3,118

The temperature stratification for summer day and winter night, with 304 K and 265 K outdoor temperatures, respectively, shows earth ambient temperature and thermal zone contributions to the energy performance of new house.

On summer day, underground space airflow rates maximize, especially in the vicinity of its vent, and vortices that are major components of turbulent flow are observed in the underground space. Flow at the center of that space was determined to be turbulent, based on Re values that were $> 4,000$.

On summer day and winter night, pressure decreases in the y direction and heat is gradually accumulated at the DSE upper level. Airflow rates increase at the top of the north-side semi DSF and south-side semi DSF, maximizing at the DSR north and south openings. Throughout the DSR, the flow was determined to be laminar, based on Re values $< 2,300$.

10. FINANCIAL ANALYSIS OF NEW HOUSE

10.1. CONSTRUCTION COSTS

Taking the component costs (Table 10.1) which are mainly material, tax, freight and labor costs at current market rates, into consideration, the bill of materials of new house (Table Q.1 - Q.6) and reference house (Table Q.7) are prepared. Finally, the construction costs of new house and reference house are calculated as \$ 7,040 and \$ 4,524, respectively.

Table 10.1. Component costs

Material - seller	Thickness (m)	Density (kg/m ³)	Cost
Lightweight Concrete – Betonsa İzobeton	0.1	1,280	62 \$/m ³
Galvanized Steel – Assan Demir ve Saç	0.0005	7,850	680 \$/ton
Styrofoam – Termopanel	0.0889	32	18 \$/m ²
Radiant Barrier – Özerden Plastik	0.013	1,070	1 \$/m ²
Metal Surface – Assan Demir ve Saç	0.008	7,824	640 \$/ton
Insulation Board – Termopanel	0.025	43	18 \$/m ²
Glazing – Trakya Cam TRC Helio	0.006	2,400	8 \$/m ²
Plywood – Sağlamlar	0.018	550	17 \$/m ²
Handles, etc. – Winsa	-	-	10 \$/piece
Unleaded PVC Glazing Frames - Winsa Dorado Gold	0.003	1,390	10 \$/m
As of June 2015, distributor quotations including VAT, freight and labor are calculated at 2.6 TL/\$ parity.			

10.2. ENERGY SAVINGS AND PAYBACK PERIOD

Comparison of Turkey's approximately \$ 0.15 household electricity price and the prices in Europe in the second half of 2014 can be found in the study of Eurostat (Figure R.1), the statistical office of the European Union [111]. According to Eurostat, the average price of electricity for household consumers in Europe (the prices for each EU Member State are

weighted according to their consumption by the household sector) was approximately \$ 0.25 per kWh in the second half of 2014. Therefore, energy savings of new house is calculated based on an expected average retail electricity price expectation of approximately \$ 0.19 (including taxes) for the next 10 years.

Energy demands, construction costs and the incremental payback periods for the component combinations introduced in Chapter 7.2.1.7 “Component Combinations” are presented in Table 10.2.

Table 10.2. Benefit/cost comparison of component combinations

Component combination	Total demand (kWh)	Total demand difference compared to new house	Construction cost (\$)	Total construction cost difference compared to new house	Incremental payback period (years)
Combination 1	2,166	21.5%	5,031	-39.9%	-
Combination 2	2,118	19.7%	5,439	-29.4%	-
Combination 3	2,023	15.9%	6,125	-14.9%	111
Combination 4	1,950	12.8%	5,619	-25.3%	38
Combination 5	1,744	2.5%	6,533	-7.8%	30
New house	1,701	0%	7,040	0%	33
Reference house	2,098	18.9%	4,524	-55.6%	-

The energy savings difference of a component combination from the energy savings of reference house is called “incremental energy savings”. Additionally, the cost difference of a component combination from the construction cost of reference house which is the lowest among all component combinations, is called “incremental construction cost”. The incremental energy savings and the incremental construction cost are taken into account for the calculation of incremental payback period.

As seen in Table 10.2, compared to the reference house, the new house generates incremental energy savings of 397 kWh (2098 kWh - 1701 kWh) which accounts for \$ 76, annually. On the other hand, compared to the reference house, the incremental construction

cost of new house is \$ 2,516 (\$ 7,040 - \$ 4,524). As a result, Combination 5 which delivers the shortest incremental payback period (30 years) has the second best energy performance with 1,744 kWh. On the other hand, new house which delivers the second shortest incremental payback period (33 years) has the best energy performance with 1,701 kWh.

The cost of new house is mainly sensitive to the price of Styrofoam which is the major component in its construction and the payback period is sensitive to the electricity prices.



11. DISCUSSION OF FINDINGS

11.1. DESIGN IMPLICATIONS

From a DSF design perspective, the study introduces the following:

- i) The first partial DSF, DSR, underground space and earth tube integration into PH architecture, forming a surrounding thermal zone from top to bottom that minimizes energy consumption while providing required comfort.
- ii) The partial DSF design is more suitable for retrofitting relative to a full DSF design, because it uses less building material and occupies less space, making it easier to apply to existing buildings.

11.2. ENERGY PERFORMANCE

From an energy performance perspective, the following is concluded:

- i) The maximum winter heating demands for the new house and the reference house are approximately 478 and 591 kWh, respectively. The new house heating demand is 19.1 per cent lower than that of the reference house.
- ii) The maximum summer cooling demand for the new house and the reference house are approximately 1,223 and 1,507 kWh, respectively. The new house cooling demand is 18.8 per cent lower than that of the reference house.
- iii) The new house mean temperature in its living quarters is 0.5 per cent higher than that of the reference house in winter, and 1.9 per cent lower in summer, indicating that energy performance of new house does not result from deteriorated living quarter temperatures.
- iv) If the roof and earth tube vents of new house are closed during summer, the cooling demand of the house is increased by 4.3 per cent, to 1,278 kWh, revealing the airflow performance contribution to the new house from a different perspective.

- v) The new house can deliver better heating and cooling demands (kWh) compared to those of the reference house while achieving indoor comfort level temperatures ($^{\circ}\text{C}$), even though the reference house design is almost a PH.

11.3. AIRFLOW CONTRIBUTION

It is also concluded that airflow in the new house DSE contributes to energy performance in two major ways:

- i) Turbulent airflow inside DSE and especially the underground space enhances heat transfer through wakes and momentum transfer between fluid particles, which in turn increases the friction force and convective heat transfer coefficient. Hence, heat loss occurs on summer days when it is needed. Strong convective heat transfer from the turbulent nature of the airflow in the underground space is favourable, because the zone has greater benefit from earth ambient temperature.
- ii) When there is no sunshine, the convective airflow velocity is slower than the sunny day time convection airflow. At nights, smaller pressure and temperature differences in DSE produce a weaker flow. Slow laminar airflow in the DSR produces thermal resistance because heat transfer via the wakes is non-existent. As airflow in DSR becomes less turbulent, more heat is preserved on winter nights.

11.4. FINANCIAL ASPECTS

- i) Taking the uncertainty of the future prices into consideration for this long term financial analysis, the new house which delivers the highest energy savings, is considered to be financially the most promising even though, for the time being, its payback period is not the shortest under current Styrofoam and electricity market conditions.
- ii) The payback period of new house is reduced as the cost of Styrofoam decreases and electricity prices increase.

12. CONTRIBUTION AND FUTURE WORKS

12.1. CONTRIBUTION

In this study, a new design PH with a double-skin envelope was developed with better performance in energy consumption for heating and cooling, while achieving comfort-level indoor temperatures as compared with a conventional reference house. A comprehensive method which helps designers make better decisions in the earliest design stage is applied for conceptual model development and comparison. Eliminating the shortcomings of existing double-skin house designs, the new PH introduced the first partial DSF design, which is integrated with a DSR, underground space and earth tube to form a surrounding thermal zone from top to bottom while utilizing earth ambient temperature. The partial DSF design is more suitable for retrofitting relative to a full DSF design, because it uses less building material and occupies less space, making it easier to apply to existing buildings. Additionally, the fluid dynamics behaviour of air inside DSE zones demonstrated the airflow's contribution to the energy performance.

12.2. LIMITATION AND RECOMMENDATIONS FOR FUTURE WORK

There have been major technological advances in envelope and its components over the past 30 years. Innovation and product development is expected to continue. However, in this study it is critical to understand which performance goals are being met by current technology and design solutions, and which ones need further development and refinement.

Outcomes of this study can be further studied based on five levels:

- i)** Construction of an actual new house to compare the numerical results with the experimental data to validate the simulations.
- ii)** Energy performance analysis of different geometries such as:
 - volume, shape and position of the underground space, DSR and north partial DSF

to increase turbulence flow in summer and laminar flow in winter,

- elimination of glazing for hotter regions. A preliminary analysis analysis in this study showed that replacing glazing on the south-side partial DSF with Styrofoam would decrease annual cooling demand by 5.7 per cent while increasing annual heating demand by the same percentage. The design with external glazing which generates lower heating demands is preferred in parallel with PHI standards,
 - fenestration area to enhance the illumination,
 - new house in larger size or as prefab.
- iii)** Energy performance analysis of different materials such as:
- low thermal resistance material for the interior wall of north-side partial DSF to further decrease cooling demand in summer,
 - PCMs as thermal mass for storing heat during daytime and releasing during nighttime to enhance the thermal behaviour of the house as PCMs become more cost effective. A preliminary analysis in this study showed that for a significant improvement in temperatures in DSE cavity and living quarters, the required PCM mass on the interior wall of south-side partial DSF would neither fit in the current geometry nor be cost effective.
- iv)** Energy performance analysis of different equipments such as heat exchangers, photovoltaic systems and roof and underground space vent automation with sensor-based enthalpy control systems.
- v)** Energy performance - cost optimization models.

REFERENCES

1. World Commission on Environment and Development. *Our Common Future: the Brundtland Report*, Oxford University Press, Oxford, 1987.
2. V. Olgyay. *Design with Climate: Bio Climatic Approach to Architectural Regionalism*, Princeton University Press, Princeton, 1936.
3. W. Streicher. Bestfaçade: Best Practice for Double-skin Façades, Graz Institute of Thermal Engineering, Report, 2005.
4. International Passive House Association, “Passive House Advantages”, http://www.passivehouse-international.org/index.php?page_id=79 [retrieved 1 October 2014].
5. International Passive House Association, “Passive House Criteria”, http://www.passivehouse-international.org/index.php?page_id=150&level1_id=78 [retrieved 1 October 2014].
6. Passive House Institute, “Database Information”, <http://www.passivhausprojekte.de/index.php?lang=en> [retrieved 1 October 2014].
7. European Commission, “Directorate - General Transport and Energy, CEPHEUS”, <http://www.cepheus.de/eng/> [retrieved 1 September 2014].
8. L. Hartweg. *The Second Generation Envelope House*, (5th edition), Natural Energy Applied Research, 1984.
9. J. Hilmarsson. Double-skin Façade Evaluating the Viability of the Component, Copenhagen Technical Academy, B.Sc. Dissertation, 2008.
10. H. Poirazis. Double-skin Façades for Office Buildings – Literature Review, Lund Institute of Technology, Report EBD-R-04/3, 2004.

11. S. Sadineni, S. Madala and R. Boehm. Passive building energy savings: a review of building envelope components. *Renewable and Sustainable Energy Reviews*, 15:3617–3631, 2011.
12. P. Tavares and A. Martins. Energy efficient building design using sensitivity analysis – a case study. *Energy and Buildings*, 39:23–31, 2007.
13. Y. Yıldız and Z. Arsan. Identification of the building parameters that influence heating and cooling energy loads for apartment buildings in hot-humid climates. *Energy*, 36:4287–4296, 2011.
14. N. Wang, T. Esramb, L. Martinez and M. McCulley. A marketable all-electric solar house: a report of a Solar Decathlon project. *Renewable Energy*, 34:2860–2871, 2009.
15. H. Tommerup, J. Rose and S. Svendsen. Energy-efficient houses built according to the energy performance requirements introduced in Denmark in 2006. *Energy and Buildings*, 39:1123–1130, 2007.
16. C. Filippin, S. Larsen, A. Beascochea and G. Lesino. Response of conventional and energy-saving buildings to design and human dependent factors. *Solar Energy*, 78:455–470, 2005.
17. L. Wang, J. Gwilliam and P. Jones. Case study of zero energy house design in UK. *Energy and Buildings*, 41:1215–1222, 2009.
18. H. Fath and K. Abdelrahman. Micro-climatic environmental conditions inside a greenhouse with a built-in solar distillation system. *Desalination*, 171:267-287, 2004.
19. M. Persson, A. Roos and M. Wall. Influence of window size on the energy balance of low energy houses. *Energy and Buildings*, 38:181–188, 2006.
20. K. Hassouneh, A. Alshboul and A. Al-Salaymeh. Influence of windows on the

- energy balance of apartment buildings in Amman. *Energy Conversion and Management*, 51:1583–1591, 2010.
21. A. Lee, H. Kelly, R. Jagoda, A. Rosenfeld, E. Stube, J. Colaco, A. Gadgil, H. Akbari, L. Norford and H. Burik. Affordable, safe housing based on expanded polystyrene (EPS) foam and a cementitious coating. *J Mater Sci*, 41:6908–6916, 2006.
 22. J. Liu, R. Wang, R. Hu, L. Yang and D. Liu. Energy efficiency of rural residential buildings: a sustainable case study in Daping Village, Sichuan Province. *Front. Energy Power Eng. China*, 4(1):117–121, 2010.
 23. Bestfaçade Project, “Introduction”,
http://www.bestfaçade.com/textde/02_intro_gesamt.htm [retrieved 1 September 2014].
 24. E. Oesterle, R. Lieb, M. Lutz and W. Heusler. *Double-skin façades – Integrated Planning*, Prestel Verlag, Munich, 2001.
 25. L. Xu and T. Ojima. Field experiments on natural energy utilization in a residential house with a double-skin façade system. *Building and Environment*, 42:2014–2023, 2007.
 26. A. Chan, T. Chow, K. Fong and Z. Lin. Investigation on energy performance of double-skin façade in Hong Kong. *Energy and Buildings*, 41:1135–1142, 2009.
 27. V. Gavan. Full-scale Experimental Evaluation and Modeling of a Double-skin Façade, l'Institut National des Sciences Appliquées de Lyon, Ph.D. Dissertation, 2009.
 28. V. Gavan, M. Woloszyn, F. Kuznik and J-J Roux. Experimental study of a

- mechanically ventilated double-skin façade with venetian sun-shading device: a full-scale investigation in controlled environment. *Solar Energy*, 84:183–195, 2010.
29. T. Jiru, Y. Tao and F. Haghighat. Airflow and heat transfer in double-skin façades. *Energy and Buildings*, 43:2760–2766, 2011.
 30. R. Fuliotto, F. Cambuli, N. Mandas, N. Bacchin, G. Manara and Q. Chen. Experimental and numerical analysis of heat transfer and airflow on an interactive building Façade. *Energy and Buildings*, 42:23–28, 2010.
 31. F. Kuznik, T. Katalina, L. Gauzere, M. Woloszyn and J-J. Roux. Numerical modeling of combined heat transfers in a double-skin façade - full-scale laboratory experiment validation. *Applied Thermal Engineering*, 31:3043-3054, 2011.
 32. M. Tascon. Experimental and Computational Evaluation of Thermal Performance and Overheating in Double-skin Façades, University of Nottingham, Ph.D. Dissertation, 2008.
 33. N. Mingotti, T. Chenvidyakarn and A. Woods. The fluid mechanics of the natural ventilation of a narrow-cavity double-skin façade. *Building and Environment*, 46:807–823, 2011.
 34. O. Kalyanova and P. Heiselberg. *Empirical Validation of Building Simulation Software: Modeling of Double Façades Final Report*, International Energy Agency (IEA), 2009.
 35. A. Fallahi. Thermal Performance of Double-skin Façade with Thermal Mass, Concordia University, Ph.D. Dissertation, 2009.
 36. W. Ding, Y. Hapartial and T. Yamada. Natural ventilation performance of a double-skin façade with a solar chimney. *Energy and Buildings*, 37:411–418, 2005.
 37. M. Shameria, M. Alghoul, K. Sopian, M. Zain and O. Elayeb. Perspectives of

- double-skin façade systems in buildings and energy saving. *Renewable and Sustainable Energy Reviews*, 15:1468–1475, 2011.
38. A. Aksamija. Context based design of double-skin façades. *Perkins+Will Research Journal*, 1(1):54-69, 2009.
 39. İ. Çetiner and E. Özkan. An approach for the evaluation of energy and cost efficiency of glass façades. *Energy and Buildings*, 37:673–684, 2005.
 40. Z. Yılmaz and F. Cetintaş. Double-skin façade's effects on heat losses of office buildings in Istanbul. *Energy and Buildings*, 37:691–697, 2005.
 41. D. Saelens, S. Roels and H. Hens. Strategies to improve the energy performance of Multiple-Skin Façades. *Building and Environment*, 43(4):638–650, 2008.
 42. N. Papadaki, S. Papantoniou and D. Kolokotsa. A parametric study of the energy performace of double-skin façades in climatic conditions of Crete, Greece. *International Journal of Low-Carbon Technologies*, 0:1–9, 2013.
 43. G. Caroli. *Robust Double-skin Façades*, ArcelorMittal Liège Research and Development, 2009.
 44. G. Gan. Simulation of buoyancy-induced flow in open cavities for natural ventilation. *Energy and Buildings*, 38(5):410-420, 2006.
 45. J. Hensen, M. Bartak and F. Drkal. Modeling and simulation of a double-skin façade system. *ASHRAE Transactions*, 108(2), 2002.
 46. G. Baldinelli. Double-skin façades for warm climate regions: analysis of a solution. *Building and Environment*, 44:1107–1118, 2009.
 47. Y. Chiu and L. Shao. An Investigation into the Effect of Solar Double-skin Façade

- with Buoyancy-driven Natural Ventilation. *CIBSE Conference*, London, 2001.
48. W. Pasut and M. Carli. Evaluation of various CFD modeling strategies in predicting airflow and temperature. *Applied Thermal Engineering*, 37:267-274, 2012.
 49. L Mei, D.L. Loveday, D.G. Infield, V. Hanby, M. Cook, Y. Li, M. Holmes and J. Bates. The Influence of Blinds on Temperatures and Air Flows within Ventilated Double-skin Façades, *Clima Well Being Indoors*, http://usir.salford.ac.uk/15870/1/Clima_2007_B02E1606.pdf. [retrieved 1 September 2014].
 50. X. Xu and Z. Yang. Natural ventilation in the double-skin façade with venetian blind. *Energy and Buildings*, 40:1498–1504, 2008.
 51. H. Manz. Total solar energy transmittance of glass double façades with free convection. *Energy and Buildings*, 36:127–136, 2004.
 52. H. Manz and T. Frank. Thermal simulation of buildings with double-skin façades. *Energy and Buildings*, 37:1114–1121, 2005.
 53. J. Hensen. Modeling Coupled Heat and Airflow: Ping-pong versus Onions. *AIVC 16th Conference*, Palm-Springs, 1995.
 54. Z. Zhai and Q. Chen. Performance of coupled building energy and CFD simulations. *Energy and Buildings*, 37:333–344, 2005.
 55. Z. Zhai, Q. Chen, P. Haves and J.H. Klems. On approaches to couple energy simulation and computational fluid dynamics programs. *Building and Environment*, 37:857- 864, 2002.
 56. J. Srebric, Q. Chen and L. Glicksman. A coupled airflow-and-energy simulation

- program for indoor thermal environmental studies. *ASHRAE Transactions*, 106(1):465–76, 2000.
57. J. Kooi and Q. Chen. Accuracy - a computer program for combined problems of energy analysis, indoor airflow, and air quality. *ASHRAE Transactions*, 94(2):196–214, 1988.
 58. L. Wang and N. Wong. Coupled simulations for naturally ventilated residential buildings. *Automation in Construction*, 17:386–398, 2008.
 59. M. Holmes, J. Lam, K. Ruddick and G. Whittle. Computation of Conduction, Convection, and Radiation in the Perimeter Zone of an Office Space. *Roomvent Conference*, Oslo, 1990.
 60. Q. Chen, X. Peng and A. Paassen. Prediction of room thermal response by CFD technique with conjugate heat transfer and radiation models. *ASHRAE Transactions*, 3884 (196):50-60, 1995.
 61. A. Moser, A. Schalin, F. Off and X. Yuan. Numerical modeling of heat transfer by radiation and convection in an atrium with thermal inertia. *ASHRAE Transactions*, 101(2):1136–1143, 1995.
 62. P. Schild. Accurate Prediction of Indoor Climate in Glazed Enclosures, Norwegian University of Science and Technology, Ph.D. Dissertation, 1997.
 63. C. Thompson and G. Leaf. Application of a multigrid method to a buoyancy induced flow problem. In: S. McCormick, editor, *Multigrid Methods Theory, Applications and Supercomputing*, Marcel Dekker, New York, 1988.
 64. R. Zhang, K. Lam, S. Yao and Y. Zhang. Coupled EnergyPlus and computational fluid dynamics simulation for natural ventilation. *Building and Environment*, 68:100–113, 2013.
 65. H. Feustel and A. Rayner-Hooson. *COMIS Fundamentals, Tech. Rep. LBNL-28560*,

Lawrence Berkeley National Laboratory, 1990.

66. L. Mora, A. Gadgil and E. Wurtz. Comparing zonal and CFD model pre-dictions of isothermal indoor airflows to experimental data. *Indoor Air*, 13:77-85, 2003.
67. N. Khan, Y. Su and S. Riffat. A review on wind driven ventilation techniques. *Energy and Buildings*, 40(8):1586-1604, 2008.
68. Alfa Steel Building Solutions,” Insulated Sheets”,
<http://www.alfasteel.net/insulated-sheet.html> [retrieved 1 September 2014].
69. Rockwool Building Materials, “Products”,
<http://www.rockwoolasia.com/products/residential+-c12+commercial+buildings/single+-c12-+double+skin+roof+solutions> [retrieved 1 June 2014].
70. Astron, “Product Selector”,
http://www.astron.biz/export/shared/.content/pdfs/wwwarticle/Astron_ProductSelector_GB.pdf [retrieved 1 September 2014].
71. P. Chang, C. Chiang and C. Lai. Development and preliminary evaluation of double roof prototypes incorporating RBS (Radiant Barrier System). *Energy and Buildings*, 40:140–147, 2008.
72. P. Biwole, M. Woloszyn and C. Pompeo. Heat transfers in a double-skin roof ventilated by natural convection in summer time. *Energy and Buildings*, 40:1487–1497, 2008.
73. S. Irwan, A. Ahmed, N. Ibrahim and N. Zakaria. Roof Angle for Optimum Thermal and Energy Performance of Insulated Roof. *ICEE 3rd Conference*, Malacca, 2009.
74. K. Ong. Temperature reduction in attic and ceiling via insulation of several passive

- roof designs. *Energy Conversion and Management*, 52:2405–2411, 2011.
75. C. Lai, J. Huang and J. Chiou. Optimal spacing for double-skin roofs. *Building and Environment*, 43:1749–1754, 2008.
 76. L. Susanti, H. Homma, H. Matsumoto, Y. Suzuki and M. Shimizu. A laboratory experiment on natural ventilation through a roof cavity for reduction of solar heat gain. *Energy and Buildings*, 40:2196–2206, 2008.
 77. T. Hooff, B. Blocken, L. Aanen and B. Bronsema. A venturi-shaped roof for wind-induced natural ventilation of buildings wind tunnel and CFD evaluation of different design configurations. *Building and Environment*, 46:1797–1807, 2011.
 78. K. Rabah. Development of energy-efficient passive solar building design in Nicosia Cyprus. *Renewable Energy*, 30:937–956, 2005.
 79. Y. Zhu, B. Lin and B. Yuan. Low-cost green building practice in China: Library of Shandong Transportation College. *Front. Energy Power Eng. China*, 4(1):100–105, 2010.
 80. D.E. Avison and V. Taylor. Information Systems Development Methodologies: A Classification According to Problem Situation. *Journal of Information Technology*, 12(1):73–81, 1997.
 81. D. Patching. *Practical Soft Systems Analysis*, Pitman, London, 1990.
 82. K. Maani and R. Cavana. *Systems Thinking, Systems Dynamics*, Pearson Education, Canada, 2007.
 83. P. Checkland. *Systems Thinking, Systems Practice*, Wiley, 1981.
 84. A. Pappas and Z. Zhai. Numerical investigation on thermal performance and

- correlations of double-skin façade with buoyancy-driven airflow. *Energy and Buildings*, 40:466–475, 2008.
85. M. Azarbayjani. Beyond Arrows: Energy Performance of a New, Naturally Ventilated Double-Skin Façade Configuration for a High-rise Office Building in Chicago, University of Illinois at Urbana-Champaign, Ph.D. Dissertation, 2010.
86. D. Saelens. Energy Performance Assessment of Single Storey Multiple-Skin Façades, Katholieke Universiteit Leuven, Ph.D. Dissertation, 2002.
87. U.S. Department of Energy, “EnergyPlus 8.0”,
http://apps1.eere.energy.gov/buildings/energyplus/?utm_source=EnergyPlus&utm_medium=redirect&utm_campaign=EnergyPlus%2Bredirect%2B1 [retrieved 1 September 2014].
88. M. Yazdanian and J.H. Klems. Measurement of the exterior convective film coefficient for windows in low-rise buildings. *ASHRAE Transaction*, 100 (1):1087-1096, 1994.
89. Ansys Incorporated, “Fluent 14.0”,
<http://www.ansys.com/Products/Simulation+Technology/Fluid+Dynamics/Fluid+Dynamics+Products/ANSYS+Fluent> [retrieved 1 September 2014].
90. Z. Warsi. *Fluid Dynamics: Theoretical and Computational Approaches*, (3rd edition), CRC Press-Taylor and Francis Group, London, 2006.
91. G. Gan. Thermal transmittance of multiple glazing: computational fluid dynamics prediction. *Applied Thermal Engineering*, 21(15):1583-1592, 2001.
92. Z. Zhang, W. Zhang, Z. Zhai and Q. Chen. Evaluation of various turbulence models

- in predicting airflow and turbulence in enclosed environments by CFD: part 2 - comparison with experimental data from literature. *HVAC&R Research*, 13(6):871-886, 2007.
93. Z. Zhai, Z. Zhang, W. Zhang and Q. Chen. Evaluation of various turbulence models in predicting airflow and turbulence in enclosed environments by CFD: part 1- summary of prevalent turbulence models. *HVAC&R Research*, 13(6):853-870, 2007.
 94. P.Y. Chou. On the velocity correlations and the equations of turbulent vorticity fluctuation. *Quarterly of Applied Mathematics*, 1:33-54, 1945.
 95. A.N. Kolmogorov. Equations of turbulent motion of an incompressible fluid. *Physics*, 6(1-2):56-58, 1942.
 96. Fluent Incorporated. *Fluent 6.3 User's Guide*, 2005.
 97. R. Avva, C. Smith and A. Singhal. Comparative Study of High and Low Reynolds Number Version of k-e Models. *AIAA Aerospace Sciences Meeting*, Reno, 1990.
 98. M. Raisee and S. Hejazi. Application of linear and non-linear low-Re k-epsilon models in two-dimensional predictions of convective heat transfer in passages with sudden contractions. *International Journal of Heat and Fluid Flow*, 28(3):429-440, 2007.
 99. B. Launder and D. Spalding. *Lectures in Mathematical Models of Turbulence*, Academic Press Inc., London, 1972.
 100. B. Launder and D. Spalding. The Numerical Computation of Turbulent Flows. *Computer Methods in Applied Mechanics and Engineering*, 3:269-289, 1974.
 101. P. Bernard. Limitations of the near-wall k-e turbulence model. *AIAA*, 24(4):619-622, 1986.
 102. U.S. Department of Energy, "Legacy OpenStudio Plug-in for SketchUp Version

- 1.0.10”,
<http://apps1.eere.energy.gov/buildings/energyplus/openstudio.cfmOpenStudio-1-0-10> [retrieved 1 September 2014].
103. NREL, “OpenStudio 0.11.5”,
<http://openstudio.nrel.gov/downloads> [retrieved 1 September 2014].
104. Ansys Incorporated, “ICEM CFD 14.0”,
<http://www.ansys.com/Products/Other+Products/ANSYS+ICEM+CFD> [retrieved 1 September 2014].
105. Trimble Navigation Limited, “SketchUp 8.0”,
<http://sketchup.google.es/intl/en/download/index.html> [retrieved 1 September 2014].
106. Dassault Systèmes, “Solidworks 2013”,
<http://www.3ds.com/products-services/solidworks/overview/> [retrieved 1 September 2014].
107. Dow Chemical Company, “Products:Styrofoam”
<http://building.dow.com/en-us/products#!%7CUS%7C0%7C0%7C0%7C0%7C0%7C0> [retrieved 1 September 2014].
108. Kama Energy Efficient Building Systems Incorporated, Kama Product Overview, 2008.
109. Steelroofing, “Trade and Technical Information”,
<http://www.steelroofing.com/trade.htm> [retrieved 1 September 2014].
110. Attic Foil Radiant Barrier Supply LLC, “Products”,
<http://www.atticfoil.com/> [retrieved 1 September 2014].

111. Eurostat, Electricity prices for household consumers, second half 2014. Available on site
[http://ec.europa.eu/eurostat/statisticsexplained/index.php/File:Electricity_prices_for_household_consumers,_second_half_2014_\(%C2%B9\)_\(EUR_per_kWh\)_YB15.png](http://ec.europa.eu/eurostat/statisticsexplained/index.php/File:Electricity_prices_for_household_consumers,_second_half_2014_(%C2%B9)_(EUR_per_kWh)_YB15.png)
[Retrieved 1 July 2015].
112. U.S. Department of Energy, Weather Data. Available on site
http://apps1.eere.energy.gov/buildings/energyplus/cfm/weather_data3.cfm/region=6_europe_wmo_region_6/country=TUR/cname=Turkey [Retrieved 1 September 2014].
113. ANSI/ASHRAE. Standard 90.1: Energy Standard for Buildings except Low-Rise Residential Buildings, (SI edition), 2007.
114. ANSI/ASHRAE. Standard 90.2: Energy Efficient Design of Low-Rise Residential Buildings, 2007.

APPENDIX A: SAELENS' MEASUREMENTS

Saelens tests a mechanically and naturally ventilated DSF with a roller screen sun-shading device. The measurements were taken at the Vliet test building of the Laboratory of Building Physics in Leuven (Belgium) (Figure 5.1). The test building and the DSF are subjected to outside weather conditions. Thus, the solar radiation and the air temperature are not controlled but precisely monitored. The DSF system (1.2 m x 2.7 m x 0.5 m in dimensions) consists of a single (8 mm) sheet of glass at the exterior, a roller screen sun-shading device in the middle of the cavity and double (4 mm + 15 mm Argon + 4 mm) glazing on the interior. The test cell is made up of an aluminum frame with thermal break, a double pane low-e interior glazing and a clear single pane exterior glazing with a conductivity of 0.04536 W/m.K. The space behind the DSF is air-conditioned. The roller screen sun-shading device has an automated control system. If the solar radiation exceeds 150 W/m² the sun-shading device is lowered completely. The shade with a material of $\rho = 0.51$, $\varepsilon = 0.39$, is modeled as 2,145 mm x 1,100 mm and it is positioned 185 mm below the top of the cavity (Figure 5.1).

Measurements were taken during the winter and summer seasons. Temperature and airflow measurements were conducted. The airflow rate through the cavity was monitored using the tracer gas technique. The pressure difference over the lower ventilation grids was also measured with tubes connected to a differential pressure transducer. For all configurations, airflow rate values between 20 m³/hr and 80 m³/hr were measured. The surface temperatures were measured on both sides of the double glazing and on one side of the single pane glazing. The cavity air temperature was monitored on either side of the sun-shading device. Sensors were installed at three different heights in order to measure the vertical temperature profile. The air inlet and outlet temperature, as well as the interior temperature, were monitored.

During winter measurements the cavity of the outdoor air curtain DSF is warmer than the exterior. According to Saelens, the cavity air can be used as preheated ventilation air. With solar radiation, the temperature difference between the inlet and the outlet easily exceeds 10 °C, and sometimes 20 °C. The temperature difference between the inlet and the outlet is defined by Saelens as the temperature difference between the outdoor air temperature and the temperature at the top or the bottom of the cavity depending on the airflow direction. When the cavity ventilation was enabled in winter conditions, the cavity temperature was

2.8 °C warmer than the outdoor air. When the DSF was closed creating an air buffer, the cavity is on average 6.4 °C warmer than the outdoor air.

During summer measurements the increase in temperature exceeds, according to Saelens, 15 °C, and may reach 28 °C. Especially during the daytime, the cavity temperature is higher than the indoor temperature. According to Saelens, the high temperatures make it impossible to use the cavity air to ventilate the building without influencing the cooling load.



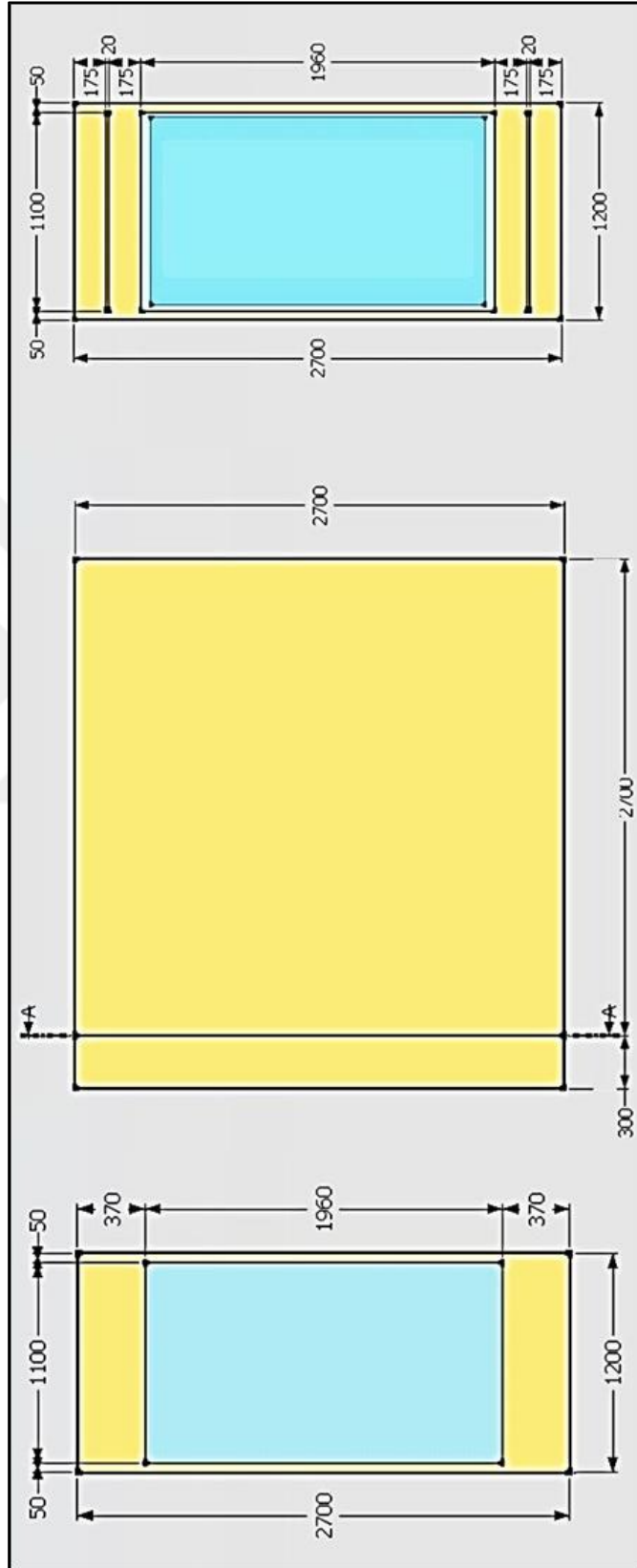


Figure B.1. Energy zone dimensions of DSF model

APPENDIX C: ENERGYPLUS SETUP OF DSF MODEL

Algorithm

- i) Solar distribution is set as full exterior with reflections in “Building” class of EnergyPlus.
- ii) “Surface Convection Algorithm Inside”, default indoor surface heat transfer convection algorithm to be used for all zones, is set as TARP (variable natural convection based on temperature difference by ASHRAE and Walton).
- iii) “Surface Convection Algorithm Outside”, default outside surface heat transfer convection algorithm to be used for all zones, is set as MoWiTT (correlation from measurements by Klems and Yazdanian for smooth surfaces at Mobile Window Thermal Test facility).
- iv) Conduction Finite Difference (ConFD) is used as “Heat Balance Algorithm”.
- v) “Timestep” which is used in the Heat Balance Model calculation for heat transfer and load calculations, is selected as 30 timesteps per hour. The minimum value suggested for ConFD is 20 timesteps per hour.

Weather and Ground

- i) Belgium Brussels 064510 IWEC weather data which is available through the U.S. Department of Energy, including temperature, relative humidity, wind, solar insolation is used in “Site Location” and “Run Period” [112].
- ii) Temperatures defined in “Site Ground Temperature Building Surface” (18 °C) are specifically used for those surfaces that have the outside environment.

Material

Regular materials including RBS, glass material, window gas, window shade and properties are described with full set of thermal properties in “Materials”, “Window Material Glazing”, “Window Material Gas” and “Window Material Shade” respectively (Table D.1).

Construction

- i) Construction layers are defined from outside layer to the inside in “Construction”.
- ii) “Building Surface Detailed” allows for detailed entry of building heat transfer surfaces. It does not include subsurfaces such as windows or doors (Table D.2).

Fenestration and Shading

- i) “Fenestration Surface Detailed” allows for detailed entry of subsurfaces (windows, doors, glass doors, tubular daylighting devices).
- ii) “Window Property Shading Control” specifies the type, location, and controls for window shades, window blinds, and switchable glazing. Shading type is defined as interior shade and shading control type as OnIfHighHorizontalSolar which turns shading is on if total (beam plus diffuse) horizontal solar irradiance exceeds SetPoint (W/m^2) and schedule, if specified, allows shading.
- iii) “Window Property Frame and Divider” used specifies the dimensions of a window frame, dividers, and inside reveal surfaces (Table D.3).

Airflow

- i) “Airflow Network Simulation Control” defines the global parameters used in an Airflow Network simulation.
- ii) “Airflow Network Multizone Zone” is used to simultaneously control a thermal zone's window and door openings.
- iii) “Airflow Network Multizone Surface” specifies the properties of a surface linkage through which air flows.
- iv) “Airflow Network Multizone Component Simple Opening” specifies the properties of airflow through windows and doors (window, door and glass door heat transfer subsurfaces) when they are closed or open (Table D.4).

Heating, Ventilating and Air Conditioning

Even though there is no mechanical ventilation, “Zone HVAC Ideal Load Air System” and “HVAC Template Thermostat Zone HVAC Equipment List” need to be defined to run the simulation.

Output

“Output Variable Dictionary”, “Output Surfaces Drawing”, “Output Table Summary Reports” “Output Control Table Style”, “Output Variable”, “Output Meter” and “Output SQLite” need to be defined in order to obtain the simulation outputs.

APPENDIX D: ENERGYPLUS INPUT DATA OF DSF MODEL

Field	Units	Obj1	Obj2	Obj3	Obj4	Obj5	Obj6
Name		Aluminum wo thermal break	Radiant Barrier	8 in concrete block	4 in concrete sand and gravel	1/2 in gyp seathing board	4 in polystrene
Roughness		Smooth	Smooth	MediumRough	MediumRough	Smooth	Rough
Thickness	m	0.005	0.0005	0.2032	0.1014984	0.012710161	0.1016
Conductivity	W/m-K	221.38	0.1	0.754	1.729577	0.1601589	0.035
Density	kg/m3	2739.15	1070	1842	2242.585	784.9047	29
Specific Heat	J/kg-K	890	897	837	836.8	836.8	1213
Thermal Absorptance		0.9	0.39	0.9	0.9	0.9	0.9
Solar Absorptance		0.2	0.39	0.2	0.6	0.92	0.5
Visible Absorptance		0.2	0.39	0.2	0.6	0.92	0.5

Field	Units	Obj1	Obj2
Name		Clear 8mm	Clear 4mm
Optical Data Type		SpectralAverage	SpectralAverage
Window Glass Spectral Data Set Name			
Thickness	m	0.008	0.004
Solar Transmittance at Normal Incidence		0.775	0.775
Front Side Solar Reflectance at Normal Incidence		0.071	0.071
Back Side Solar Reflectance at Normal Incidence		0.071	0.071
Visible Transmittance at Normal Incidence		0.881	0.881
Front Side Visible Reflectance at Normal Incidence		0.08	0.08
Back Side Visible Reflectance at Normal Incidence		0.08	0.08
Infrared Transmittance at Normal Incidence		0	0
Front Side Infrared Hemispherical Emissivity		0.84	0.84
Back Side Infrared Hemispherical Emissivity		0.84	0.84
Conductivity	W/m-K	0.04536	0.04536
Dirt Correction Factor for Solar and Visible Transmittance			
Solar Diffusing			
Young's modulus	Pa		
Poisson's ratio			

Field	Units	Obj1
Name		Argon 15mm
Gas Type		Argon
Thickness	m	0.015
Conductivity Coefficient A	W/m-K	0.042
Conductivity Coefficient B	W/m-K2	
Conductivity Coefficient C	W/m-K3	
Viscosity Coefficient A	kg/m-s	
Viscosity Coefficient B	kg/m-s-K	
Viscosity Coefficient C	kg/m-s-K2	
Specific Heat Coefficient A	J/kg-K	
Specific Heat Coefficient B	J/kg-K2	
Specific Heat Coefficient C	J/kg-K3	
Molecular Weight	g/mol	
Specific Heat Ratio		

Field	Units	Obj1
Name		Radiant Barrier Shades
Solar Transmittance	dimensionless	0.1
Solar Reflectance	dimensionless	0.51
Visible Transmittance	dimensionless	0.1
Visible Reflectance	dimensionless	0.51
Infrared Hemispherical Emissivity	dimensionless	0.39
Infrared Transmittance	dimensionless	0
Thickness	m	0.0005
Conductivity	W/m-K	0.1
Shade to Glass Distance	m	0.15
Top Opening Multiplier		
Bottom Opening Multiplier		
Left-Side Opening Multiplier		
Right-Side Opening Multiplier		0
Airflow Permeability	dimensionless	

Figure D.1. Material data

Field	Units	Obj1	Obj2	Obj3	Obj4	Obj5	Obj6	Obj7	Obj8	Obj9	Obj10	Obj11	Obj12
Name		Exterior Wall	Exterior Window	Interior Window	Slab Floor	Zone1 Wall2	Zone1 Roof	Zone2 Floor1	Zone2 Wall1	Zone2 Wall4	Zone2 Roof1	Zone2 Wall2	Zone2 Wall3
Outside Layer		8 in concrete block	Clear 8mm	Clear 4mm	4 in concrete sand and gravel	Exterior Wall Reversed	1/2 in gyp sheathing board	4 in polystyrene	Aluminum wo thermal break				
Layer 2		4 in polystyrene		Argon 15mm									
Layer 3		1/2 in gyp sheathing board		Clear 4mm									
Layer 4													
Layer 5													
Layer 6													
Layer 7													
Layer 8													
Layer 9													
Layer 10													
Field	Units	Obj1	Obj2	Obj3	Obj4	Obj5	Obj6	Obj7	Obj8	Obj9	Obj10	Obj11	Obj12
Name		Zone1 Wall1	Zone1 Floor1	Zone1 Wall3	Zone1 Wall4	Zone1 Wall2	Zone1 Roof	Zone2 Floor1	Zone2 Wall1	Zone2 Wall4	Zone2 Roof1	Zone2 Wall2	Zone2 Wall3
Surface Type		Wall	Floor	Wall	Wall	Wall	Roof	Floor	Wall	Wall	Floor	Wall	Wall
Construction Name		Exterior Wall	Slab Floor	Exterior Wall	Exterior Wall	Exterior Wall	Exterior Wall	Slab Floor	Exterior Wall Reversed	Exterior Wall	Exterior Wall	Exterior Wall	Exterior Wall
Zone Name		Zone1	Zone1	Zone1	Zone1	Zone1	Zone1	Zone2	Zone2	Zone2	Zone2	Zone2	Zone2
Outside Boundary Condition		Outdoors	Ground	Adiabatic	Zone1	Adiabatic	Outdoors	Ground	Zone1	Adiabatic	Outdoors	Adiabatic	Adiabatic
Outside Boundary Condition Object					Zone2				Zone1				
Sun Exposure		SunExposed	NoSun	NoSun	NoSun	NoSun	NoSun	NoSun	NoSun	NoSun	NoSun	NoSun	NoSun
Wind Exposure		WindExposed	NoWind	NoWind	NoWind	NoWind	NoWind	NoWind	NoWind	NoWind	NoWind	NoWind	NoWind
View Factor to Ground		autocalculate	0	0	0	0	0	0	0	0	0	0	0
Number of Vertices		4	4	4	4	4	4	4	4	4	4	4	4
Vertex 1 X-coordinate	m	0	1.2	0	1.2	1.2	1.2	1.2	0	0	1.2	1.2	1.2
Vertex 1 Y-coordinate	m	0	0	0.3	0.3	0	0.3	0	0	2.7	2.7	0	2.7
Vertex 1 Z-coordinate	m	2.7	0	2.7	2.7	2.7	2.7	0	2.7	2.7	2.7	2.7	2.7
Vertex 2 X-coordinate	m	0	0	0	1.2	1.2	0	0	0	0	1.2	1.2	1.2
Vertex 2 Y-coordinate	m	0	0	0.3	0.3	0	0.3	0	0	2.7	2.7	0	2.7
Vertex 2 Z-coordinate	m	0	0	0	0	0	2.7	0	0	0	2.7	0	0
Vertex 3 X-coordinate	m	1.2	0	0	0	1.2	0	0	1.2	0	0	1.2	0
Vertex 3 Y-coordinate	m	0	0.3	0	0.3	0	0	2.7	0	0	0	2.7	2.7
Vertex 3 Z-coordinate	m	0	0	0	0	0	2.7	0	0	0	2.7	0	0
Vertex 4 X-coordinate	m	1.2	1.2	0	0	1.2	1.2	1.2	1.2	1.2	1.2	1.2	0
Vertex 4 Y-coordinate	m	0	0.3	0	0.3	0	0.3	0	2.7	0	0	2.7	2.7
Vertex 4 Z-coordinate	m	2.7	0	2.7	2.7	2.7	2.7	0	2.7	2.7	2.7	2.7	2.7

Figure D.2. Construction data

Field	Units	Obj1	Obj2	Obj3	Obj4	Obj5
Name		Exterior Glass	Zone1 Winint	Zone2 Winint	Outlet	Inlet
Surface Type		Window	Window	Window	Door	Door
Construction Name		Exterior Window	Interior Window	Interior Window	Grids	Grids
Building Surface Name		Zone1 Wall1	Zone1 Wall3	Zone2 Wall1	Zone1 Wall1	Zone1 Wall1
Outside Boundary Condition Object						
View Factor to Ground						
Shading Control Name		ShadingControl				
Frame and Divider Name						
Multiplier						
Number of Vertices		4	4	4	4	4
Vertex 1 X-coordinate	m	0.05	1.15	0.05	0.05	0.05
Vertex 1 Y-coordinate	m	0	0.3	0	0	0
Vertex 1 Z-coordinate	m	2.33	2.33	2.33	2.525	0.195
Vertex 2 X-coordinate	m	0.05	1.15	0.05	0.05	0.05
Vertex 2 Y-coordinate	m	0	0.3	0	0	0
Vertex 2 Z-coordinate	m	0.37	0.37	0.37	2.505	0.175
Vertex 3 X-coordinate	m	1.15	0.05	1.15	1.15	1.15
Vertex 3 Y-coordinate	m	0	0.3	0	0	0
Vertex 3 Z-coordinate	m	0.37	0.37	0.37	2.505	0.175
Vertex 4 X-coordinate	m	1.15	0.05	1.15	1.15	1.15
Vertex 4 Y-coordinate	m	0	0.3	0	0	0
Vertex 4 Z-coordinate	m	2.33	2.33	2.33	2.525	0.195

Field	Units	Obj1
Name		ShadingControl
Shading Type		InteriorShade
Construction with Shading Name		
Shading Control Type		OnIfHighHorizontalSolar
Schedule Name		
Setpoint	W/m2, W or deg C	150
Shading Control Is Scheduled		Yes
Glare Control Is Active		No
Shading Device Material Name		Radiant Barrier Shades
Type of Slat Angle Control for Blinds		
Slat Angle Schedule Name		
Setpoint 2	W/m2 or deg C	

Field	Units	Obj1
Name		AI Frame w/break
Frame Width	m	
Frame Outside Projection	m	
Frame Inside Projection	m	
Frame Conductance	W/m2-K	
Ratio of Frame-Edge Glass Conductance to Center-Of-Glass Conductance		1
Frame Solar Absorptance		0.7
Frame Visible Absorptance		0.7
Frame Thermal Hemispherical Emissivity		0.9
Divider Type		DividedLite
Divider Width	m	
Number of Horizontal Dividers		
Number of Vertical Dividers		
Divider Outside Projection	m	
Divider Inside Projection	m	
Divider Conductance	W/m2-K	
Ratio of Divider-Edge Glass Conductance to Center-Of-Glass Conductance		1
Divider Solar Absorptance		
Divider Visible Absorptance		
Divider Thermal Hemispherical Emissivity		0.9
Outside Reveal Solar Absorptance		
Inside Sill Depth	m	
Inside Sill Solar Absorptance		

Figure D.3. Fenestration and shading data

Field	Units	Obj1	Obj2
Name		Natural Summer Ventilation	
AirflowNetwork Control		MultizoneWithoutDistribution	
Wind Pressure Coefficient Type		SurfaceAverageCalculation	
AirflowNetwork Wind Pressure Coefficient Array Name			
Height Selection for Local Wind Pressure Calculation			
Building Type		LowRise	
Maximum Number of Iterations	dimensionless	500	
Initialization Type		ZeroNodePressures	
Relative Airflow Convergence Tolerance	dimensionless	0.00001	
Absolute Airflow Convergence Tolerance	kg/s	0.000001	
Convergence Acceleration Limit	dimensionless	-0.5	
Azimuth Angle of Long Axis of Building	deg	90	
Ratio of Building Width Along Short Axis to Width Along Long Axis		0.4444	
Field	Units	Obj1	Obj2
Zone Name		Zone1	
Ventilation Control Mode		Constant	
Ventilation Control Zone Temperature Setpoint Schedule Name			
Minimum Venting Open Factor	dimensionless	1	
Indoor and Outdoor Temperature Difference Lower Limit For Maximum Venting Open Factor	deltaC	0	
Indoor and Outdoor Temperature Difference Upper Limit for Minimum Venting Open Factor	deltaC	100	
Indoor and Outdoor Enthalpy Difference Lower Limit For Maximum Venting Open Factor	deltaJ/kg	0	
Indoor and Outdoor Enthalpy Difference Upper Limit for Minimum Venting Open Factor	deltaJ/kg	300000	
Venting Availability Schedule Name			
Field	Units	Obj1	Obj2
Surface Name		Inlet	Outlet
Leakage Component Name		Exterior Open	Exterior Open
External Node Name			
Window/Door Opening Factor, or Crack Factor	dimensionless	1	1
Ventilation Control Mode		Constant	Constant
Ventilation Control Zone Temperature Setpoint Schedule Name			
Minimum Venting Open Factor	dimensionless	1	1
Indoor and Outdoor Temperature Difference Lower Limit	deltaC		
Indoor and Outdoor Temperature Difference Upper Limit	deltaC		
Indoor and Outdoor Enthalpy Difference Lower Limit For	deltaJ/kg		
Indoor and Outdoor Enthalpy Difference Upper Limit for	deltaJ/kg		
Venting Availability Schedule Name			
Field	Units	Obj1	Obj2
Name		Exterior Open	
Air Mass Flow Coefficient When Opening is Closed	kg/s-m	0.00001	
Air Mass Flow Exponent When Opening is Closed	dimensionless	0.5	
Minimum Density Difference for Two-Way Flow	kg/m3	0.0001	
Discharge Coefficient	dimensionless	1	

Figure D.4. Airflow network data

APPENDIX E: FLUENT BOUNDARY CONDITIONS OF DSF MODEL

Table E.1. Boundary conditions of DSF model

Fluent boundary conditions	Boundary type	Model A	Model B
Shade convective heat flux (W/m ²)	Wall	0	81.6
Exterior glass inside face temperature (°C)	Wall	17.0	43.2
Interior glass inside face temperature (°C)	Wall	18.1	30.4
Floor inside face temperature (°C)	Wall	18.1	22.6
Roof inside face temperature (°C)	Wall	17.8	32.5
Wall 1 inside face temperature (°C)	Wall	18.2	31.6
Wall 2 inside face temperature (°C)	Wall	18.3	32.8
Wall 3 inside face temperature (°C)	Wall	18.1	33.5
Wall 4 inside face temperature (°C)	Wall	18.3	32.8
Inlet opening	Inlet	16.8	29.3
Outlet opening	Outlet	16.7	28.8

Table E.2. Operating conditions of DSF model

Fluent operating conditions	Model A	Model B
Gravitational acceleration g (m/s ²)	-9.807	-9.807
Operating temperature (K)	291.43	316.38
Operating density (kg/m ³)	1.2129	1.117
Operating pressure	101,325	101,325

Table E.3. Boussinesq model air properties at operating temperatures

Boussinesq model air properties	Model A	Model B
Thermal expansion coefficient (1/K)	0.00345	0.00316
Density (kg/m ³)	1.2129	1.117
Specific heat Cp (J/kgK)	1.006	1.007
Thermal conductivity K (W/mK)	0.0256	0.0273
Dynamic viscosity (kg/ms)	0.0000183	0.0000195

APPENDIX F: FLUENT SCALED RESIDUALS OF DSF MODEL

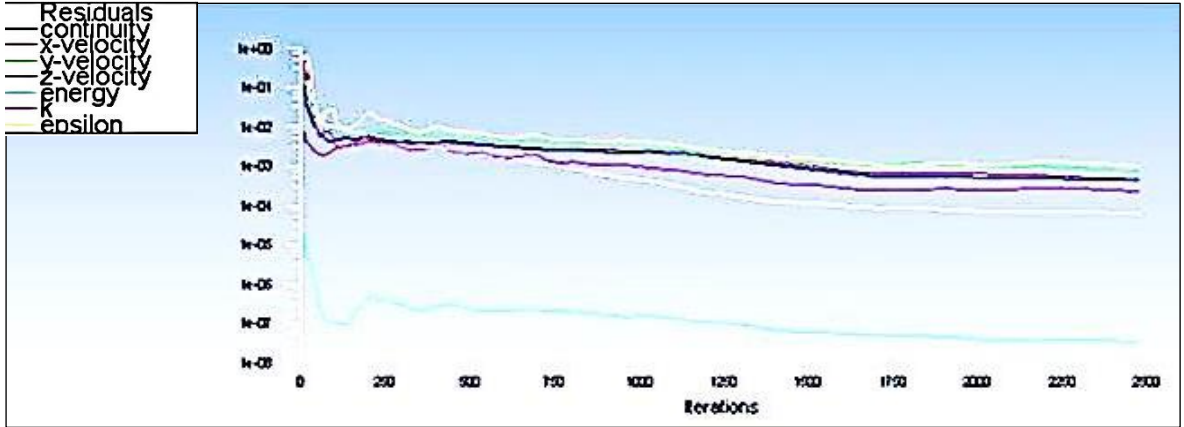


Figure F.1. Scaled residuals of DSF Model A

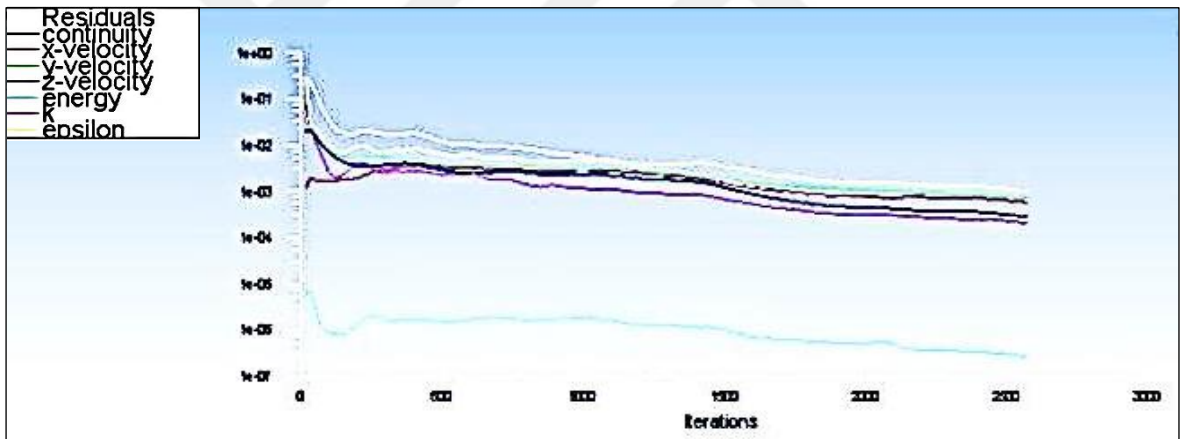


Figure F.2. Scaled residuals of DSF Model B

APPENDIX G: ENERGY ZONE DIMENSIONS OF NEW HOUSE

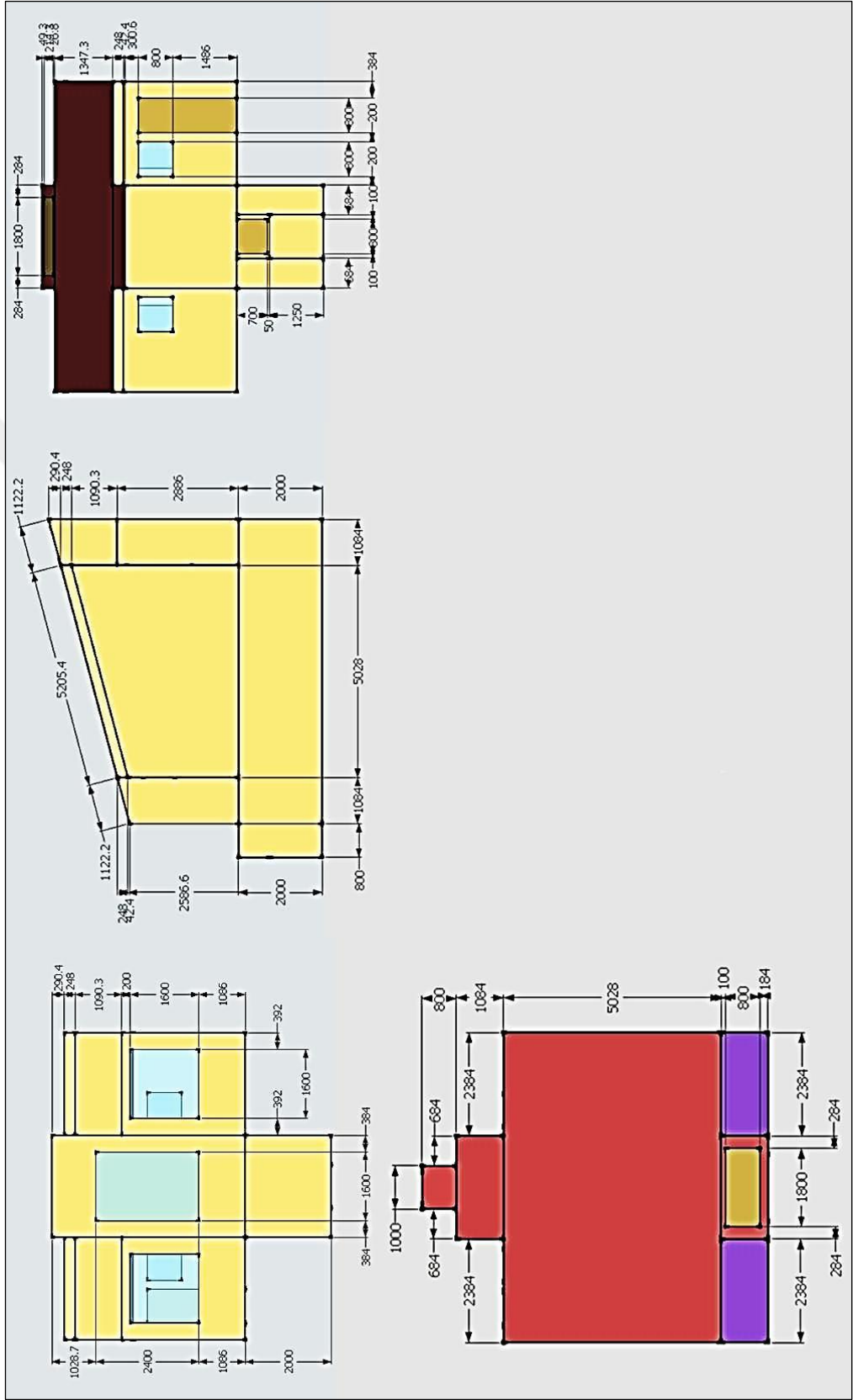


Figure G.1.1. Energy zone dimensions of new house

APPENDIX H: ENERGYPLUS SETUP OF NEW HOUSE

Algorithm

- i) Solar distribution is set as full exterior with reflections in “Building” class of EnergyPlus 8.0.
- ii) “Surface Convection Algorithm Inside”, default indoor surface heat transfer convection algorithm to be used for all zones, is set as TARP (variable natural convection based on temperature difference by ASHRAE and Walton).
- iii) “Surface Convection Algorithm Outside”, default outside surface heat transfer convection algorithm to be used for all zones, is set as MoWiTT (correlation from measurements by Klems and Yazdanian for smooth surfaces).
- iv) Conduction Finite Difference (ConFD) is used as “Heat Balance Algorithm”.
- v) “Timestep” which is used in the Heat Balance Model calculation for heat transfer and load calculations, is selected as 30 timesteps per hour. The minimum value suggested for ConFD is 20 timesteps per hour.

Weather and Ground

- i) Turkey Istanbul 170600 IWEC weather data available through the U.S. Department of Energy is used, including temperature, relative humidity, wind, and solar insolation in “Site Location” and “Run Period” [112].
- ii) Temperatures defined in “Site Ground Temperature FC factor Method” with the C-factor and F-factor methods, are specifically used for underground walls and ground floors. These temperatures are close to the monthly average outdoor air temperature delayed by 3 months for the location. These values and perimeters of underground space and earth tube are taken into account as advised by ASHRAE [113] [114] (Table I.1).

Schedule

- i) “Schedule Compact” is used to create activity, efficiency, clothing, air velocity, occupancy, intermittent, lighting, window vent, shade.

- ii) Winter/summer vent and shade schedules are introduced in order to open all air vents and the south-side shades from 5 May until 1 October (summer period).
- iii) The heating setpoint is defined as 18 °C between 7:00 and 22:00, and 14 °C otherwise. The cooling setpoint is defined as 26 °C between 7:00 and 22:00, and 30 °C otherwise. (Table I.1).

Material

Regular materials including RBS, glass material, window gas, window shade and properties are described with full set of thermal properties in “Materials”, “Window Material Glazing”, “Window Material Gas” and “Window Material Shade” respectively (Table I.2).

Construction

- i) Construction layers are defined from outside layer to the inside in “Construction”, underground walls are defined in “Construction C factor Underground Wall” and underground floors (or slab-on-grade) in “Construction F factor Ground Floor”.
- ii) “Building Surface Detailed” allows for detailed entry of building heat transfer surfaces. It does not include subsurfaces such as windows or doors (Table I.3).

Fenestration and Shading

- i) “Fenestration Surface Detailed” allows for detailed entry of subsurfaces (windows, doors, glass doors, tubular daylighting devices).
- ii) “Window Property Shading Control” specifies the type, location, and controls for window shades, window blinds, and switchable glazing. Shading type is defined as interior shade.
- iii) “Shading Building Detailed” used is used for shading elements such as trees, other buildings, parts of this building not being modeled. Each pair of windows on the south-side of the living quarters has 1,084 mm x 2,384 mm outside shades which screen the sun in summer (Table I.4).

Occupancy and Equipment

- i) “People” sets internal gains and contaminant rates for occupants in the zone. Thermal comfort model type is set as AdaptiveCEN15251.
- ii) “Lights” sets internal gains for lights in the zone. Lighting level is set as 300 W.
- iii) “Electric Equipment” sets internal gains for electric equipment in the zone. Design level is set as 5.38 W/m² (Table I.5).

Airflow

- i) “Airflow Network Simulation Control” defines the global parameters used in an Airflow Network simulation.
- ii) “Airflow Network Multizone Zone” is used to simultaneously control a thermal zone's window and door openings.
- iii) “Airflow Network Multizone Surface” specifies the properties of a surface linkage through which air flows.
- iv) “Airflow Network Multizone Reference Crack Conditions” specifies the conditions under which the air mass flow coefficient was measured.
- v) “Airflow Network Multizone Surface Crack” specifies the properties of airflow through a crack.
- vi) “Airflow Network Multizone Component Simple Opening” specifies the properties of airflow through windows and doors (window, door and glass door heat transfer subsurfaces) when they are closed or open.
- vii) “Airflow Network Multizone Component Horizontal Opening” specifies the properties of airflow through a horizontal opening (Table I.6).

Heating, Ventilating and Air Conditioning

- i) “Zone Control Thermostat” defines the Thermostat settings for a zone or list of zones and “Thermostat Setpoint Dual Setpoint” is used for a heating and cooling thermostat with dual setpoints.

- ii) Even though there is no mechanical ventilation, “Zone HVAC Ideal Load Air System”, “Zone HVAC Equipment List” and “Zone HVAC Equipment Connections” need to be defined to run the simulation (Table I.7).

Output

“Output Variable Dictionary”, “Output Surfaces Drawing”, “Output Table Summary Reports” “Output Control Table Style”, “Output Variable”, “Output Meter” and “Output SQLite” need to be defined in order to obtain the simulation outputs.



APPENDIX I: ENERGYPLUS INPUT DATA OF NEW HOUSE

Field	Units	Obt1	Obt2	Obt3	Obt4	Obt5	Obt6	Obt7	Obt8	Obt9	Obt10	Obt11	Obt12
Schedule Type	Units	Obt1	Obt2	Obt3	Obt4	Obt5	Obt6	Obt7	Obt8	Obt9	Obt10	Obt11	Obt12
Name	Units	Obt1	Obt2	Obt3	Obt4	Obt5	Obt6	Obt7	Obt8	Obt9	Obt10	Obt11	Obt12
Activity Sch	Any Number	Through: 12/31	Through: 12/31	Through: 12/31	Through: 12/31	Fraction	Fraction	Temperature	Temperature	Temperature	Fraction	Fraction	Fraction
Any Number	Any Number	For: AIDays	For: AIDays	For: AIDays	For: AIDays	Through: 12/31	Through: 12/31	Through: 12/31	Through: 12/31	Through: 12/31	Through: 12/31	Through: 12/31	Through: 12/31
Unit: 24.00	Unit: 24.00	Unit: 24.00	Unit: 24.00	Unit: 24.00	Unit: 24.00	Unit: 8.00	Unit: 18.00	Unit: 7.00	Unit: 7.00	Unit: 7.00	Unit: 24.00	Unit: 24.00	Unit: 1.00
Unit: 131.8	0	1	0	1	0.137	1	0	14	30	4	0	0	0.45
January Ground Temperature	C	11.4											
February Ground Temperature	C	7.9											
March Ground Temperature	C	5.8											
April Ground Temperature	C	4.9											
May Ground Temperature	C	7.3											
June Ground Temperature	C	12.2											
July Ground Temperature	C	16.8											
August Ground Temperature	C	21.6											
September Ground Temperature	C	24.1											
October Ground Temperature	C	24.2											
November Ground Temperature	C	20.8											
December Ground Temperature	C	16.5											
Field 1	varies												
Field 2	varies												
Field 3	varies												
Field 4	varies												
Field 5	varies												
Field 6	varies												
Field 7	varies												
Field 8	varies												
Field 9	varies												
Field 10	varies												
Field 11	varies												
Field 12	varies												
Field 13	varies												
Field 14	varies												
Field 15	varies												
Field 16	varies												
Field 17	varies												
Field 18	varies												
Field 19	varies												
Field 20	varies												
Field 21	varies												
Field 22	varies												
Field 23	varies												
Field 24	varies												
Field 25	varies												
Field 26	varies												
Field 27	varies												
Field 28	varies												
Field 29	varies												
Field 30	varies												
Field 31	varies												
Field 32	varies												
Field 33	varies												
Field 34	varies												
Field 35	varies												
Field 36	varies												
Field 37	varies												
Field 38	varies												
Field 39	varies												
Field 40	varies												
Field 41	varies												
Field 42	varies												
Field 43	varies												
Field 44	varies												
Field 45	varies												
Field 46	varies												

Figure I.1. Ground and schedule data

Field	Units	Obj1	Obj2	Obj3	Obj4	Obj5	Obj6
Name		M11 100mm lightweight concrete	1/2mm Galvanized Steel	3 1/2" Styrofoam	Radiant Barrier	101 25mm insulation board	F08 Metal surface
Roughness		MediumRough	Smooth	MediumSmooth	Smooth	MediumRough	Smooth
Thickness	m	0.1016	0.0005	0.0889	0.013	0.0254	0.008
Conductivity	W/m-K	0.53	18	0.036057	235	0.03	45.28
Density	kg/m3	1280	7850	32	1070	43	7824
Specific Heat	J/kg-K	840	452	1400	897	1210	500
Thermal Absorptance					0.03		
Solar Absorptance					0.03		
Visible Absorptance					0.03		

Field	Units	Obj1
Name		CLEAR 6MM
Optical Data Type		SpectralAverage
Window Glass Spectral Data Set Name		
Thickness	m	0.006
Solar Transmittance at Normal Incidence		0.775
Front Side Solar Reflectance at Normal Incidence		0.071
Back Side Solar Reflectance at Normal Incidence		0.071
Visible Transmittance at Normal Incidence		0.881
Front Side Visible Reflectance at Normal Incidence		0.08
Back Side Visible Reflectance at Normal Incidence		0.08
Infrared Transmittance at Normal Incidence		0
Front Side Infrared Hemispherical Emissivity		0.84
Back Side Infrared Hemispherical Emissivity		0.84
Conductivity	W/m-K	0.9
Dirt Correction Factor for Solar and Visible Transmittance		
Solar Diffusing		
Young's modulus	Pa	
Poisson's ratio		

Field	Units	Obj1
Name		AIR 6MM
Gas Type		Air
Thickness	m	0.0063
Conductivity Coefficient A	W/m-K	
Conductivity Coefficient B	W/m-K2	
Conductivity Coefficient C	W/m-K3	
Viscosity Coefficient A	kg/m-s	
Viscosity Coefficient B	kg/m-s-K	
Viscosity Coefficient C	kg/m-s-K2	
Specific Heat Coefficient A	J/kg-K	
Specific Heat Coefficient B	J/kg-K2	
Specific Heat Coefficient C	J/kg-K3	
Molecular Weight	g/mol	
Specific Heat Ratio		

Field	Units	Obj1
Name		Radiant Barrier Shades
Solar Transmittance	dimensionless	0.28
Solar Reflectance	dimensionless	0.7
Visible Transmittance	dimensionless	0
Visible Reflectance	dimensionless	0.97
Infrared Hemispherical Emissivity	dimensionless	0.018
Infrared Transmittance	dimensionless	0.9
Thickness	m	0.00013
Conductivity	W/m-K	235
Shade to Glass Distance	m	0.04
Top Opening Multiplier		
Bottom Opening Multiplier		
Left-Side Opening Multiplier		
Right-Side Opening Multiplier		0
Airflow Permeability	dimensionless	

Figure I.2. Material data

FBID	Units	Obj1	Obj2	Obj3	Obj4	Obj5	Obj6	Obj7	Obj8	Obj9	Obj10	Obj11	Obj12
Name		Underground Surface	House Floor	House Wall	House Ceiling	House Window	House Door	House Window	House Roof	Underground Ceiling	PCM Wall of Zone04	PCM Wall of Zone02	Air Vent
Outside Layer		M11 100mm lightweight concrete	M11 100mm lightweight concrete	3 1/2" Styrofoam	3 1/2" Styrofoam	CLEAR BMH	F08 Metal surface	CLEAR BMH	17/2mm Galvanized Steel	3 1/2" Styrofoam	3 1/2" Styrofoam	3 1/2" Styrofoam	17/2mm Galvanized Steel
Layer 2						AIR BMH	I01 25mm insulation board		Resident Barrier	M11 100mm lightweight concrete			3 1/2" Styrofoam
Layer 3						CLEAR BMH							17/2mm Galvanized Steel
Units	Units	Obj1	Obj2	Obj3	Obj4	Obj5	Obj6	Obj7	Obj8	Obj9	Obj10	Obj11	Obj12
Name		Underground Wall	Underground Wall										
C-Factor	W/m2K	6.48	6.48										
Height	m	2	1.25										
FBID	Units	Obj1	Obj2	Obj3	Obj4	Obj5	Obj6	Obj7	Obj8	Obj9	Obj10	Obj11	Obj12
Name		Underground Floor	Ground Floor	Underground Floor II									
F-Factor	W/mK	1.264	1.264										
Area	m2	17.04	11.987	0.8									
PerimeterExposed	m	18.128	9.796	2.6									
FBID	Units	Obj1	Obj2	Obj3	Obj4	Obj5	Obj6	Obj7	Obj8	Obj9	Obj10	Obj11	Obj12
Name		Zone01:Wall01	Zone01:Wall02	Zone01:Wall03	Zone01:Wall04	Zone01:Wall05	Zone01:Wall06	Zone01:Wall07	Zone01:Wall08	Zone01:Wall09	Zone01:Wall10	Zone01:Wall11	Zone01:Wall12
Surface Type		Wall	Wall	Wall	Wall	Wall	Wall	Wall	Wall	Wall	Wall	Wall	Wall
Construction Name		Underground Wall	Underground Wall	Underground Wall	Underground Surface	Underground Wall	Underground Wall	Underground Wall	Underground Ceiling	Underground Ceiling	Underground Ceiling	Underground Ceiling	Underground Ceiling
Zone Name		Zone01	Zone01	Zone01	Zone01	Zone01	Zone01	Zone01	Zone01	Zone01	Zone01	Zone01	Zone01
Outside Boundary Condition		GroundDiactorMethod	GroundDiactorMethod	GroundDiactorMethod	GroundDiactorMethod	GroundDiactorMethod	GroundDiactorMethod	GroundDiactorMethod	GroundDiactorMethod	GroundDiactorMethod	GroundDiactorMethod	GroundDiactorMethod	GroundDiactorMethod
Outside Boundary Condition Object		NoSun	NoSun	NoSun	NoSun	NoSun	NoSun	NoSun	NoSun	NoSun	NoSun	NoSun	NoSun
Sun Exposure		NoWind	NoWind	NoWind	NoWind	NoWind	NoWind	NoWind	NoWind	NoWind	NoWind	NoWind	NoWind
View Factor to Ground		0	0	0	0	0	0	0	0	0	0	0	0
Number of Vertices		4	4	4	4	4	4	4	4	4	4	4	4
Vertex 1 X-coordinate	m	-1.184	-1.184	-0.5	0.5	1.184	1.184	-1.184	-1.184	-1.184	-1.184	-1.184	-1.184
Vertex 1 Y-coordinate	m	-0.184	7.012	7.012	7.012	7.012	-0.184	0.9	5.928	7.012	7.012	7.012	7.012
Vertex 1 Z-coordinate	m	2.1	2.1	2.1	2.1	2.1	2.1	2.1	2.1	2.1	2.1	2.1	2.1
Vertex 2 X-coordinate	m	-1.184	-1.184	-0.5	0.5	1.184	1.184	-1.184	-1.184	-1.184	-1.184	-1.184	-1.184
Vertex 2 Y-coordinate	m	-0.184	7.012	7.012	7.012	7.012	-0.184	0.9	5.928	7.012	7.012	7.012	7.012
Vertex 2 Z-coordinate	m	0.1	0.1	0.1	0.1	0.1	0.1	0.1	0.1	0.1	0.1	0.1	0.1
Vertex 3 X-coordinate	m	1.184	-1.184	-0.5	-0.5	1.184	1.184	-1.184	-1.184	-1.184	-1.184	-1.184	-1.184
Vertex 3 Y-coordinate	m	-0.184	-0.184	7.012	7.012	7.012	7.012	-0.184	0.9	5.928	7.012	7.012	7.012
Vertex 3 Z-coordinate	m	0.1	0.1	0.1	0.1	0.1	0.1	0.1	0.1	0.1	0.1	0.1	0.1
Vertex 4 X-coordinate	m	1.184	-1.184	-0.5	-0.5	1.184	1.184	-1.184	-1.184	-1.184	-1.184	-1.184	-1.184
Vertex 4 Y-coordinate	m	-0.184	-0.184	7.012	7.012	7.012	7.012	-0.184	0.9	5.928	7.012	7.012	7.012
Vertex 4 Z-coordinate	m	2.1	2.1	2.1	2.1	2.1	2.1	2.1	2.1	2.1	2.1	2.1	2.1
FBID	Units	Obj10	Obj11	Obj12	Obj13	Obj14	Obj15	Obj16	Obj17	Obj18	Obj19	Obj20	
Name		Zone01:Floor01	Zone02:Wall01	Zone02:Wall02	Zone02:Wall03	Zone02:Wall04	Zone02:Wall05	Zone02:Wall06	Zone02:Wall07	Zone02:Wall08	Zone02:Wall09	Zone02:Wall10	
Surface Type		Floor	Wall	Wall	Wall	Wall	Wall	Wall	Wall	Wall	Wall	Floor	
Construction Name		Underground Floor	House Wall	House Wall	House Wall	House Wall	House Wall	House Wall	House Wall	House Wall	House Wall	House Wall	
Zone Name		Zone01	Zone02	Zone02	Zone02	Zone02	Zone02	Zone02	Zone02	Zone02	Zone02	Zone02	
Outside Boundary Condition		GroundDiactorMethod	Surface	Surface	Surface	Surface	Surface	Surface	Surface	Surface	Surface	Surface	
Outside Boundary Condition Object		NoSun	NoSun	NoSun	NoSun	NoSun	NoSun	NoSun	NoSun	NoSun	NoSun	NoSun	
Sun Exposure		NoWind	NoWind	NoWind	NoWind	NoWind	NoWind	NoWind	NoWind	NoWind	NoWind	NoWind	
View Factor to Ground		0	0	0	0	0	0	0	0	0	0	0	
Number of Vertices		4	4	4	4	4	4	4	4	4	4	4	
Vertex 1 X-coordinate	m	1.184	-1.184	-0.92	-0.92	-0.92	-0.92	-0.92	-0.92	-0.92	-0.92	-0.92	
Vertex 1 Y-coordinate	m	7.012	7.012	3.9763	3.9763	3.9763	3.9763	3.9763	3.9763	3.9763	3.9763	3.9763	
Vertex 1 Z-coordinate	m	0.1	0.1	0.1	0.1	0.1	0.1	0.1	0.1	0.1	0.1	0.1	
Vertex 2 X-coordinate	m	1.184	-1.184	-0.92	-0.92	-0.92	-0.92	-0.92	-0.92	-0.92	-0.92	-0.92	
Vertex 2 Y-coordinate	m	-0.184	-0.184	7.012	7.012	7.012	7.012	7.012	7.012	7.012	7.012	7.012	
Vertex 2 Z-coordinate	m	0.1	0.1	0.1	0.1	0.1	0.1	0.1	0.1	0.1	0.1	0.1	
Vertex 3 X-coordinate	m	-1.184	-1.184	-0.92	-0.92	-0.92	-0.92	-0.92	-0.92	-0.92	-0.92	-0.92	
Vertex 3 Y-coordinate	m	-0.184	-0.184	7.012	7.012	7.012	7.012	7.012	7.012	7.012	7.012	7.012	
Vertex 3 Z-coordinate	m	0.1	0.1	0.1	0.1	0.1	0.1	0.1	0.1	0.1	0.1	0.1	
Vertex 4 X-coordinate	m	1.184	-1.184	-0.92	-0.92	-0.92	-0.92	-0.92	-0.92	-0.92	-0.92	-0.92	
Vertex 4 Y-coordinate	m	7.012	7.012	3.9763	3.9763	3.9763	3.9763	3.9763	3.9763	3.9763	3.9763	3.9763	
Vertex 4 Z-coordinate	m	0.1	0.1	0.1	0.1	0.1	0.1	0.1	0.1	0.1	0.1	0.1	

Figure I.3. Construction data

Field	Unit	01b21	01b22	01b23	01b24	01b25	01b26	01b27	01b28	01b29	01b30	01b31	01b32
Name		Zone02.Floor02	Zone02.Floor03	Zone03.Wall01	Zone03.Wall02	Zone03.Wall03	Zone03.Wall04	Zone03.Wall05	Zone03.Wall06	Zone03.Wall07	Zone03.Wall08	Zone03.Floor01	Zone03.Floor01
Surface Type		Floor	Floor	Wall	Wall	Wall	Wall	Wall	Wall	Wall	Wall	Floor	Floor
Construction Name		Ground Floor	Ground Floor	House Wall	House Wall	House Wall	House Wall	House Wall	House Wall	House Wall	House Wall	House Wall	House Wall
Zone Name		Zone02	Zone02	Zone03	Zone03	Zone03	Zone03	Zone03	Zone03	Zone03	Zone03	Zone03	Zone03
Outside Boundary Condition		Surface	GroundDictaMethod	Surface	Surface	Surface	Surface	Surface	Surface	Surface	Surface	Surface	Surface
Outside Boundary Condition Object		Zone01.Ceiling02	NoSun	Zone04.Wall03	Zone04.Wall03	Zone04.Wall03	Zone04.Wall03	Zone04.Wall03	Zone05.Wall01	Zone05.Wall01	Zone05.Wall01	Zone02.Ceiling01	Zone02.Ceiling01
Sun Exposure		NoSun	NoSun	NoWind	NoWind	NoWind	NoWind	NoWind	NoWind	NoWind	NoWind	NoSun	NoSun
Wind Exposure		NoWind	NoWind	SurfExposed	WindExposed	WindExposed	WindExposed	WindExposed	WindExposed	WindExposed	WindExposed	WindExposed	WindExposed
View Factor to Ground		0	0	0	0	0	0	0	0	0	0	0	0
Number of Vertices		4	4	4	4	4	4	4	4	4	4	4	4
Vertex 1 X-coordinate	m	1.184	-1.184	1.184	-1.184	-3.568	-1.184	-1.184	1.184	3.568	3.568	-3.568	-3.568
Vertex 1 Y-coordinate	m	4.935	4.935	0	0	5.028	5.028	5.028	5.028	5.028	5.028	0	0
Vertex 1 Z-coordinate	m	0	0	0.348	0.348	-0.9953	-0.9953	-0.9953	-0.9953	-0.9953	-0.9953	0.348	0.1
Vertex 2 X-coordinate	m	1.184	-1.184	1.184	-1.184	-3.568	-1.184	-1.184	1.184	3.568	3.568	-3.568	-3.568
Vertex 2 Y-coordinate	m	-0.092	-0.092	0	0	5.028	5.028	5.028	5.028	5.028	5.028	0	0
Vertex 2 Z-coordinate	m	0	0	0.1	0.1	-1.2473	-1.2473	-1.2473	-1.2473	-1.2473	-1.2473	0.1	-0.9953
Vertex 3 X-coordinate	m	-1.184	-3.568	3.568	1.184	-1.184	-3.568	-1.184	-1.184	1.184	3.568	-3.568	-3.568
Vertex 3 Y-coordinate	m	-0.092	-0.092	0	0	5.028	5.028	5.028	5.028	5.028	5.028	0	0
Vertex 3 Z-coordinate	m	0	0	0.1	0.1	-1.2473	-1.2473	-1.2473	-1.2473	-1.2473	-1.2473	0.1	-0.9953
Vertex 4 X-coordinate	m	-1.184	-3.568	3.568	1.184	-1.184	-3.568	-1.184	-1.184	1.184	3.568	-3.568	-3.568
Vertex 4 Y-coordinate	m	4.935	4.935	0	0	5.028	5.028	5.028	5.028	5.028	5.028	0	0
Vertex 4 Z-coordinate	m	0	0	0.348	0.348	-0.9953	-0.9953	-0.9953	-0.9953	-0.9953	-0.9953	0.348	0.1
Field		01b33	01b34	01b35	01b36	01b37	01b38	01b39	01b40	01b41	01b42	01b43	01b44
Name		Zone04.Wall01	Zone04.Wall02	Zone04.Wall03	Zone04.Wall04	Zone04.Wall05	Zone04.Floor01	Zone04.Floor01	Zone05.Wall01	Zone05.Wall02	Zone05.Wall03	Zone05.Wall04	Zone05.Wall05
Surface Type		Wall	Wall	Wall	Wall	Wall	Floor	Floor	Wall	Wall	Wall	Wall	Wall
Construction Name		House Wall	House Wall	House Wall	PCH Wall of Zone04	House Wall	House Floor	House Floor	House Wall	House Wall	House Wall	House Wall	House Wall
Zone Name		Zone04	Zone04	Zone04	Zone04	Zone04	Zone04	Zone04	Zone05	Zone05	Zone05	Zone05	Zone05
Outside Boundary Condition		Surface	Surface	Surface	Surface	Surface	Surface	Surface	Surface	Surface	Surface	Surface	Surface
Outside Boundary Condition Object		Zone03.Wall02	Zone02.Wall02	Zone03.Wall02	Zone02.Wall02	Zone03.Wall02	Zone01.Ceiling01	Zone01.Ceiling01	Zone03.Wall05	Zone02.Wall06	Zone02.Wall06	Zone02.Wall06	Zone02.Wall06
Sun Exposure		SurfExposed	SurfExposed	SurfExposed	NoSun	SurfExposed	SurfExposed	SurfExposed	NoSun	NoSun	SurfExposed	SurfExposed	SurfExposed
Wind Exposure		WindExposed	WindExposed	WindExposed	NoWind	WindExposed	WindExposed	WindExposed	NoWind	NoWind	WindExposed	WindExposed	WindExposed
View Factor to Ground		4	4	4	4	4	4	4	4	4	4	4	4
Number of Vertices		4	4	4	4	4	4	4	4	4	4	4	4
Vertex 1 X-coordinate	m	-1.184	-1.184	1.184	1.184	1.184	1.184	1.184	-1.184	-1.184	-1.184	1.184	1.184
Vertex 1 Y-coordinate	m	0	1.084	1.084	1.084	4.5147	4.5147	4.5147	0	2.877	2.877	2.877	2.877
Vertex 1 Z-coordinate	m	4.5147	4.2243	4.2243	3.9763	4.2243	4.2243	4.2243	0	2.877	2.877	2.877	2.877
Vertex 2 X-coordinate	m	-1.184	-1.184	1.184	1.184	1.184	1.184	1.184	-1.184	-1.184	-1.184	1.184	1.184
Vertex 2 Y-coordinate	m	0	1.084	1.084	1.084	4.5147	4.5147	4.5147	0	2.877	2.877	2.877	2.877
Vertex 2 Z-coordinate	m	0	3.9763	3.9763	0	4.2243	4.2243	4.2243	0	2.877	2.877	2.877	2.877
Vertex 3 X-coordinate	m	-1.184	-1.184	1.184	1.184	1.184	1.184	1.184	-1.184	-1.184	-1.184	1.184	1.184
Vertex 3 Y-coordinate	m	0	1.084	1.084	1.084	4.5147	4.5147	4.5147	0	2.877	2.877	2.877	2.877
Vertex 3 Z-coordinate	m	0	3.9763	3.9763	0	4.2243	4.2243	4.2243	0	2.877	2.877	2.877	2.877
Vertex 4 X-coordinate	m	-1.184	-1.184	1.184	1.184	1.184	1.184	1.184	-1.184	-1.184	-1.184	1.184	1.184
Vertex 4 Y-coordinate	m	0	1.084	1.084	1.084	4.5147	4.5147	4.5147	0	2.877	2.877	2.877	2.877
Vertex 4 Z-coordinate	m	0	3.9763	3.9763	0	4.2243	4.2243	4.2243	0	2.877	2.877	2.877	2.877
Field		01b45	01b46	01b47	01b48	01b49	01b50	01b51	01b52	01b53	01b54	01b55	01b56
Name		Zone05.Wall05	Zone05.Floor01	Zone06.Wall01	Zone06.Wall02	Zone06.Wall03	Zone06.Wall04	Zone06.Ceiling01	Zone06.Floor01	Zone06.Floor01	Zone06.Wall01	Zone06.Wall02	Zone06.Wall03
Surface Type		Wall	Floor	Wall	Wall	Wall	Wall	Ceiling	Floor	Floor	Wall	Wall	Wall
Construction Name		House Wall	House Floor	Underground Surface	Underground Wall	Underground Wall	Underground Wall	Underground Surface	Underground Floor II	Underground Floor II	Underground Floor II	Underground Floor II	Underground Floor II
Zone Name		Zone05	Zone05	Zone06	Zone06	Zone06	Zone06	Zone06	Zone06	Zone06	Zone06	Zone06	Zone06
Outside Boundary Condition		Surface	Surface	Surface	Surface	Surface	Surface	Surface	Surface	Surface	Surface	Surface	Surface
Outside Boundary Condition Object		Zone01.Ceiling03	Zone01.Ceiling03	Zone01.Wall04	Zone01.Wall04	Zone01.Wall04	Zone01.Wall04	Zone01.Wall04	Zone05	Zone05	Zone05	Zone05	Zone05
Sun Exposure		SurfExposed	SurfExposed	NoSun	NoSun	NoSun	NoSun	SurfExposed	SurfExposed	SurfExposed	NoSun	NoSun	NoSun
Wind Exposure		WindExposed	WindExposed	NoWind	NoWind	NoWind	NoWind	WindExposed	WindExposed	WindExposed	NoWind	NoWind	NoWind
View Factor to Ground		4	4	4	4	4	4	4	4	4	4	4	4
Number of Vertices		4	4	4	4	4	4	4	4	4	4	4	4
Vertex 1 X-coordinate	m	1.184	1.184	-0.5	-0.5	0.5	0.5	-0.5	0.5	0.5	0.5	0.5	0.5
Vertex 1 Y-coordinate	m	2.877	2.877	0	0.8	0.8	0.8	0.8	0.8	0.8	0.8	0.8	0.8
Vertex 1 Z-coordinate	m	1.184	1.184	-0.5	-0.5	0.5	0.5	-0.5	0.5	0.5	0.5	0.5	0.5
Vertex 2 X-coordinate	m	0	1.084	0	0.8	0.8	0.8	0.8	0.8	0.8	0.8	0.8	0.8
Vertex 2 Y-coordinate	m	0	1.084	0	0.8	0.8	0.8	0.8	0.8	0.8	0.8	0.8	0.8
Vertex 2 Z-coordinate	m	0	2.9688	0	-0.5	-0.5	-0.5	0.5	0.5	0.5	-0.5	-0.5	-0.5
Vertex 3 X-coordinate	m	1.184	1.184	-0.5	-0.5	0.5	0.5	-0.5	0.5	0.5	0.5	0.5	0.5
Vertex 3 Y-coordinate	m	0	1.084	0	0.8	0.8	0.8	0.8	0.8	0.8	0.8	0.8	0.8
Vertex 3 Z-coordinate	m	0	2.9688	0	-0.5	-0.5	-0.5	0.5	0.5	0.5	-0.5	-0.5	-0.5
Vertex 4 X-coordinate	m	1.184	1.184	-0.5	-0.5	0.5	0.5	-0.5	0.5	0.5	0.5	0.5	0.5
Vertex 4 Y-coordinate	m	0	1.084	0	0.8	0.8	0.8	0.8	0.8	0.8	0.8	0.8	0.8
Vertex 4 Z-coordinate	m	0	2.9688	0	-0.5	-0.5	-0.5	0.5	0.5	0.5	-0.5	-0.5	-0.5
Vertex 4 Z-coordinate	m	1.084	1.084	0	0.8	0.8	0.8	0.8	0.8	0.8	0.8	0.8	0.8
Vertex 4 Z-coordinate	m	2.877	2.877	0	2	2	2	2	2	2	2	2	2

Figure I.4. Construction data continued

Field	Units	Obj1	Obj2	Obj3	Obj4	Obj5	Obj6	Obj7	Obj8	Obj9	Obj10	Obj11
Name		Zone01:Vent01NB	Zone01:Vent02NT	Zone01:Vent03ST	Zone02:Win01S	Zone02:Win02S	Zone02:Win03N	Zone02:Win04N	Door_1	Zone03:Vent01S	Zone03:Vent02N	Zone04:Win01S
Surface Type		Door	Door	Door	Window	Window	Window	Window	Door	Door	Door	Window
Construction Name		Air Vent	Air Vent	Air Vent	House Window	House Window	House Window	House Window	House Door	Air Vent	Air Vent	South Shell Window
Building Surface Name		Zone01:Wall04	Zone01:Ceiling03	Zone01:Ceiling01	Zone02:Wall03	Zone02:Wall01	Zone02:Wall07	Zone02:Wall05	Zone02:Wall05	Zone03:Wall02	Zone03:Wall06	Zone04:Wall01
Outside Boundary Condition Object		Zone05:Vent02B	Zone05:Vent01B	Zone04:Vent01B						Zone04:Vent03RT	Zone05:Vent02RT	
View Factor to Ground												
Shading Control Name					ShadingControl	ShadingControl						ShadingControl
Frame and Divider Name												
Multiplier												
Number of Vertices		4	4	4	4	4	4	4	4	4	4	4
Vertex 1 X-coordinate	m	0.4	-0.8	-0.8	-3.176	1.576	2.184	-1.384	-2.384	-1	1	-0.8
Vertex 1 Y-coordinate	m	7.012	6.728	0.8	-0.092	-0.092	4.936	4.936	4.936	0	5.028	0
Vertex 1 Z-coordinate	m	0.65	2.1	2.1	2.686	2.686	2.286	2.286	2.286	0.2553	-1.092	3.486
Vertex 2 X-coordinate	m	0.4	-0.8	-0.8	-3.176	1.576	2.184	-1.384	-2.384	-1	1	-0.8
Vertex 2 Y-coordinate	m	7.012	6.028	0.1	-0.092	-0.092	4.936	4.936	4.936	0	5.028	0
Vertex 2 Z-coordinate	m	0.25	2.1	2.1	1.086	1.086	1.486	1.486	0	0.1	-1.2473	1.086
Vertex 3 X-coordinate	m	-0.4	0.8	0.8	-1.576	3.176	1.384	-2.184	-3.184	1	-1	0.8
Vertex 3 Y-coordinate	m	7.012	6.028	0.1	-0.092	-0.092	4.936	4.936	4.936	0	5.028	0
Vertex 3 Z-coordinate	m	0.25	2.1	2.1	1.086	1.086	1.486	1.486	0	0.1	-1.2473	1.086
Vertex 4 X-coordinate	m	-0.4	0.8	0.8	-1.576	3.176	1.384	-2.184	-3.184	1	-1	0.8
Vertex 4 Y-coordinate	m	7.012	6.728	0.8	-0.092	-0.092	4.936	4.936	4.936	0	5.028	0
Vertex 4 Z-coordinate	m	0.65	2.1	2.1	2.686	2.686	2.286	2.286	2.286	0.2553	-1.092	3.486

Field	Units	Obj12	Obj13	Obj14	Obj15	Obj16	Obj17	Obj18
Name		Zone04:Vent01B	Zone04:Vent02T	Zone04:Vent03RT	Zone05:Vent01B	Zone05:Vent02RT	Zone06:Vent01Out	Zone06:Vent02B
Surface Type		Door	Door	Door	Door	Door	Door	Door
Construction Name		Air Vent	Air Vent	Air Vent	Air Vent	Air Vent	Air Vent	Air Vent
Building Surface Name		Zone04:Floor01	Zone04:Floor01	Zone04:Wall03	Zone05:Floor01	Zone05:Wall01	Zone06:Wall03T	Zone06:Wall01
Outside Boundary Condition Object		Zone01:Vent03ST		Zone03:Vent01S	Zone01:Vent02NT	Zone03:Vent02N		Zone01:Vent01NB
View Factor to Ground								
Shading Control Name								
Frame and Divider Name								
Multiplier								
Number of Vertices		4	4	4	4	4	4	4
Vertex 1 X-coordinate	m	0.8	0.9	1	0.8	-1	0.4	-0.4
Vertex 1 Y-coordinate	m	0.984	0.184011285455	1.084	0.8	0	0.8	0
Vertex 1 Z-coordinate	m	0	4.465403987734	4.1316	0	2.7843	2	0.55
Vertex 2 X-coordinate	m	0.8	0.9	1	0.8	-1	0.4	-0.4
Vertex 2 Y-coordinate	m	0.284	0.984001556332	1.084	0.1	0	0.8	0
Vertex 2 Z-coordinate	m	0	4.251089250944	3.9763	0	2.629	1.3	0.15
Vertex 3 X-coordinate	m	-0.8	-0.9	-1	-0.8	1	-0.4	0.4
Vertex 3 Y-coordinate	m	0.284	0.984001556332	1.084	0.1	0	0.8	0
Vertex 3 Z-coordinate	m	0	4.251089250944	3.9763	0	2.629	1.3	0.15
Vertex 4 X-coordinate	m	-0.8	-0.9	-1	-0.8	1	-0.4	0.4
Vertex 4 Y-coordinate	m	0.984	0.184011285455	1.084	0.8	0	0.8	0
Vertex 4 Z-coordinate	m	0	4.465403987734	4.1316	0	2.7843	2	0.55

Field	Units	Obj1
Name		ShadingControl
Shading Type		InteriorShade
Construction with Shading Name		
Shading Control Type		OhlIScheduleAllows
Schedule Name		WinterSummerShade
Setpoint	W/m2, W or deg C	
Shading Control Is Scheduled		Yes
Glare Control Is Active		No
Shading Device Material Name		Radiant Barrier Shades
Type of Slat Angle Control for Blinds		
Slat Angle Schedule Name		
Setpoint 2	W/m2 or deg C	

Field	Units	Obj1	Obj2
Name		Shading_2	Shading_1
Transmittance Schedule Name			
Number of Vertices		4	4
Vertex 1 X-coordinate	m	-3.568	1.184
Vertex 1 Y-coordinate	m	0.9	0.9
Vertex 1 Z-coordinate	m	4.986	4.986
Vertex 2 X-coordinate	m	-3.568	1.184
Vertex 2 Y-coordinate	m	-0.184	-0.184
Vertex 2 Z-coordinate	m	4.986	4.986
Vertex 3 X-coordinate	m	-1.184	3.568
Vertex 3 Y-coordinate	m	-0.184	-0.184
Vertex 3 Z-coordinate	m	4.986	4.986
Vertex 4 X-coordinate	m	-1.184	3.568
Vertex 4 Y-coordinate	m	0.9	0.9
Vertex 4 Z-coordinate	m	4.986	4.986

Figure I.5. Fenestration and shading data

Field	Units	Obj1
Name		Residents
Zone or ZoneList Name		Zone02
Number of People Schedule Name		OCCUPANCY
Number of People Calculation Method		People
Number of People		2
People per Zone Floor Area	person/m2	
Zone Floor Area per Person	m2/person	
Fraction Radiant		0.3
Sensible Heat Fraction		
Activity Level Schedule Name		Activity Sch
Carbon Dioxide Generation Rate	m3/s-W	0.000000382
Enable ASHRAE 55 Comfort Warnings		
Mean Radiant Temperature Calculation Type		zoneaveraged
Surface Name/Angle Factor List Name		
Work Efficiency Schedule Name		Eff Sch
Clothing Insulation Schedule Name		Clothing Sch
Air Velocity Schedule Name		Air Velo Sch
Thermal Comfort Model 1 Type		AdaptiveCEN15251

Field	Units	Obj1
Name		Lights
Zone or ZoneList Name		Zone02
Schedule Name		LIGHTING
Design Level Calculation Method		LightingLevel
Lighting Level	W	300
Watts per Zone Floor Area	W/m2	
Watts per Person	W/person	
Return Air Fraction		0
Fraction Radiant		0.2
Fraction Visible		0.2
Fraction Replaceable		0
End-Use Subcategory		GeneralLights

Field	Units	Obj1
Name		Electrical Equipment
Zone or ZoneList Name		Zone02
Schedule Name		APT_EQP_SCH
Design Level Calculation Method		Watts/Area
Design Level	W	
Watts per Zone Floor Area	W/m2	5.38
Watts per Person	W/person	
Fraction Latent		0
Fraction Radiant		0.3
Fraction Lost		0

Figure I.6. Occupancy and equipment data

Field	Units	Obj1	Obj2	Obj3	Obj4	Obj5	Obj6	Obj7	Obj8
Name		AFN Ventilation							
AirflowNetwork Control		Multizone/WithoutDistribution							
Wind Pressure Coefficient Type		SurfaceAverageCalculation							
AirflowNetwork Wind Pressure Coefficient Array Name									
Height Selection for Local Wind Pressure Calculation									
Building Type		LOWRISE							
Maximum Number of Iterations	dimensionless	30000							
Initialization Type		ZeroNodePressures							
Relative Airflow Convergence Tolerance	dimensionless	0.00001							
Absolute Airflow Convergence Tolerance	kg/s	0.000001							
Convergence Acceleration Limit	dimensionless	-0.5							
Azimuth Angle of Long Axis of Building	deg	90							
Ratio of Building Width Along Short Axis to Width Along Long Axis		0.704596							
Field	Units	Obj1	Obj2	Obj3	Obj4	Obj5	Obj6	Obj7	Obj8
Zone Name		Zone02	Zone06	Zone05	Zone01	Zone04	Zone03	Zone04	Zone03
Ventilation Control Mode		Constant	Constant	Constant	Constant	Constant	Constant	Constant	Constant
Ventilation Control Zone Temperature Setpoint Schedule Name									
Minimum Venting Open Factor	dimensionless	1	1	1	1	1	1	1	1
Indoor and Outdoor Temperature Difference Lower Limit For Maximum Venting Open Factor	deltac	0	0	0	0	0	0	0	0
Indoor and Outdoor Temperature Difference Upper Limit For Minimum Venting Open Factor	deltac	100	100	100	100	100	100	100	100
Indoor and Outdoor Enthalpy Difference Lower Limit For Maximum Venting Open Factor	deltal/kg	0	0	0	0	0	0	0	0
Indoor and Outdoor Enthalpy Difference Upper Limit For Minimum Venting Open Factor	deltal/kg	300000	300000	300000	300000	300000	300000	300000	300000
Venting Availability Schedule Name									
Field	Units	Obj1	Obj2	Obj3	Obj4	Obj5	Obj6	Obj7	Obj8
Surface Name		Zone02:Wall04	Zone02:Wall08	Zone06:Ceiling01	Zone05:Vent018	Zone05:Vent01B	Zone05:Vent018	Zone05:Vent01B	Zone03:Vent02N
Leakage Component Name		CR-1	CR-1	CR-1	CR-1	CR-1	CR-1	CR-1	CR-1
External Node Name									
Window/Door Opening Factor, or Crack Factor	dimensionless	1	1	1	1	1	1	1	1
Ventilation Control Mode				Constant				Constant	
Ventilation Control Zone Temperature Setpoint Schedule Name									
Minimum Venting Open Factor	dimensionless			1				1	
Indoor and Outdoor Temperature Difference Lower Limit For Maximum Venting Open Factor	deltac								
Indoor and Outdoor Temperature Difference Upper Limit For Minimum Venting Open Factor	deltac	100	100	100	100	100	100	100	100
Indoor and Outdoor Enthalpy Difference Lower Limit For Maximum Venting Open Factor	deltal/kg								
Indoor and Outdoor Enthalpy Difference Upper Limit For Minimum Venting Open Factor	deltal/kg	300000	300000	300000	300000	300000	300000	300000	300000
Venting Availability Schedule Name				WinterSummerVent				WinterSummerVent	

Figure I.7. Airflow network data

Field	Units	Obj8	Obj9	Obj10	Obj11	Obj12	Obj13
Surface Name		Zone03:Vent02N	Zone03:Roof01	Zone03:Vent01S	Zone04:Roof01	Zone04:Vent01B	Zone04:Vent02T
Leakage Component Name		SO_Zone03:Vent02	CR-1	SO_Zone03:Vent01S	CR-1	HO_Zone04:Vent01B	SO_Zone04:Vent02T
External Node Name							
Window/Door Opening Factor, or Crack Factor	dimensionless	1	1	1	1	1	1
Ventilation Control Mode		Constant		Constant		Constant	Constant
Ventilation Control Zone Temperature Setpoint Schedule							
Minimum Venting Open Factor	dimensionless	1		1		1	
Indoor and Outdoor Temperature Difference Lower Limit	deltaC						
Indoor and Outdoor Temperature Difference Upper Limit	deltaC		100		100		
Indoor and Outdoor Enthalpy Difference Lower Limit For	deltaJ/kg						
Indoor and Outdoor Enthalpy Difference Upper Limit For	deltaJ/kg		300000		300000		
Venting Availability Schedule Name							WinterSummerVent

Field	Units	Obj1
Name		CR-1
ReferenceCrackConditions		
Reference Temperature	C	20
Reference Barometric Pressure	Pa	101325
Reference HumidRat	kgWater/kgDryAir	0

Field	Units	Obj1	Obj2	Obj3	Obj4	Obj5
Name		CR-1				
Air Mass Flow Coefficient at Reference Conditions	kg/s	0.01				
Air Mass Flow Exponent	dimensionless	0.667				
ReferenceCrackConditions						
Name		Obj1	Obj2	Obj3	Obj4	Obj5
Air Mass Flow Coefficient When Opening is Closed	kg/s-m	SO_Zone01:Vent01B	SO_Zone03:Vent01S	SO_Zone03:Vent02N	SO_Zone04:Vent02T	SO_Zone06:Wall03T
Air Mass Flow Exponent When Opening is Closed	dimensionless	0.00001	0.00001	0.00001	0.00001	0.00001
Minimum Density Difference for Two-Way Flow	kg/m3	0.5	0.5	0.5	0.5	0.5
Discharge Coefficient	dimensionless	0.0001	0.0001	0.0001	0.0001	0.0001
Name		Obj1	Obj2	Obj3	Obj4	Obj5
Air Mass Flow Coefficient When Opening is Closed	kg/s-m	HO_Zone04:Vent01B	HO_Zone05:Vent01B			
Air Mass Flow Exponent When Opening is Closed	dimensionless	0.5	0.5			
Sloping Plane Angle	deg	90	90			
Discharge Coefficient	dimensionless	1	1			

Figure I.8. Airflow network data continued

Field	Units	Obj1
Name		Zone02 Thermostat
Zone or ZoneList Name		Zone02
Control Type Schedule Name		HVACTemplate-Always 4
Control 1 Object Type		ThermostatSetpoint: DualSetpoint
Control 1 Name		Thermo_All Dual SP Control
Control 2 Object Type		
Control 2 Name		
Control 3 Object Type		
Control 3 Name		
Control 4 Object Type		
Control 4 Name		

Field	Units	Obj1
Name		Thermo_All Dual SP Control
Heating Setpoint Temperature Schedule Name		Heating Setpoints
Cooling Setpoint Temperature Schedule Name		Cooling Setpoints

Field	Units	Obj1
Name		Zone02ZoneHVAC:IdealLoadsAirSystem
Availability Schedule Name		
Zone Supply Air Node Name		Zone02 Supply Inlet
Zone Exhaust Air Node Name		
Maximum Heating Supply Air Temperature	C	50
Minimum Cooling Supply Air Temperature	C	13
Maximum Heating Supply Air Humidity Ratio	kgWater/kgDryAir	0.008
Minimum Cooling Supply Air Humidity Ratio	kgWater/kgDryAir	0.009
Heating Limit		NoLimit
Maximum Heating Air Flow Rate	m3/s	
Maximum Sensible Heating Capacity	W	
Cooling Limit		NoLimit
Maximum Cooling Air Flow Rate	m3/s	
Maximum Total Cooling Capacity	W	
Heating Availability Schedule Name		
Cooling Availability Schedule Name		
Dehumidification Control Type		ConstantSensibleHeatRatio
Cooling Sensible Heat Ratio	dimensionless	0.7
Humidification Control Type		ConstantSupplyHumidityRatio
Design Specification Outdoor Air Object Name		
Outdoor Air Inlet Node Name		
Demand Controlled Ventilation Type		None
Outdoor Air Economizer Type		NoEconomizer
Heat Recovery Type		None
Sensible Heat Recovery Effectiveness	dimensionless	0.7
Latent Heat Recovery Effectiveness	dimensionless	0.65

Field	Units	Obj1
Name		Zone02 Equipment
Zone Equipment 1 Object Type		ZoneHVAC:IdealLoadsAirSystem
Zone Equipment 1 Name		Zone02ZoneHVAC:IdealLoadsAirSystem
Zone Equipment 1 Cooling Sequence		1
Zone Equipment 1 Heating or NoLoad Sequence		1

Field	Units	Obj1
Zone Name		Zone02
Zone Conditioning Equipment List Name		Zone02 Equipment
Zone Air Inlet Node or NodeList Name		Zone02 Supply Inlet
Zone Air Exhaust Node or NodeList Name		
Zone Air Node Name		Zone02 Zone Air Node
Zone Return Air Node Name		Zone02 Return Outlet

Figure I.9. Heating, ventilating and air conditioning data

APPENDIX J: ENERGY ZONE DIMENSIONS OF REFERENCE HOUSE

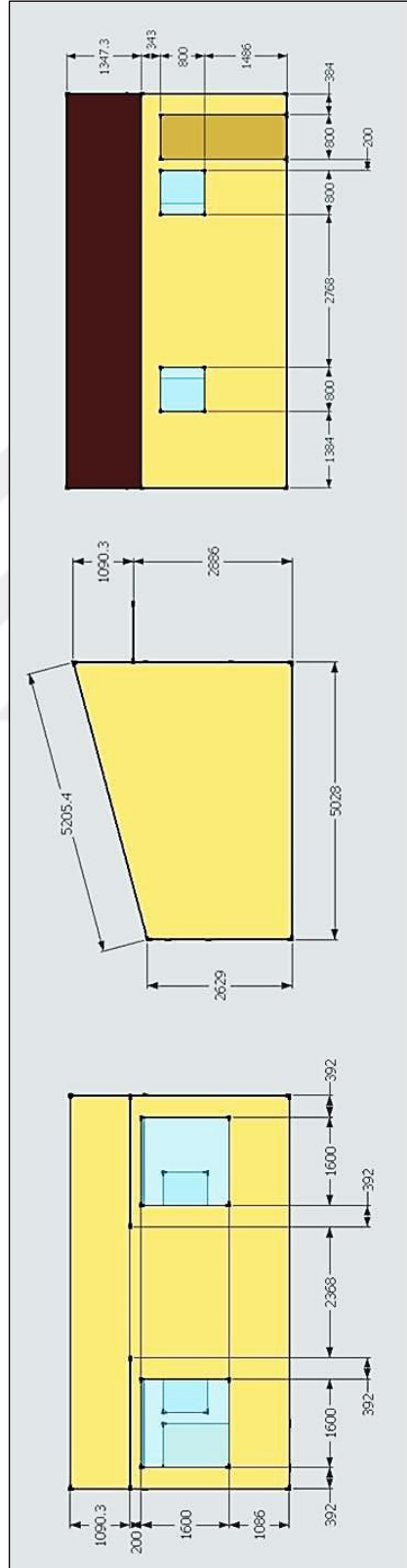


Figure J.1. Energy zone dimensions of reference house

APPENDIX K: ENERGYPLUS SETUP OF REFERENCE HOUSE

Algorithm

- i)** Solar distribution is set as full exterior with reflections in “Building” class of EnergyPlus 8.0.
- ii)** “Surface Convection Algorithm Inside”, default indoor surface heat transfer convection algorithm to be used for all zones, is set as TARP (variable natural convection based on temperature difference by ASHRAE and Walton).
- iii)** “Surface Convection Algorithm Outside”, default outside surface heat transfer convection algorithm to be used for all zones, is set as MoWiTT (correlation from measurements by Klems and Yazdanian for smooth surfaces).
- iv)** Conduction Finite Difference (ConFD) is used as “Heat Balance Algorithm”.
- v)** “Timestep” which is used in the Heat Balance Model calculation for heat transfer and load calculations, is selected as 30 timesteps per hour. The minimum value suggested for ConFD is 20 timesteps per hour.

Weather and Ground

- i)** Turkey Istanbul 170600 IWEC weather data available through the U.S. Department of Energy is used, including temperature, relative humidity, wind, and solar insolation in “Site Location” and “Run Period” [112].
- ii)** Temperatures defined in “Site Ground Temperature FC factor Method” with the F-factor method is specifically used for ground floors. These temperatures are close to the monthly average outdoor air temperature delayed by 3 months for the location. These values and perimeters of ground floor are taken into account as advised by ASHRAE [113] [114] (Table L.1).

Schedule

- i)** “Schedule Compact” is used to create activity, efficiency, clothing, air velocity, occupancy, intermittent, lighting, window vent, shade.

ii) Shade schedule is introduced in order to open the south-side shades from 5 May until 1 October (summer period).

iii) The heating setpoint is defined as 18 °C between 7:00 and 22:00, and 14 °C otherwise. The cooling setpoint is defined as 26 °C between 7:00 and 22:00, and 30 °C otherwise. (Table L.1).

Material

Regular materials including RBS, glass material, window gas, window shade and properties are described with full set of thermal properties in “Materials”, “Window Material Glazing”, “Window Material Gas” and “Window Material Shade” respectively (Table L.2).

Construction

i) Construction layers are defined from outside layer to the inside in “Construction”, underground floors (or slab-on-grade) are defined in “Construction F factor Ground Floor”.

ii) “Building Surface Detailed” allows for detailed entry of building heat transfer surfaces. It does not include subsurfaces such as windows or doors (Table L.3).

Fenestration and Shading

i) “Fenestration Surface Detailed” allows for detailed entry of subsurfaces (windows, doors, glass doors, tubular daylighting devices).

ii) “Window Property Shading Control” specifies the type, location, and controls for window shades, window blinds, and switchable glazing. Shading type is defined as interior shade.

iii) “Shading Building Detailed” used is used for shading elements such as trees, other buildings, parts of this building not being modeled. Each pair of windows on the south-side of the living quarters has 1,084 mm x 2,384 mm outside shades which screen the sun in summer (Table L.4).

Occupancy and Equipment

- i) “People” sets internal gains and contaminant rates for occupants in the zone. Thermal comfort model type is set as AdaptiveCEN15251.
- ii) “Lights” sets internal gains for lights in the zone. Lighting level is set as 300 W.
- iii) “Electric Equipment” sets internal gains for electric equipment in the zone. Design level is set as 5.38 W/m² (Table L.5).

Airflow

- i) “Airflow Network Simulation Control” defines the global parameters used in an Airflow Network simulation.
- ii) “Airflow Network Multizone Zone” is used to simultaneously control a thermal zone's window and door openings.
- iii) “Airflow Network Multizone Surface” specifies the properties of a surface linkage through which air flows.
- iv) “Airflow Network Multizone Reference Crack Conditions” specifies the conditions under which the air mass flow coefficient was measured.
- v) “Airflow Network Multizone Surface Crack” specifies the properties of airflow through a crack (Table L.6).

Heating, Ventilating and Air Conditioning

- i) “Zone Control Thermostat” defines the Thermostat settings for a zone or list of zones and “Thermostat Setpoint Dual Setpoint” is used for a heating and cooling thermostat with dual setpoints.
- ii) Even though there is no mechanical ventilation, “Zone HVAC Ideal Load Air System”, “Zone HVAC Equipment List” and “Zone HVAC Equipment Connections” need to be defined to run the simulation (Table L.7).

Output

“Output Variable Dictionary”, “Output Surfaces Drawing”, “Output Table Summary

Reports” “Output Control Table Style”, “Output Variable”, “Output Meter” and “Output SQLite” need to be defined in order to obtain the simulation outputs.



APPENDIX L: ENERGYPLUS INPUT DATA OF REFERENCE HOUSE

Field	Units	Ob1	Ob2	Ob3	Ob4	Ob5	Ob6	Ob7	Ob8	Ob9	Ob10	Ob11
Name	Units	Activity Sch	Eff Sch	Clothing Sch	Air Velo Sch	OCCUPANCY	LIGHTING	Heating Setpoints	Cooling Setpoints	HVAC Template-Always 4	WritersSummerShade	APT_EQP_SCH
Schedule Type/Limit Name		Any Number	Any Number	Any Number	Any Number	Fraction	Fraction	Temperature	Temperature	HVAC Template-Always 4	Fraction	Fraction
January Ground Temperature	C	11.4										
February Ground Temperature	C	7.9										
March Ground Temperature	C	5.8										
April Ground Temperature	C	4.9										
May Ground Temperature	C	7.3										
June Ground Temperature	C	12.2										
July Ground Temperature	C	16.8										
August Ground Temperature	C	21.6										
September Ground Temperature	C	24.1										
October Ground Temperature	C	24.2										
November Ground Temperature	C	20.8										
December Ground Temperature	C	16.5										
Field 1	varies											
Field 2	varies											
Field 3	varies											
Field 4	varies	131.8			0.137							
Field 5	varies											
Field 6	varies											
Field 7	varies											
Field 8	varies											
Field 9	varies											
Field 10	varies											
Field 11	varies											
Field 12	varies											
Field 13	varies											
Field 14	varies											
Field 15	varies											
Field 16	varies											
Field 17	varies											
Field 18	varies											
Field 19	varies											
Field 20	varies											
Field 21	varies											
Field 22	varies											
Field 23	varies											
Field 24	varies											
Field 25	varies											
Field 26	varies											
Field 27	varies											
Field 28	varies											
Field 29	varies											
Field 30	varies											
Field 31	varies											
Field 32	varies											
Field 33	varies											
Field 34	varies											
Field 35	varies											
Field 36	varies											
Field 37	varies											
Field 38	varies											
Field 39	varies											
Field 40	varies											
Field 41	varies											
Field 42	varies											
Field 43	varies											
Field 44	varies											
Field 45	varies											
Field 46	varies											

Figure L.1. Ground and schedule data

Field	Units	Obj1	Obj2	Obj3	Obj4	Obj5	Obj6
Name		M11 100mm lightweight concrete	1/2mm Galvanized Steel	3 1/2" Styrofoam	Radiant Barrier	I01 25mm insulation board	F08 Metal surface
Roughness		MediumRough	Smooth	MediumSmooth	Smooth	MediumRough	Smooth
Thickness	m	0.1016	0.0005	0.0889	0.013	0.0254	0.008
Conductivity	W/m-K	0.53	18	0.036057	235	0.03	45.28
Density	kg/m3	1280	7850	32	1070	43	7824
Specific Heat	J/kg-K	840	452	1400	897	1210	500
Thermal Absorptance					0.03		
Solar Absorptance					0.03		
Visible Absorptance					0.03		

Field	Units	Obj1
Name		CLEAR 6MM
Optical Data Type		SpectralAverage
Window Glass Spectral Data Set Name		
Thickness	m	0.006
Solar Transmittance at Normal Incidence		0.775
Front Side Solar Reflectance at Normal Incidence		0.071
Back Side Solar Reflectance at Normal Incidence		0.071
Visible Transmittance at Normal Incidence		0.881
Front Side Visible Reflectance at Normal Incidence		0.08
Back Side Visible Reflectance at Normal Incidence		0.08
Infrared Transmittance at Normal Incidence		0
Front Side Infrared Hemispherical Emissivity		0.84
Back Side Infrared Hemispherical Emissivity		0.84
Conductivity	W/m-K	0.9
Dirt Correction Factor for Solar and Visible Transmittance		
Solar Diffusing		
Young's modulus	Pa	
Poisson's ratio		

Field	Units	Obj1
Name		AIR 6MM
Gas Type		Air
Thickness	m	0.0063
Conductivity Coefficient A	W/m-K	
Conductivity Coefficient B	W/m-K2	
Conductivity Coefficient C	W/m-K3	
Viscosity Coefficient A	kg/m-s	
Viscosity Coefficient B	kg/m-s-K	
Viscosity Coefficient C	kg/m-s-K2	
Specific Heat Coefficient A	J/kg-K	
Specific Heat Coefficient B	J/kg-K2	
Specific Heat Coefficient C	J/kg-K3	
Molecular Weight	g/mol	
Specific Heat Ratio		

Field	Units	Obj1
Name		Radiant Barrier Shades
Solar Transmittance	dimensionless	0.28
Solar Reflectance	dimensionless	0.7
Visible Transmittance	dimensionless	0
Visible Reflectance	dimensionless	0.97
Infrared Hemispherical Emissivity	dimensionless	0.018
Infrared Transmittance	dimensionless	0.9
Thickness	m	0.00013
Conductivity	W/m-K	235
Shade to Glass Distance	m	0.04
Top Opening Multiplier		
Bottom Opening Multiplier		
Left-Side Opening Multiplier		
Right-Side Opening Multiplier		0
Airflow Permeability	dimensionless	

Figure L.2. Material data

Field	Units	Obj1	Obj2	Obj3	Obj4		
Name		House Wall	House Window	House Door	House Roof New		
Outside Layer		3 1/2" Styrofoam	CLEAR 6MM	F08 Metal surface	1/2mm Galvanized Steel		
Layer 2			AIR 6MM	I01 25mm insulation board	3 1/2" Styrofoam		
Layer 3			CLEAR 6MM		Radiant Barrier		
Field	Units	Obj1					
Name		Ground Floor					
F-Factor	W/m-K	0.4					
Area	m2	35.87					
PerimeterExposed	m	24.328					
Field	Units	Obj1	Obj2	Obj3	Obj4	Obj5	Obj6
Name		Zone02:Wall01	Zone02:Wall04	Zone02:Wall05	Zone02:Wall08	Zone02:Ceiling01	Zone02:Floor01
Surface Type		Wall	Wall	Wall	Wall	Roof	Floor
Construction Name		House Wall	House Wall	House Wall	House Wall	House Roof New	Ground Floor
Zone Name		Zone02	Zone02	Zone02	Zone02	Zone02	Zone02
Outside Boundary Condition		Outdoors	Outdoors	Outdoors	Outdoors	Outdoors	GroundFCfactorMethod
Outside Boundary Condition Object							
Sun Exposure		SunExposed	SunExposed	SunExposed	SunExposed	SunExposed	NoSun
Wind Exposure		WindExposed	WindExposed	WindExposed	WindExposed	WindExposed	NoWind
View Factor to Ground						0	0
Number of Vertices		4	4	4	4	4	4
Vertex 1 X-coordinate	m	-3.568	-3.568	3.568	3.568	3.568	3.568
Vertex 1 Y-coordinate	m	-0.092	4.936	4.936	-0.092	-0.092	4.936
Vertex 1 Z-coordinate	m	3.9763	2.629	2.629	3.9763	3.9763	0
Vertex 2 X-coordinate	m	-3.568	-3.568	3.568	3.568	3.568	3.568
Vertex 2 Y-coordinate	m	-0.092	4.936	4.936	-0.092	4.936	-0.092
Vertex 2 Z-coordinate	m	0	0	0	0	2.629	0
Vertex 3 X-coordinate	m	3.568	-3.568	-3.568	3.568	-3.568	-3.568
Vertex 3 Y-coordinate	m	-0.092	-0.092	4.936	4.936	4.936	-0.092
Vertex 3 Z-coordinate	m	0	0	0	0	2.629	0
Vertex 4 X-coordinate	m	3.568	-3.568	-3.568	3.568	-3.568	-3.568
Vertex 4 Y-coordinate	m	-0.092	-0.092	4.936	4.936	-0.092	4.936
Vertex 4 Z-coordinate	m	3.9763	3.9763	2.629	2.629	3.9763	0

Figure L.3. Construction data

Field	Units	Obj1	Obj2	Obj3	Obj4	Obj5
Name		Zn02:Win01S	Zn02:Win02S	Zone02:Win03N	Zone02:Win04N	Door_1
Surface Type		Window	Window	Window	Window	Door
Construction Name		House Window	House Window	House Window	House Window	House Door
Building Surface Name		Zone02:Wall01	Zone02:Wall01	Zone02:Wall05	Zone02:Wall05	Zone02:Wall05
Outside Boundary Condition Object						
View Factor to Ground						
Shading Control Name		ShadingControl	ShadingControl			
Frame and Divider Name						
Multiplier						
Number of Vertices		4	4	4	4	4
Vertex 1 X-coordinate	m	-3.176	1.576	2.184	-1.384	-2.384
Vertex 1 Y-coordinate	m	-0.092	-0.092	4.936	4.936	4.936
Vertex 1 Z-coordinate	m	2.686	2.686	2.286	2.286	2.286
Vertex 2 X-coordinate	m	-3.176	1.576	2.184	-1.384	-2.384
Vertex 2 Y-coordinate	m	-0.092	-0.092	4.936	4.936	4.936
Vertex 2 Z-coordinate	m	1.086	1.086	1.486	1.486	0
Vertex 3 X-coordinate	m	-1.576	3.176	1.384	-2.184	-3.184
Vertex 3 Y-coordinate	m	-0.092	-0.092	4.936	4.936	4.936
Vertex 3 Z-coordinate	m	1.086	1.086	1.486	1.486	0
Vertex 4 X-coordinate	m	-1.576	3.176	1.384	-2.184	-3.184
Vertex 4 Y-coordinate	m	-0.092	-0.092	4.936	4.936	4.936
Vertex 4 Z-coordinate	m	2.686	2.686	2.286	2.286	2.286

Field	Units	Obj1
Name		ShadingControl
Shading Type		InteriorShade
Construction with Shading Name		
Shading Control Type		OnIfScheduleAllows
Schedule Name		WinterSummerShade
Setpoint	W/m2, W or deg C	
Shading Control Is Scheduled		Yes
Glare Control Is Active		No
Shading Device Material Name		Radiant Barrier Shades
Type of Slat Angle Control for Blinds		
Slat Angle Schedule Name		
Setpoint 2	W/m2 or deg C	

Field	Units	Obj1	Obj2
Name		Shading_2	Shading_1
Transmittance Schedule Name			
Number of Vertices		4	4
Vertex 1 X-coordinate	m	-3.568	1.184
Vertex 1 Y-coordinate	m	0.9	0.9
Vertex 1 Z-coordinate	m	4.936	4.936
Vertex 2 X-coordinate	m	-3.568	1.184
Vertex 2 Y-coordinate	m	-0.184	-0.184
Vertex 2 Z-coordinate	m	4.936	4.936
Vertex 3 X-coordinate	m	-1.184	3.568
Vertex 3 Y-coordinate	m	-0.184	-0.184
Vertex 3 Z-coordinate	m	4.936	4.936
Vertex 4 X-coordinate	m	-1.184	3.568
Vertex 4 Y-coordinate	m	0.9	0.9
Vertex 4 Z-coordinate	m	4.936	4.936

Figure L.4. Fenestration and shading data

Field	Units	Obj1
Name		Residents
Zone or ZoneList Name		Zone02
Number of People Schedule Name		OCCUPANCY
Number of People Calculation Method		People
Number of People		2
People per Zone Floor Area	person/m2	
Zone Floor Area per Person	m2/person	
Fraction Radiant		0.3
Sensible Heat Fraction		
Activity Level Schedule Name		Activity Sch
Carbon Dioxide Generation Rate	m3/s-W	0.000000382
Enable ASHRAE 55 Comfort Warnings		
Mean Radiant Temperature Calculation Type		zoneaveraged
Surface Name/Angle Factor List Name		
Work Efficiency Schedule Name		Eff Sch
Clothing Insulation Schedule Name		Clothing Sch
Air Velocity Schedule Name		Air Velo Sch
Thermal Comfort Model 1 Type		AdaptiveCEN15251
Field	Units	Obj1
Name		Lights
Zone or ZoneList Name		Zone02
Schedule Name		LIGHTING
Design Level Calculation Method		LightingLevel
Lighting Level	W	300
Watts per Zone Floor Area	W/m2	
Watts per Person	W/person	
Return Air Fraction		0
Fraction Radiant		0.2
Fraction Visible		0.2
Fraction Replaceable		0
End-Use Subcategory		GeneralLights
Field	Units	Obj1
Name		Electrical Equipment
Zone or ZoneList Name		Zone02
Schedule Name		APT_EQP_SCH
Design Level Calculation Method		Watts/Area
Design Level	W	
Watts per Zone Floor Area	W/m2	5.38
Watts per Person	W/person	
Fraction Latent		0
Fraction Radiant		0.3
Fraction Lost		0

Figure L.5. Occupancy and equipment data

Field	Units	Obj1	
Name		NaturalVentilation	
AirflowNetwork Control		MultizoneWithoutDistribution	
Wind Pressure Coefficient Type		SurfaceAverageCalculation	
AirflowNetwork Wind Pressure Coefficient Array Name			
Height Selection for Local Wind Pressure Calculation			
Building Type		LOWRISE	
Maximum Number of Iterations	dimensionless	500	
Initialization Type		ZeroNodePressures	
Relative Airflow Convergence Tolerance	dimensionless	0.00001	
Absolute Airflow Convergence Tolerance	kg/s	0.000001	
Convergence Acceleration Limit	dimensionless	-0.5	
Azimuth Angle of Long Axis of Building	deg	90	
Ratio of Building Width Along Short Axis to Width Along Long Axis		0.704596	
Field	Units	Obj1	
Zone Name		Zone02	
Ventilation Control Mode		Constant	
Ventilation Control Zone Temperature Setpoint Schedule Name			
Minimum Venting Open Factor	dimensionless		
Indoor and Outdoor Temperature Difference Lower Limit For Maximum Venting Open Factor	deltaC		
Indoor and Outdoor Temperature Difference Upper Limit for Minimum Venting Open Factor	deltaC	100	
Indoor and Outdoor Enthalpy Difference Lower Limit For Maximum Venting Open Factor	deltaJ/kg		
Indoor and Outdoor Enthalpy Difference Upper Limit for Minimum Venting Open Factor	deltaJ/kg	300000	
Venting Availability Schedule Name			
Field	Units	Obj1	Obj2
Surface Name		Zone02:Wall04	Zone02:Wall08
Leakage Component Name		CR-1	CR-1
External Node Name			
Window/Door Opening Factor, or Crack Factor	dimensionless	1	1
Ventilation Control Mode			
Ventilation Control Zone Temperature Setpoint Schedule Name			
Minimum Venting Open Factor	dimensionless		
Indoor and Outdoor Temperature Difference Lower Limit For Maximum Venting Open Factor	deltaC		
Indoor and Outdoor Temperature Difference Upper Limit for Minimum Venting Open Factor	deltaC	100	100
Indoor and Outdoor Enthalpy Difference Lower Limit For Maximum Venting Open Factor	deltaJ/kg		
Indoor and Outdoor Enthalpy Difference Upper Limit for Minimum Venting Open Factor	deltaJ/kg	300000	300000
Venting Availability Schedule Name			
Field	Units	Obj1	
Name		ReferenceCrackConditions	
Reference Temperature	C	20	
Reference Barometric Pressure	Pa	101325	
Reference Humidity Ratio	kgWater/kgDryAir	0	
Field	Units	Obj1	
Name		CR-1	
Air Mass Flow Coefficient at Reference Conditions	kg/s	0.01	
Air Mass Flow Exponent	dimensionless	0.667	
Reference Crack Conditions		ReferenceCrackConditions	

Figure L.6. Airflow network data

Field	Units	Obj1
Name		Zone02 Thermostat
Zone or ZoneList Name		Zone02
Control Type Schedule Name		HVACTemplate-Always 4
Control 1 Object Type		ThermostatSetpoint: DualSetpoint
Control 1 Name		Thermo_All Dual SP Control
Control 2 Object Type		
Control 2 Name		
Control 3 Object Type		
Control 3 Name		
Control 4 Object Type		
Control 4 Name		

Field	Units	Obj1
Name		Thermo_All Dual SP Control
Heating Setpoint Temperature Schedule Name		Heating Setpoints
Cooling Setpoint Temperature Schedule Name		Cooling Setpoints

Field	Units	Obj1
Name		Zone02ZoneHVAC:IdealLoadsAirSystem
Availability Schedule Name		
Zone Supply Air Node Name		Zone02 Supply Inlet
Zone Exhaust Air Node Name		
Maximum Heating Supply Air Temperature	C	50
Minimum Cooling Supply Air Temperature	C	13
Maximum Heating Supply Air Humidity Ratio	kgWater/kgDryAir	0.008
Minimum Cooling Supply Air Humidity Ratio	kgWater/kgDryAir	0.009
Heating Limit		NoLimit
Maximum Heating Air Flow Rate	m3/s	
Maximum Sensible Heating Capacity	W	
Cooling Limit		NoLimit
Maximum Cooling Air Flow Rate	m3/s	
Maximum Total Cooling Capacity	W	
Heating Availability Schedule Name		
Cooling Availability Schedule Name		
Dehumidification Control Type		ConstantSensibleHeatRatio
Cooling Sensible Heat Ratio	dimensionless	0.7
Humidification Control Type		ConstantSupplyHumidityRatio
Design Specification Outdoor Air Object Name		
Outdoor Air Inlet Node Name		
Demand Controlled Ventilation Type		None
Outdoor Air Economizer Type		NoEconomizer
Heat Recovery Type		None
Sensible Heat Recovery Effectiveness	dimensionless	0.7
Latent Heat Recovery Effectiveness	dimensionless	0.65

Field	Units	Obj1
Name		Zone02 Equipment
Zone Equipment 1 Object Type		ZoneHVAC:IdealLoadsAirSystem
Zone Equipment 1 Name		Zone02ZoneHVAC:IdealLoadsAirSystem
Zone Equipment 1 Cooling Sequence		1
Zone Equipment 1 Heating or No-Load Sequence		1

Field	Units	Obj1
Zone Name		Zone02
Zone Conditioning Equipment List Name		Zone02 Equipment
Zone Air Inlet Node or NodeList Name		Zone02 Supply Inlet
Zone Air Exhaust Node or NodeList Name		...
Zone Air Node Name		Zone02 Zone Air Node
Zone Return Air Node Name		Zone02 Return Outlet

Figure L.7. Heating, ventilating and air conditioning data

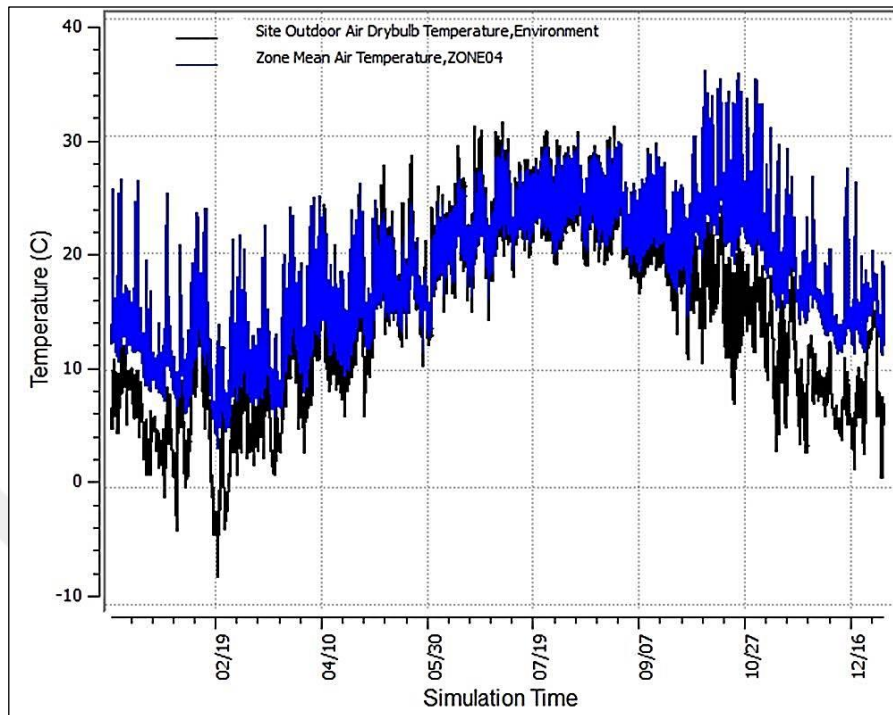
APPENDIX M: ENERGYPLUS OUTPUT DATA OF NEW HOUSE

Figure M.1. Annual air temperatures in south-side partial DSF versus outside

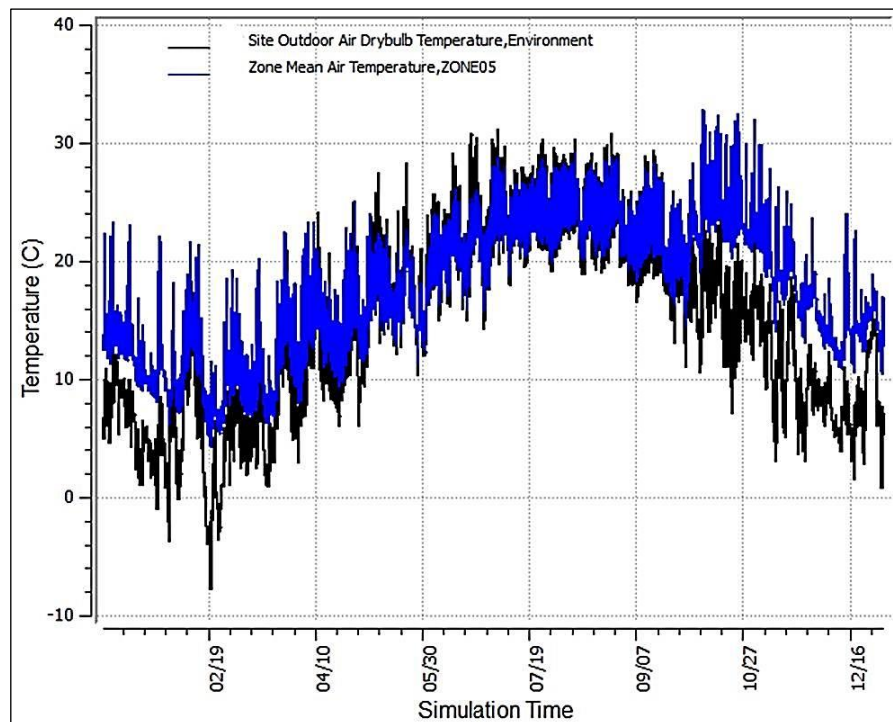


Figure M.2. Annual air temperatures in north-side partial DSF versus outside

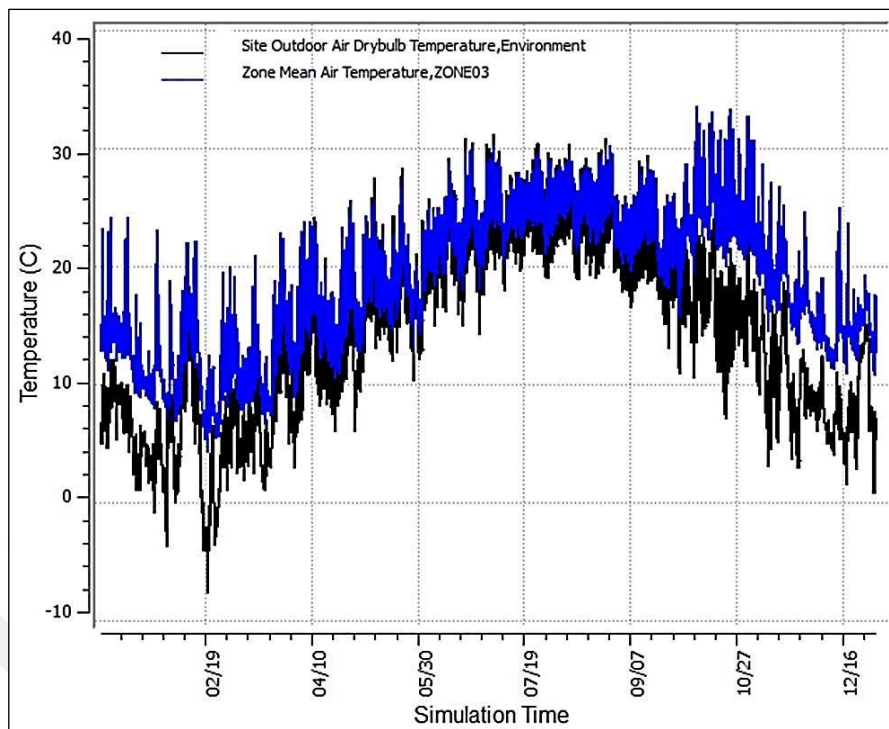


Figure M.3. Annual air temperatures in DSR versus outside

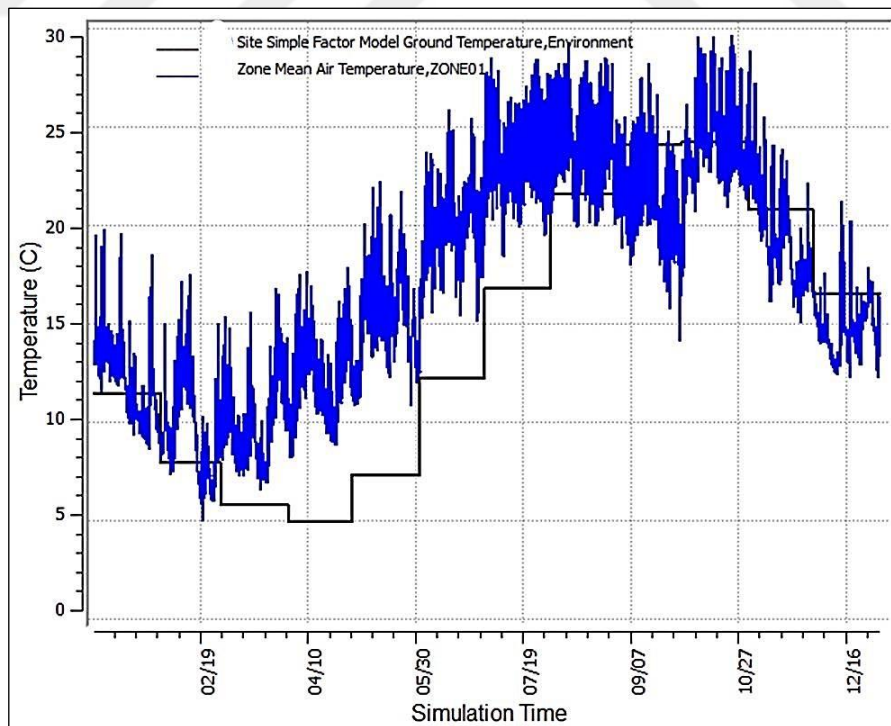


Figure M.4. Annual air temperatures in underground space versus ground

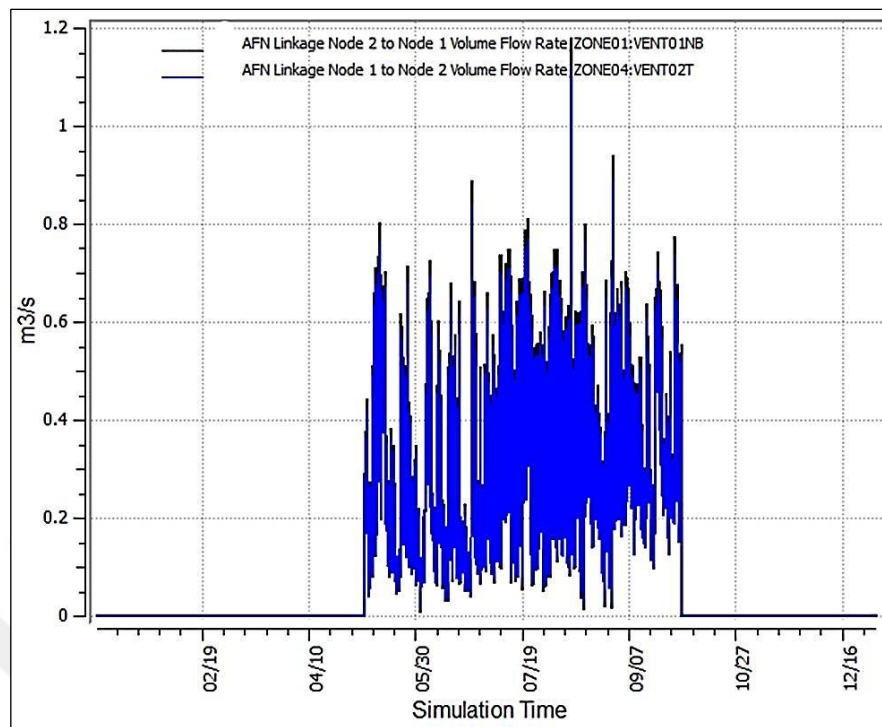


Figure M.5. Annual airflow rates at roof and underground space vent nodes

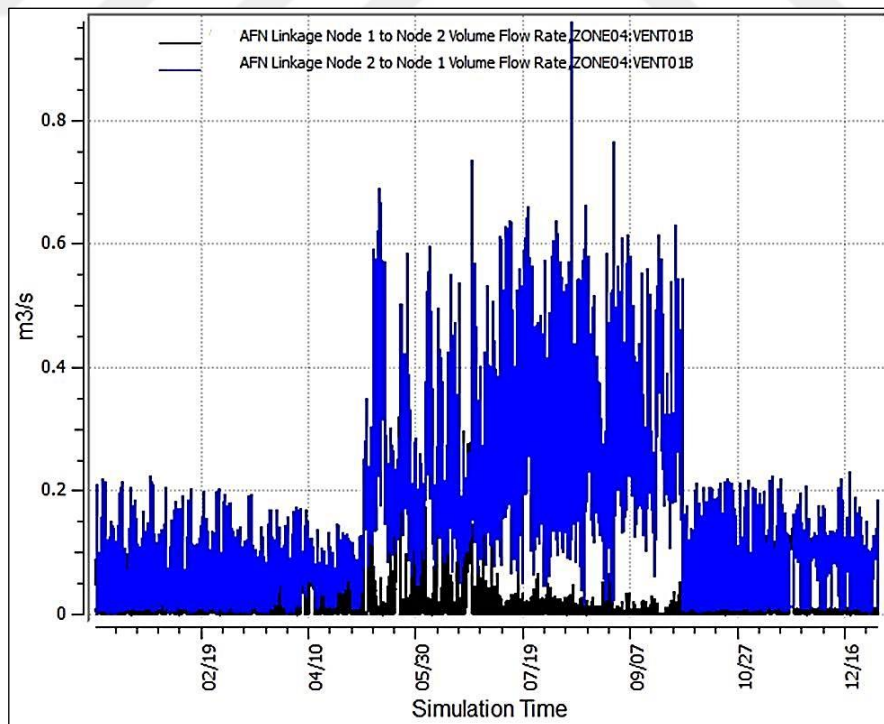


Figure M.6. Annual airflow rates at south-side partial DSF bottom opening node

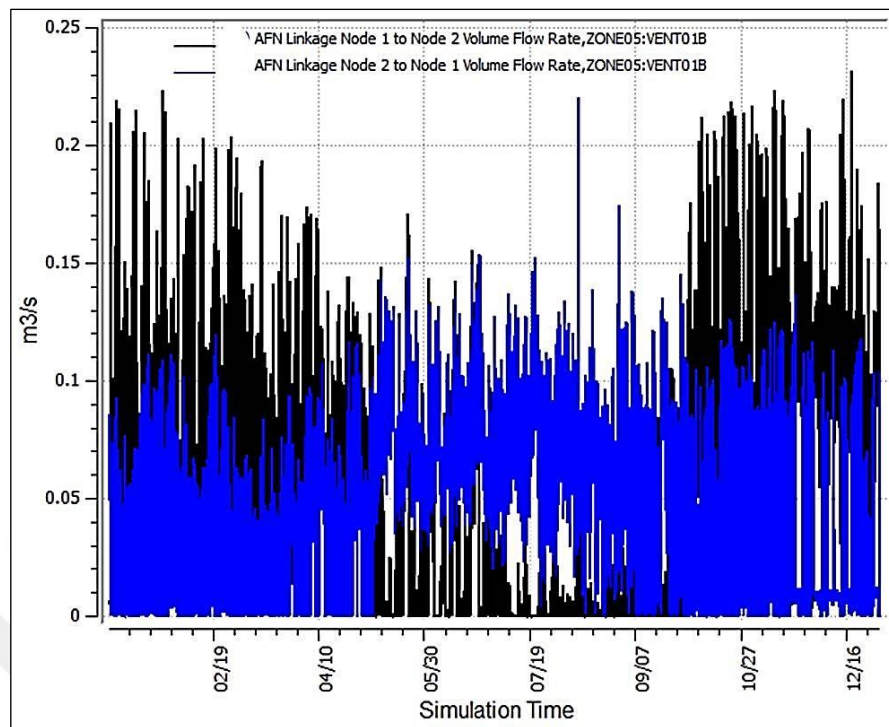


Figure M.7. Annual airflow rates at north-side partial DSF bottom opening node

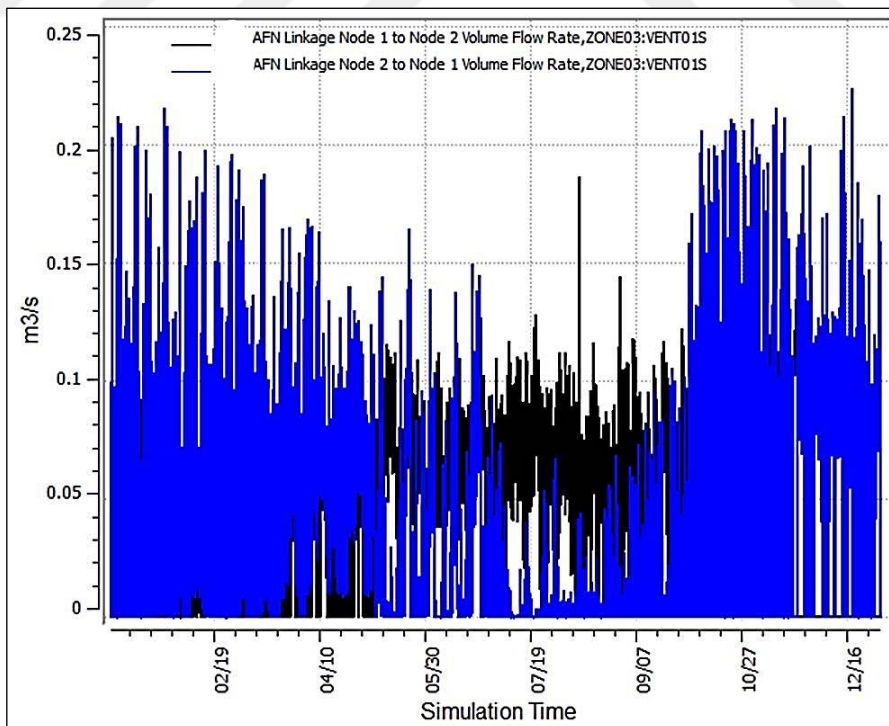


Figure M.8. Annual airflow rates at DSR south opening node

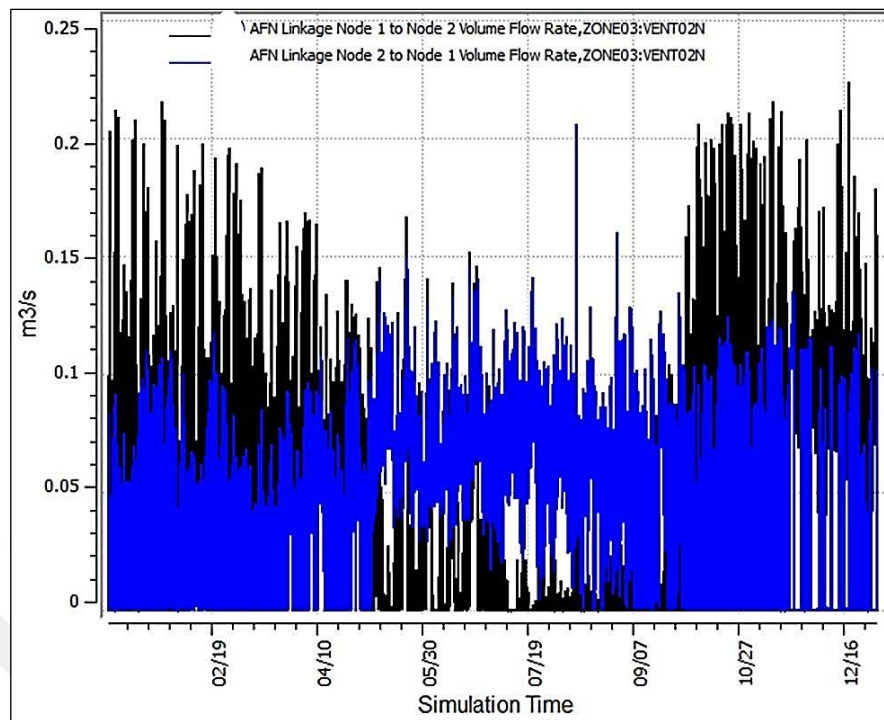


Figure M.9. Annual airflow rates at DSR north opening node

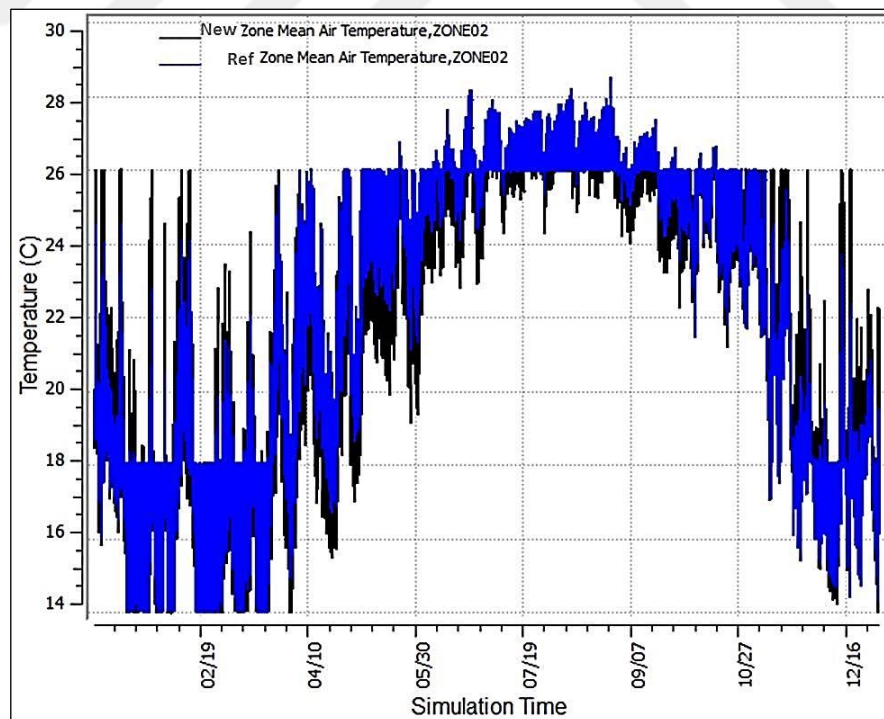


Figure M.10. Annual air temperatures in new house and reference house living quarters

APPENDIX N: AIRFLOW ZONE DIMENSIONS OF NEW HOUSE

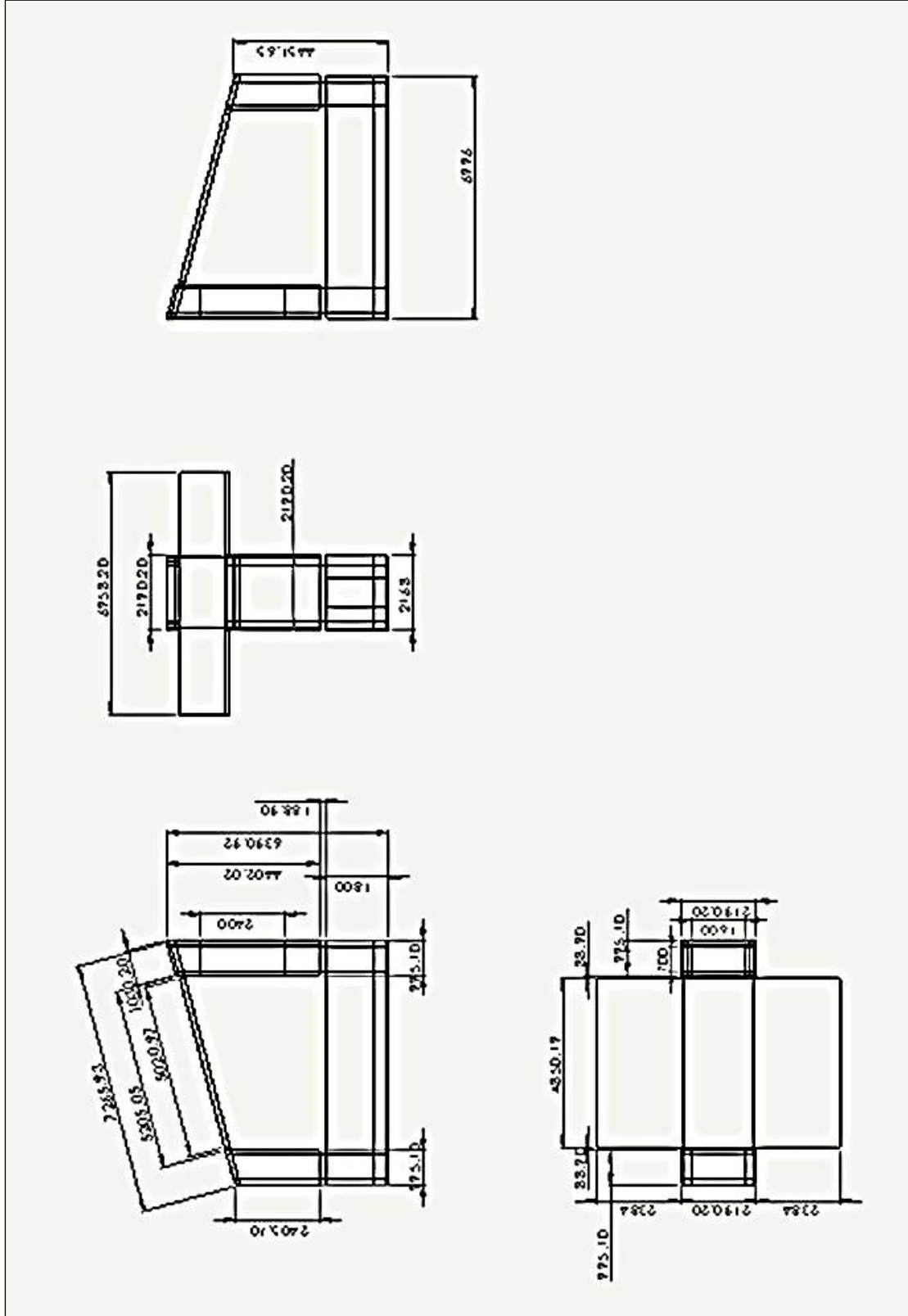


Figure N.1. Airflow zone dimensions of new house

APPENDIX O: FLUENT BOUNDARY CONDITIONS OF NEW HOUSE

Table O.1. Average temperatures of air zones at summer daytime and winter night time extremes

Air zones of new house	Average summer temperature (K)	Air zones of new house	Average winter temperature (K)
Outdoor	304.39	Outdoor	265.39
Earth tube	303.97	Earth tube	278.69
North-side semi DSF	301.76	North-side semi DSF	277.53
South-side semi DSF	302.28	South-side semi DSF	276.49
DSR	303.20	DSR	277.42
Underground space	301.26	Underground space	278.20

Table O.2. Boundary conditions of new house at summer daytime and winter night time extremes

Fluent surface boundary conditions	Boundary type	Summer surface temperature (K)	Fluent surface boundary conditions	Boundary type	Winter surface temperature (K)
DSR			DSR		
Roof vent	outlet	306.37	Roof vent	Wall	274.73
Floor	Wall	302.95	Floor	Wall	278.55
Back	Wall	303.39	Back	Wall	277.24
Left	Wall	303.41	Left	Wall	277.24
Front	Wall	304.06	Front	Wall	277.25
Right	Wall	304.54	Right	Wall	277.24
Ceiling	Wall	304.77	Ceiling	Wall	276.14
North-side semi DSF			North-side semi DSF		
Floor	Wall	301.77	Floor	Wall	277.05
Back	Wall	302.45	Back	Wall	276.17
Left	Wall	302.38	Left	Wall	276.15
Front	Wall	302.09	Front	Wall	277.27
Right	Wall	303.08	Right	Wall	276.15
Ceiling	Wall	303.66	Ceiling	Wall	275.85
South-side semi DSF			South-side semi DSF		
Glazing	Wall	304.63	Glazing	Wall	268.30
Floor	Wall	305.71	Floor	Wall	274.73
Back	Wall	306.23	Back	Wall	274.96
Left	Wall	306.38	Left	Wall	274.00
Front	Wall	306.54	Front	Wall	274.35
Right	Wall	306.97	Right	Wall	274.00
Ceiling	Wall	304.32	Ceiling	Wall	275.33

Table O.2. Boundary conditions of new house at summer daytime and winter night time extremes continued

Fluent surface boundary conditions	Boundary type	Summer surface temperature (K)	Fluent surface boundary conditions	Boundary type	Winter surface temperature (K)
Underground space			Underground space		
Underground space vent	Inlet	295.46	Underground space vent	Wall	280.43
Floor	Wall	294.22	Floor	Wall	280.55
Back	Wall	295.31	Back	Wall	280.35
Left	Wall	294.80	Left	Wall	280.59
Front	Wall	294.79	Front	Wall	280.59
Right	Wall	294.80	Right	Wall	280.59
Ceiling	Wall	296.09	Ceiling	Wall	280.80
Openings (with adiabatic surfaces)			Openings (with adiabatic surfaces)		
South-side semi DSF bottom opening	Wall	303.39	South-side semi DSF bottom opening	Wall	276.25
North-side semi DSF bottom opening	Wall	299.24	North-side semi DSF bottom opening	Wall	278.32
DSR South opening	Wall	300.71	DSR South opening	Wall	279.19
DSR North opening	Wall	300.59	DSR North opening	Wall	279.34
Infiltration			Infiltration		
South-side semi DSF left	Outlet	303.32	South-side semi DSF left	Outlet	274.33
South-side semi DSF right	outlet	303.32	South-side semi DSF right	outlet	274.33
North-side semi DSF left	outlet	303.66	North-side semi DSF left	inlet	275.85
North-side semi DSF right	outlet	303.66	North-side semi DSF right	inlet	275.85

Table O.3. Operating conditions of new house

Fluent operating conditions	Summer	Winter
Gravitational acceleration g (m/s^2)	-9.807	-9.807
Operating temperature (K)	306.97	280.80
Operating density (kg/m^3)	1.1512	1.2587
Operating pressure	101,325	101,325

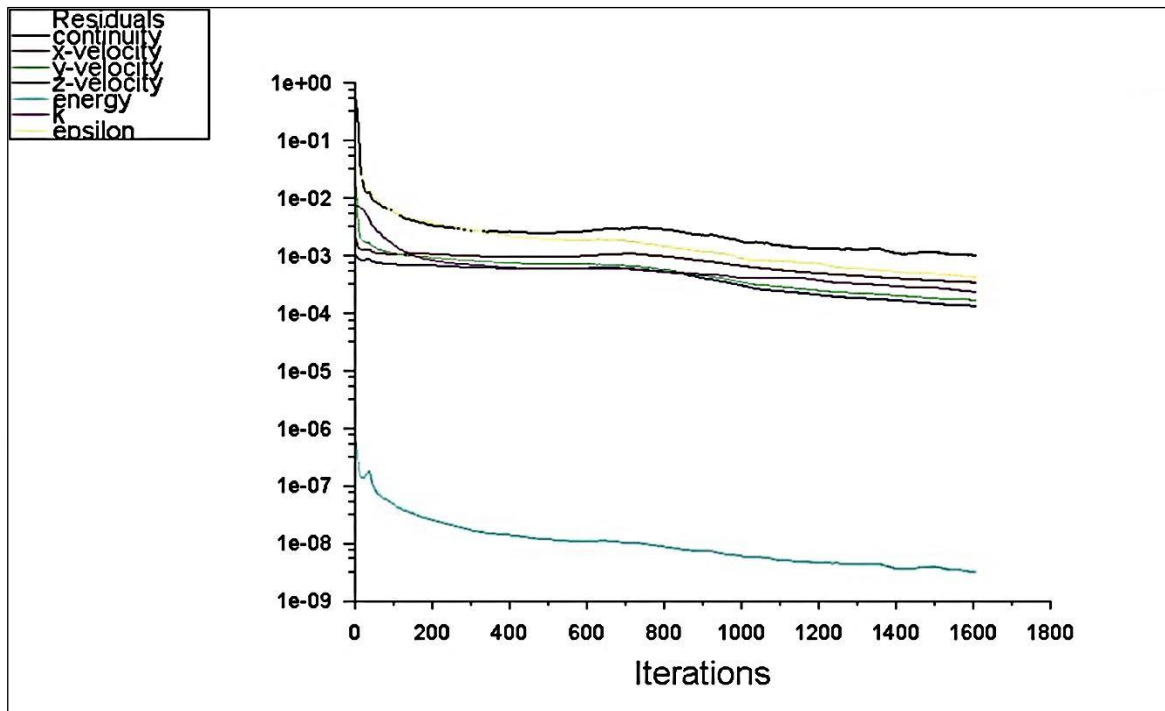
APPENDIX P: FLUENT SCALED RESIDUALS OF NEW HOUSE

Figure P.1. Scaled residuals of new house at summer daytime extremes

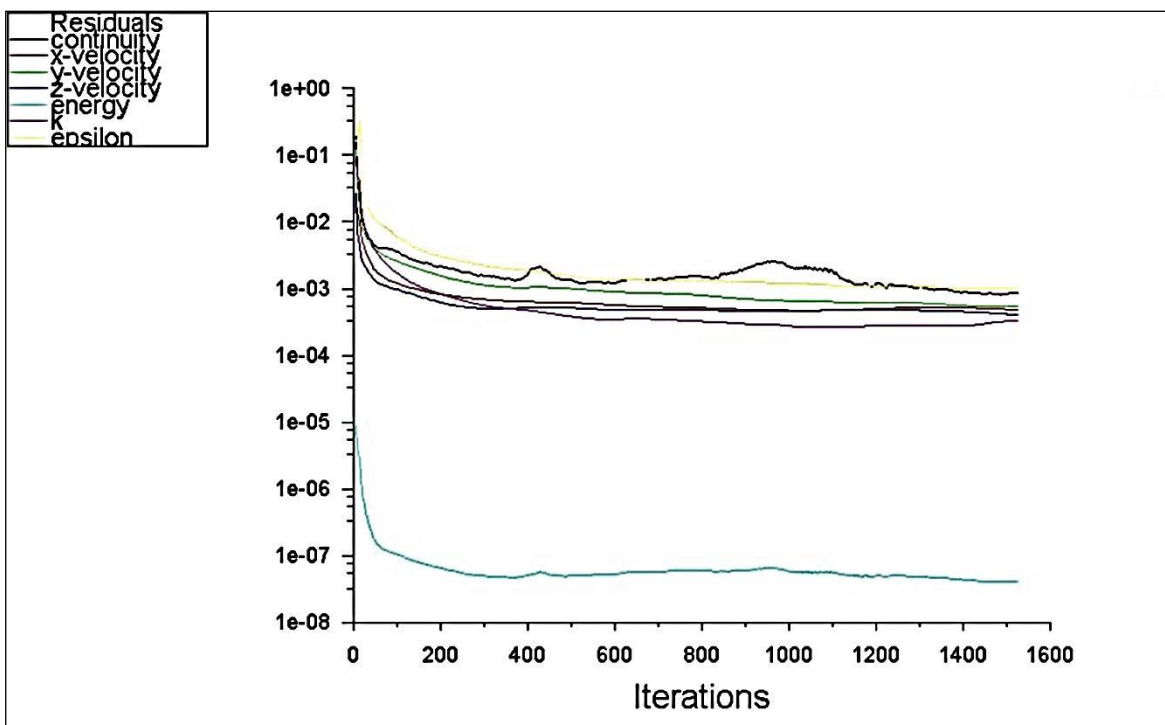


Figure P.2. Scaled residuals of new house at winter nighttime extremes

APPENDIX Q: CONSTRUCTION COSTS

Table Q.1. Bill of materials and cost data of new house living quarters

Living quarters	Quantity	Area (m ²)	Total (m ²)	Construction cost (\$)
Ceiling wall - Styrofoam	1	37.1	37.1	674
North wall - Styrofoam	1	15.7	15.7	285
North wall - double glazings	4	0.6	2.4	20
North wall - door metal surface	1	1.8	1.8	1,152
North wall - door insulation board	1	1.8	1.8	33
South wall - Styrofoam	1	23.3	23.3	423
South wall - double glazings	4	2.6	10.4	85
South wall - shading radiant barriers	2	2.6	5.2	7
East wall - Styrofoam	1	16.6	16.6	301
West wall - Styrofoam	1	16.6	16.6	301
Floor wall - Styrofoam	1	11.9	11.9	216
Floor wall - lightweight concrete	1	24	24	148
Plywood - Sağlamlar	1	35.9	35.9	626
Handles, etc. - Winsa	5	-	-	51
Unleaded PVC glazing frames - Winsa Dorado Gold (19.2 m)	-	-	-	194
Total	-	-	-	4,515

Table Q.2. Bill of materials and cost data of new house DSR

DSR	Quantity	Area (m²)	Total (m²)	Construction cost (\$)
Ceiling wall - galvanized steel	1	37.1	37.1	99
Ceiling wall - Styrofoam	1	37.1	37.1	674
Ceiling wall - radiant barrier	1	37.1	37.1	53
North wall - Styrofoam	1	1.5	1.5	27
South wall - Styrofoam	1	1.5	1.5	27
East wall - Styrofoam	1	1.2	1.2	22
West wall - Styrofoam	1	1.2	1.2	22
Total	-	-	-	924

Table Q.3. Bill of materials and cost data of new house underground space

Underground space	Quantity	Area (m²)	Total (m²)	Construction cost (\$)
Ceiling wall - lightweight concrete	1	14.7	14.7	90
North wall - lightweight concrete	1	4.5	4.5	28
North wall - air vent galvanized steel	2	0.3	0.6	2
North wall - air vent Styrofoam	1	0.3	0.3	5
South wall - lightweight concrete	1	4.7	4.7	29
East wall - lightweight concrete	1	14.4	14.4	89
West wall - lightweight concrete	1	14.4	14.4	89
Floor wall - lightweight concrete	1	17	17	105
Total	-	-	-	436

Table Q.4. Bill of materials and cost data of new house earth tube

Earth tube	Quantity	Area (m²)	Total (m²)	Construction cost (\$)
Ceiling wall - lightweight concrete	1	0.8	0.8	5
North wall - lightweight concrete	1	1.5	1.5	9
North wall - air Vent galvanized steel	2	0.6	1.2	3
North wall - air vent Styrofoam	1	0.6	0.6	11
South wall - lightweight concrete	1	1.7	1.7	10
South wall - air vent galvanized steel	2	0.3	0.6	2
South wall - air vent Styrofoam	1	0.3	0.3	5
East wall - lightweight concrete	1	1.6	1.6	10
West wall - lightweight concrete	1	1.6	1.6	10
Floor wall - lightweight concrete	1	0.8	0.8	5
Total	-	-	-	70

Table Q.5. Bill of materials and cost data of new house North-side semi DSF

North-side semi DSF	Quantity	Area (m²)	Total (m²)	Construction cost (\$)
Ceiling wall - galvanized steel	1	2.7	2.7	7
Ceiling wall - Styrofoam	1	2.7	2.7	49
Ceiling wall - radiant barrier	1	2.7	2.7	4
North wall - Styrofoam	1	6.1	6.1	111
South wall - Styrofoam	1	6.5	6.5	118
East wall - Styrofoam	1	3	3	54
West wall - Styrofoam	1	3	3	54
Floor wall - Styrofoam	1	1.4	1.4	25
Total	-	-	-	423

Table Q.6. Bill of materials and cost data of new house South-side semi DSF

South-side semi DSF	Quantity	Area (m²)	Total (m²)	Construction cost (\$)
Ceiling wall - galvanized steel	1	1.2	1.2	3
Ceiling wall - Styrofoam	1	1.2	1.2	22
Ceiling wall - radiant barrier	1	1.2	1.2	2
Ceiling wall - air vent galvanized steel	2	1.5	3	8
Ceiling wall - air vent Styrofoam	1	1.5	1.5	27
North wall - Styrofoam	1	9.7	9.7	176
South wall - Styrofoam	1	6.9	6.9	125
South wall - single glazing	1	3.8	3.8	31
East wall - Styrofoam	1	4.7	4.7	85
West wall - Styrofoam	1	4.7	4.7	85
Floor wall - Styrofoam	1	1.4	1.4	25
Unleaded PVC glazing frames - Winsa Dorado Gold (8 m)	-	-	-	81
Total	-	-	-	671

Table Q.7. Bill of materials and cost data of reference house

Living quarters	Quantity	Area (m²)	Total (m²)	Construction cost (\$)
Ceiling wall - galvanized steel	1	37.1	37.1	99
Ceiling wall - Styrofoam	1	37.1	37.1	674
Ceiling wall - radiant barrier	1	37.1	37.1	53
North wall - Styrofoam	1	15.7	15.7	285
North wall - double glazings	4	0.6	2.4	20
North wall - door metal surface	1	1.8	1.8	1,152
North wall - door insulation board	1	1.8	1.8	33
South wall - Styrofoam	1	23.3	23.3	423
South wall - double glazings	4	2.6	10.4	85
South wall - shading radiant barriers	2	2.6	5.2	7
East wall - Styrofoam	1	16.6	16.6	301
West wall - Styrofoam	1	16.6	16.6	301
Floor wall - lightweight concrete	1	35.9	35.9	221
Plywood - Sağlamlar	1	35.9	35.9	626
Handles, etc. - Winsa	5	-	-	51
Unleaded PVC glazing frames - Winsa Dorado Gold (19.2 m)	-	-	-	194
Total	-	-	-	4,524

APPENDIX R: ELECTRICITY COSTS

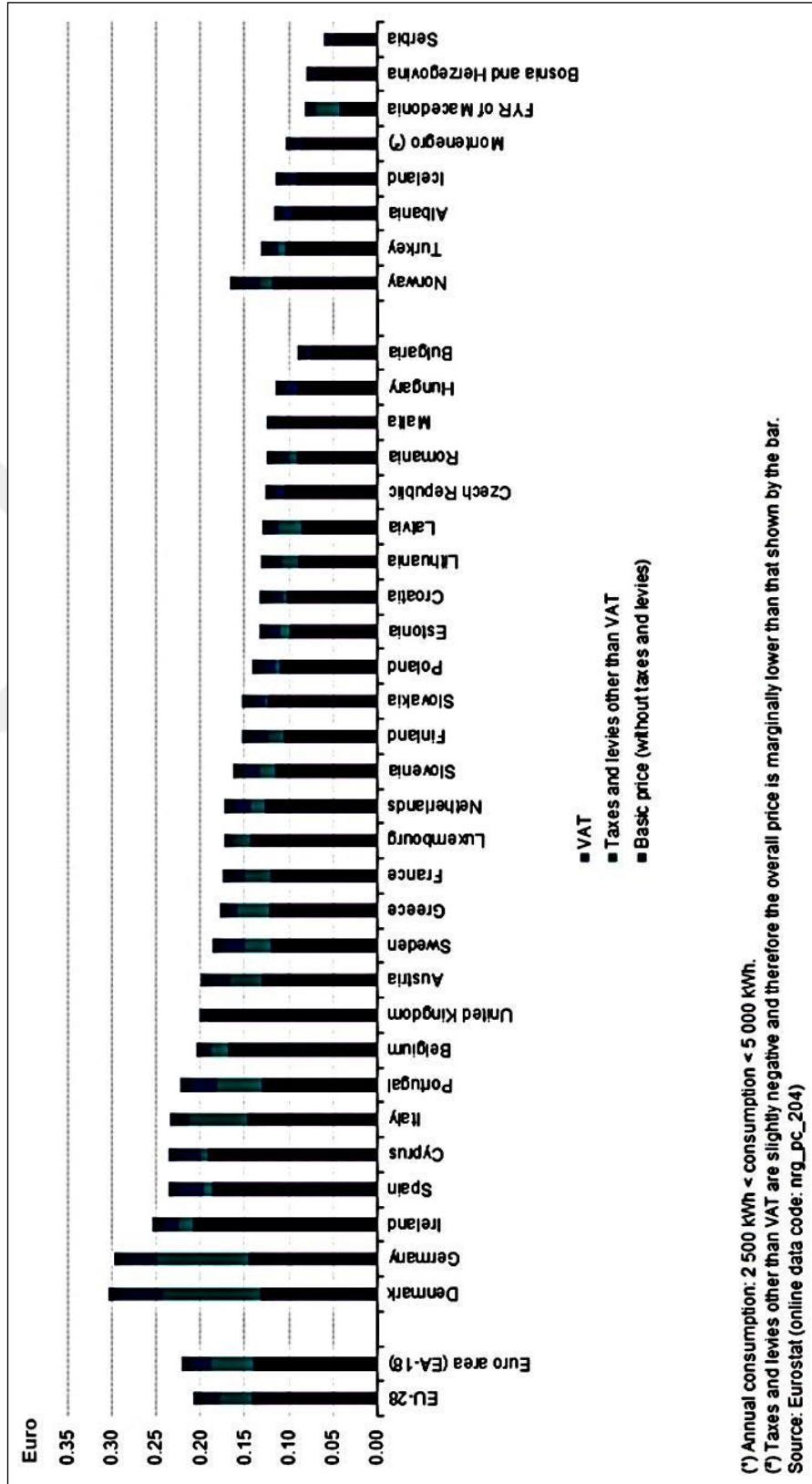


Figure R.1.1. Household electricity prices in Europe in the second half of 2014 [111]